Dosage sensitivity in Pumilio1-related phenotypes reflects distinct disease mechanisms

Salvatore Botta[1,2], Nicola de Prisco[1], Alexei Chemiakine[1], Maximilian Cabaj[1], Purvi Patel[3], Ella Doron-Mandel[4], Colton J. Treadway[5], Marko Jovanovic[4], Nicholas G. Brown[5], Rajesh K. Soni[3], and Vincenzo A. Gennarino[1,6,7,8,*]

[1]Department of Genetics and Development, Columbia University Irving Medical Center, New York, NY.
[2]Department of Translational Medical Science, University of Campania Luigi Vanvitelli, Caserta, Italy.
[3]Proteomics and Macromolecular Crystallography Shared Resource, Herbert Irving Comprehensive Cancer Center, Columbia University Irving Medical Center, New York, NY, USA.
[4]Department of Biological Sciences, Columbia University, New York, NY, USA.
[5]Department of Pharmacology and Lineberger Comprehensive Cancer Center, University of North Carolina School of Medicine, Chapel Hill, NC, USA.
[6]Departments of Pediatrics and Neurology, Columbia University Irving Medical Center, New York, NY.
[7]Columbia Stem Cell Initiative, Columbia University Irving Medical Center, New York, NY.
[8]Initiative for Columbia Ataxia and Tremor, Columbia University Irving Medical Center, New York, NY.
[*]Corresponding author: Tel: +1 212-305-7863; Email: vag2138@cumc.columbia.edu

Abstract

Mutations in the RNA-binding protein (RBP) Pumilio1 (PUM1) can cause dramatically different phenotypes. We previously noted that phenotypic severity tracked with protein dosage: a mild mutation that reduces PUM1 levels by 25% causes late-onset ataxia, whereas PUM1 haploinsufficiency causes developmental delay and seizures. Why this difference in expression should cause such different phenotypes has been unclear: PUM1 targets are de-repressed to equal degrees in both cases, and the more severe mutation does not hinder PUM1's RNA-binding ability. We therefore developed a PUM1 interactome in the murine brain. We find that mild PUM1 loss de-represses PUM1-specific targets, but PUM1 haploinsufficiency disrupts several interactors and regulation of their targets. We validated these phenomena in patient-derived cell lines and show that normalizing PUM1 levels restores interactors and their targets to proper levels. We therefore propose that dosage sensitivity does not necessarily reflect a linear change in protein abundance but can involve distinct mechanisms. Studying the interactors of RBPs *in vivo* will be necessary to understand their functions in neurological diseases.

Keywords: Pumilio/PADDAS/PRCA/protein interactome/RNA neurobiology

Introduction

RNA-binding proteins (RBPs) modify the proteome at the post-transcriptional level, regulating RNA localization, transport, translation, splicing, and decay; they have been found to orchestrate hundreds of pathways that are responsible for proper biological functions (Hentze *et al*, 2018; Keene, 2007b). As our understanding of RBPs has grown over the past decade, it has become clear that their functions are particularly important in neurons, whose synaptic plasticity demands rapid local responses to stimuli (Mauger *et al*, 2016). Several complex neurological disorders—e.g., Fragile X syndrome, Fragile X-associated tremor and ataxia syndrome, and amyotrophic lateral sclerosis—are known to involve disruptions in the function of RBPs, which has understandably led to considerable interest in mapping their neuronal targets (Darnell & Richter, 2012; Khalil *et al*, 2018; Ravanidis *et al*, 2018).

Our work on Pumilio1 (PUM1), however, has revealed that the targets may not provide a full picture of the RBP's functioning. After discovering that PUM1 is important for mouse neurobiology (Gennarino *et al*, 2015), we searched human databases for individuals with mutations in *PUM1*. We initially found 13 individuals with deletions or missense mutations, and their phenotypes tracked with protein dosage. A mild mutation (T1035S) that reduces PUM1 levels by 25% causes a slowly progressive, pure ataxia with onset in mid-life, which we called PUM1-related cerebellar ataxia or PRCA. Deletions or the most severe missense mutation (R1147W) reduce PUM1 levels by ~50% and cause a neurodevelopmental syndrome we called PUM1-associated developmental delay and seizures, or PADDAS (Gennarino *et al*, 2018). Both the infantile and adult-onset phenotypes are now considered to be forms of spinocerebellar ataxia type 47 (SCA47). T1035S lies within a highly conserved RNA-binding domain and impairs RNA binding, so it was not surprising to find known PUM1 targets upregulated in patient cells. The puzzle came with R1147W, which lies outside this domain and does not impair target regulation, yet deregulates the same targets to the same degree as T1035S (Gennarino *et al.*, 2018). Moreover, the R1147W phenotype is quite severe, closer to that of the null mice than the heterozygous mice. Given that RBPs can interact with, influence, or compete with each other (Dassi, 2017), we hypothesized that R1147W disrupts PUM1's ability to interact with its native partners, which would then lead to de-repression of the targets of these complexes and not just the direct targets of PUM1.

Testing this hypothesis required us to identify PUM1 interactors in the mouse brain. Although a great deal is known about the PUMILIO/FBF (PUF) family of RBPs (Bohn *et al*, 2018; Friend *et al*, 2012; Goldstrohm *et al*, 2018; Kedde *et al*, 2010; Miles *et al*, 2012; Temme *et al*, 2014; Uyhazi *et al*, 2020; Van Etten *et al*, 2012; Weidmann *et al*, 2014), of which PUM1 and its homolog PUM2 are members, little is known about PUM1 function in the postnatal mammalian brain. Protein interactions in general, and those

67 of PUF (Pumilio and FBF) family members in particular, can be organism-, transcript-, and even
68 condition-specific (Marrero *et al*, 2011). We therefore took an unbiased approach by using *in vivo*
69 proteomics to identify PUM1's native partners in the mouse brain. We then studied the effect of PUM1
70 insufficiency on a subset of RBP interactors in *PUM1* heterozygous and null mice and cell lines from
71 patients bearing either the T1035S or R1147W mutation. The results support our hypothesis that two
72 different mechanisms underlie PRCA and PADDAS, underscoring the need to examine an RBP's
73 interactions as well as identify its targets.
74
75 **Results**
76 **Establishing the PUM1 interactome in the adult mouse brain**
77 We performed co-immunoprecipitation (IP) on brains from 10-week-old wild-type (WT) mice
78 followed by liquid chromatography with tandem mass spectrometry (LC-MS/MS); we used IgG as a
79 negative control (**Figure S1A**). Principal component analysis (PCA) separated IP-IgG from IP-Pum1
80 (**Figure S1B**). No residual Pum1 was detected in brain tissue by post-IP western blot (**Figure S1C**). (In
81 this paper, we will differentiate between human and mouse proteins by using all-caps only for the
82 former.) Considering only those candidates that had at least two unique peptides in at least five out of six
83 IP-Pum1 samples, this approach identified 234 putative interactors (**Figure S1C** and **Table S1**) that we
84 clustered into 10 functional groups using protein-protein interaction data from CORUM and the Human
85 Protein Atlas (Raudvere *et al*, 2019) (**Figure 1**).
86 Our list included several proteins that had been previously found to interact with Pum1, as well as
87 new members of protein complexes or families that interact with Pum1 in other contexts. For example,
88 our LC-MS/MS identified Fmrp (cluster 7), which associates with Pum1 in neural progenitor cells (Zhang
89 *et al*, 2017). We also identified Cnot1, the central scaffold of the CCR4-NOT complex (Enwerem *et al*,
90 2021; Van Etten *et al.*, 2012), which is recruited by Pum1 to shorten poly(A) tails and promote mRNA
91 degradation (Temme *et al.*, 2014; Van Etten *et al.*, 2012; Weidmann *et al.*, 2014). Translation initiation
92 factors (cluster 6) cooperate with PUF proteins in invertebrates (Blewett & Goldstrohm, 2012).
93 *Drosophila* studies showed that Pumilio partners with different proteins in different neuronal types
94 (Muraro *et al*, 2008), so we repeated the LC-MS/MS experiments in three brain regions that express
95 abundant Pum1: the cerebellum, hippocampus, and cortex (Gennarino *et al.*, 2015). PCA readily
96 separated Pum1 and IgG samples (**Figure S2A**). This analysis identified 854 putative Pum1 interactors in
97 the cerebellum, 423 in the hippocampus, and 598 in the cortex (**Figure 2A**, **Figure S2B-D** and **Table S1**).
98 489 were unique to the cerebellum, 145 to the hippocampus, 247 to the cortex, and 48 unique to the rest
99 of the brain (i.e., excluding these three regions). Only 82 candidates appeared in all three brain regions

100 and the whole brain (**Figure 2A**, *yellow dots*).

101 To determine whether these results merely reflect regional differences in protein abundance, we
102 performed quantitative proteomics in 10-week-old whole brain, cerebellum, cortex, and hippocampus.
103 Pum1 interactors in general were not the most abundant proteins in these samples (**Figure S3A, B**). For
104 example, Pum2, which turned up in only 3 out of 6 of the whole-brain samples, was one of the strongest
105 Pum1 interactors in the cortex (**Figure 2A, S3C,** and **Table S1**). It is expressed at low levels in all brain
106 regions examined (**Figure S3D**). These findings suggest that the candidate interactors represent biological
107 information rather than post-lysis effects or high abundance.

108 Components of the APC/C and mTOR pathways were consistent across the three brain regions
109 (**Figure 2A, B**, and **Table S1**), but the list of Pum1 interactors in several other pathways was expanded by
110 this regional analysis (**Figure 2**). For example, although Cnot1 turned up in all three brain regions
111 (**Figure S3C**), Cnot2 appeared only in cortex and cerebellum, and Cnot10 only in the cortex (**Figure 2A**).
112 There were many putative interactors involved in translation initiation, with Eif3b showing up in both the
113 hippocampus and the whole brain (**Figure 2A**). The splicing factors showed regional specificity in
114 interactions: Rbfox1 was restricted to the cortex, while Rbfox2 and Rbfox3 were in the cerebellum,
115 hippocampus, and whole brain (**Figure 2A**). This is consistent with previous work showing that Rbfox1
116 mediates cell-type-specific splicing in cortical interneurons (Wamsley *et al*, 2018) and that Rbfox2 is
117 needed for cerebellar development (Gehman *et al*, 2012).

118 DAVID Gene Ontology analysis revealed that the main functional categories across the three regions
119 were ubiquitin ligases (anaphase-promoting complex [APC/C], E2/E3 and Kll-linked ubiquitin) and RBPs
120 involved in various aspects of RNA metabolism (RNA silencing, 3'UTR binding, mRNA stability,
121 transport, and splicing) (**Figure 2B** and **Table S2**). To test some of these interactions biochemically, we
122 tried to purify recombinant proteins, but many of the proteins or their complexes are either quite large
123 (>100kD) or strongly tended to aggregate. We were able pull down PUM1 by recombinant GST-tagged
124 FMRP (**Figure S4A**) and GST-tagged PUM2 (**Figure S4B**), confirming their direct interactions (**Figure**
125 **S4**). We also used IP and co-IP to spot-check key candidates from the anaphase promoting complex or
126 cyclosome (APC/C, cluster 1: Anapc1, Fzr1) and mTOR (cluster 10: Rptor, Cad) pathways (**Figure S3C,**
127 **S4C**, and **D**).

128 Realizing we would need to select certain proteins for further *in vivo* study, we decided to prioritize
129 the RBPs in cluster 7 (**Figure 1**): Fmrp and Ago2 (involved in RNA silencing), Cnot1 (mRNA
130 deadenylase protein), Rbfox3 (alternative splicing factor), and Pum2. We reasoned as follows. First, RBP-
131 RBP interactions are biologically important, and RNA-related categories were prominent in the gene
132 ontology analyses for both whole brain and all three brain regions. Second, this cluster was also the most

133 highly interconnected with other clusters and likely to influence their activities. Third, these RBPs have
134 been well studied, which would enable us to more readily test the consequences of PUM1 loss.
135 Nevertheless, these proteins have been studied mostly *in vitro* and, with the exception of Fmrp and Pum2,
136 have not been previously associated with Pum1 in the murine brain, so they might shed more light on
137 Pum1 biology.
138
139 **Pum1 associates with Fmrp, Ago2, Cnot1, and Pum2 in the absence of mRNA**
140 We confirmed Pum1 associations with Pum2, Fmrp, Ago2, Rbfox3, and Cnot1 by co-IP followed by
141 western blot (**Figure 3A**, *left panel*). We also tested for murine Mov10, which binds both Fmrp and Ago2
142 *in vitro* (Kenny *et al*, 2020; Kenny *et al*, 2014), and found it pulled down with Pum1, likely in concert
143 with Fmrp (**Figure 3A**). We co-IP'd Pum1 and blotted for all six RBPs in *Pum1*$^{-/-}$ mouse brains; none
144 were detected (**Figure S5A**). We then tested other proteins associated with the RNA silencing machinery
145 that did not appear in our LC-MS/MS data, such as Ago1 and Ago3, and we found no interactions
146 (**Figure S5B**).
147 To exclude the possibility that the co-IP experiments were recovering proteins that co-bound target
148 RNAs but are not part of the same complex as the protein of interest, we treated mouse brain samples
149 with RNase and verified that no detectable RNA remained (see Materials and Methods). Pum1 still
150 associated with Pum2, Fmrp, Ago2, and Cnot1 in the absence of mRNA, but not with Rbfox3 or Mov10
151 (**Figure 3A**, *right panel*, and **S5C**). We repeated the RNase experiments in HEK293T cells, which
152 confirmed our results (except for Rbfox3, which was not detectable in these cells) (**Figure 3B**). These
153 data suggest that Pum1 interacts with Pum2, Fmrp, Ago2, and Cnot1 prior to binding RNA.
154
155 **Pum1 loss alters RBP interactors and miRNA machinery in mouse cerebella by sex**
156 If Pum1 is an important interactor for these six RBPs, loss of Pum1 should affect their stability or
157 abundance in mouse brain. *Pum1* heterozygous and null mice showed changes in the quantities of Pum2,
158 Ago2, and Mov10 proteins across the brain (**Figure S6A**), but only *Pum2* showed changes in mRNA
159 levels **(Figure S6B**). Ago2 and Mov10 levels fell only in male mice (**Figure S6A**), which led us to
160 quantify Pum2, Fmrp, Ago2, Rbfox3, Cnot1 and Mov10 mRNA and protein in the cerebellum, cortex,
161 and hippocampus of male and female mice.
162 As previously reported, Fmrp protein expression was upregulated in all three brain regions in male
163 null mice, but in female null cerebella Fmrp was almost 70% lower (**Figure 4A**) (Singh *et al*, 2007; Singh
164 & Prasad, 2008). Pum2 protein levels rose in all three brain regions, as did its mRNA (**Figure 4A-C**, and
165 **Figure S7**). Ago2, Rbfox3, and Cnot1 also showed divergent responses to Pum1 loss according to sex

166 and brain region (**Figure 4A-C**). None of these proteins showed any changes in mRNA levels (**Figure**
167 **S7**), despite the fact that *Fmr1* and *Cnot1*, like *Pum2*, have a Pumilio Response Element (PRE) (Zamore
168 *et al*, 1997) in their 3'UTR.

169 Because Pum1 loss has deleterious effects on the cerebellum in both mice (Gennarino *et al.*, 2015)
170 and humans (Gennarino *et al.*, 2018), and Pum1 interacts closely with the miRNA machinery (Kedde *et*
171 *al.*, 2010), we decided to investigate the physiological relevance of these sex-specific observations by
172 examining the effects of divergent Ago2 protein levels on cerebellar miRNAs in male and female mice.
173 Our miRNA-seq identified 701 expressed miRNAs, many of which diverged in expression between the
174 two sexes (**Figure S8A, B**). Heatmap clustering of significant miRNA expression in *Pum1*$^{-/-}$ and WT
175 male and female cerebella at 10 weeks of age revealed that the expression of 166 miRNAs diverged
176 between the two sexes in parallel with Ago2 expression (**Table S3, Figure 4D**).

177 To study the expression of downstream targets that are co-bound by those miRNAs in 10-week-old
178 WT and *Pum1*$^{-/-}$ male and female cerebella, we selected the 49 miRNAs that showed >25% change in
179 expression in either direction. Using TargetScan and CoMeTa (Agarwal *et al*, 2015; Gennarino *et al*,
180 2012) we identified 6832 putative targets that are co-bound by at least two miRNA . To reduce this list to
181 manageable size, we prioritized targets that are co-bound by at least eight miRNAs, for a total of,
182 coincidentally, 49 putative targets. *Pum1*$^{-/-}$ male and female cerebella showed gene expression changes
183 for 44 out of these 49 targets that correlated with the sex differences in Ago2 levels (**Figure 4E**, **Figure**
184 **S9** and **Table S4**).

185 To elucidate the biological pathways in which these miRNAs play an essential role, we performed
186 David Gene Ontology (GO) with all the non-redundant targets predicted by CoMeTa (Gennarino *et al.*,
187 2012) and TargetScan 7.1 (Agarwal *et al.*, 2015) that are co-bound by at least four miRNAs (GO needs a
188 larger pool of genes than 49 but fewer than 3000), 2127 targets (**Figure S10A-C**). Among 2127 targets
189 analyzed, we found enrichment for multiple categories having to do with synaptic function under "cellular
190 components." The most enriched categories under "biological processes" were organ growth and post-
191 embryonic development. Under KEGG pathways, there was a particular enrichment in Wnt signaling,
192 dopaminergic and cholinergic pathways, cancers, and protein ubiquitination.

193 We then analyzed the same targets by SynGO (Koopmans *et al*, 2019), which uses single-cell data to
194 identify genes that are expressed in specific neurons. SynGO pinpointed 117 presynpatic targets and 124
195 postsynaptic (**Figure S10D**). Among the 166 miRNAs inversely expressed between sexes were the entire
196 miR-200 family (miR-200a, miR-220b, miR-200c, miR-141, and miR-429), which regulates targets
197 involved in neurogenesis, glioma, and neurodegenerative diseases (Fu *et al*, 2019; Trumbach & Prakash,
198 2015). These results are consonant with SCA47 cerebellar deficits and suggest an intimate relation

199 between Pum1 and Ago2 in mouse cerebellum.

200

201 **Pum1, Pum2, Fmrp, Ago2, and Rbfox3 share their top targets**

202 If the complexes Pum1 forms with these RBPs are physiologically relevant, as seen for Ago2 in
203 cerebellum, then they should co-regulate at least some of the same mRNA targets. Indeed, one corollary
204 of the "regulon theory," which posits that mRNA targets in the same pathway are co-regulated
205 (Blackinton & Keene, 2014; Keene, 2007a, b; Keene & Lager, 2005), is that there should be a discernible
206 set of RBPs that do the co-regulating.

207 To test this hypothesis, we analyzed all the available high-throughput sequencing UV-crosslinking
208 and immunoprecipitation (HITS-CLIP) data available for the murine brain. These data exist for Fmrp
209 (Maurin *et al*, 2018), Ago2 (Chi *et al*, 2009), Rbfox3 (Weyn-Vanhentenryck *et al*, 2014), Pum1, and
210 Pum2 (Zhang *et al.*, 2017)). We then performed gene set enrichment analysis (GSEA) (Subramanian *et al*,
211 2005) using Fmrp as the basis for comparison (because it has the largest dataset). As negative controls,
212 we used HITS-CLIP data from mouse brain for the other four available RBPs that did not show up as
213 Pum1 interactors in our LC-MS/MS: Mbnl2 (Charizanis *et al*, 2012), Nova (Zhang *et al*, 2010), Apc
214 (Preitner *et al*, 2014), and Ptpb2 (Licatalosi *et al*, 2012).

215 Although the datasets are not perfectly matched (the mice were different ages in some cases; see
216 Methods), this analysis nonetheless revealed that Pum1 targets were concentrated in the top 5th percentile
217 of all Fmrp targets, with an enrichment score (ES) of 0.93 (the maximum is 1) and FDR of 0 (**Figure 5A,**
218 *blue line represents ES*). Pum2, Ago2, and Rbfox3 showed nearly identical patterns. There was no
219 significant overlap between the targets of Fmrp and those of any negative control (Nova had the highest
220 ES, but this was only 0.36 with a rank max of 45th percentile and FDR=1; **Figure 5B**). Neither Pum1 nor
221 its partner RBP targets were enriched among any of the ranked target lists of the negative controls
222 (**Figure S11A**).

223 To ascertain where highest-ranking Fmrp targets fell among the genes with the highest probability of
224 being Pum1 targets, we divided the Fmrp ranked target list into 10 equal bins according to percentile. We
225 then repeated GSEA of Pum1 HITS-CLIP data for each bin and found that 648 of the 1194 identified
226 Pum1 targets (54%) are in the top 10th percentile of Fmrp targets, with an ES of 0.8 (**Figure 5C**). This
227 was also true for Pum2, Ago2, and Rbfox3 (**Figure 5C**).

228 We then performed the same analysis but instead used the Pum1 target list as the basis for
229 comparison. We ran GSEA on each of the four Pum1 partners against the list of Pum1 target genes, and
230 each partner's targets were within the top 20% of the Pum1 list (**Figure 5D**). Specifically, Fmrp's targets
231 reside in the top 10th percentile (with an ES of 0.81), Pum2's targets within the 16th percentile (ES=0.9),

232 Ago2's targets within the 18th percentile (ES=0.76), and Rbofx3's targets within the 19th percentile
233 (ES=0.67). The four RBPs used here as negative controls have a minimum rank at the 37th percentile, and
234 the best ES was 0.26 for Apc; none of the five reached statistical significance (**Figure 5D**). These
235 analyses demonstrate that there is substantial overlap among the highest-ranked targets of Pum1, Pum2,
236 Fmrp, Ago2, and Rbfox3.
237 We also studied the targets shared by Pum1, Pum2, Ago2, and Rbfox3 to determine how they
238 distribute within Fmrp. We found an ES of 0.93 falling within the top 5th percentile (**Figure 5E**); 141 out
239 of 175 common targets were within the top 10th percentile (bin1) of Fmrp targets, with 99 within the top
240 5th (**Figure 5F**). This contrasts with the negative controls, for which the best ES was 0.41 within the top
241 40th-60th percentile (**Figure 5G**). DAVID gene ontology analysis of those 175 common targets between
242 Ago2, Pum1, Pum2, Fmrp, and Rbfox3 revealed pathways enriched in neurons and axonal projections
243 (**Figure S11B, C**). Previous studies have shown that Pum1 and Pum2 cooperate with the miRNA
244 machinery to suppress certain targets (Gennarino *et al.*, 2015; Kedde *et al.*, 2010). Among Fmrp HITS-
245 CLIP targets, there were almost 300 microRNAs. Pum1 HITS-CLIP had 60 miRNAs, only four of which
246 were not shared with Fmrp; Pum2 HITS-CLIP had no miRNAs that were not shared with either Pum1 or
247 Fmrp (**Figure S11D** and **Table S6**). The Pum1 complexes with these fellow RBPs are therefore
248 physiologically relevant.
249
250 **PUM1 interactors are destabilized in cell lines from infantile-onset but not adult-onset patients**
251 Having identified Pum1 interactors and shared targets, we were finally in a position to determine
252 whether either the mildest (T1035S) or most severe (R1147W) missense mutations in PUM1 destabilize
253 these key RBP interactors. We compared patient-derived cell lines (lymphoblasts for T1035S, fibroblasts
254 for R1147W) with their respective age-, sex-, and cell type matched healthy controls. IP (**Figure 6A, B**)
255 and post-IP (**Figure S12A, B**) against PUM1 followed by western blot show that our protocol pulled
256 down 100% of PUM1 protein from both patient-derived cell lines. We then confirmed that R1147W,
257 which lies outside the RNA-binding domain, retains RNA-binding activity, while T1035S does not
258 (**Figure S12C**).
259 Co-IP confirmed that PUM1 associates with FMRP, AGO2, CNOT1, and MOV10 in patient cell lines
260 (**Figure 6A, B**). (RBFOX3 and PUM2 were expressed at too low levels in the patient-derived cells.) The
261 mild T1035S variant had no effect on any of these proteins (**Figure 6B**), but R1147W impaired PUM1
262 association with AGO2, MOV10, and CNOT1 (**Figure 6A**).
263 In order to compare the effects of the mutants in the same cell type, we turned to HEK293T cells.
264 GST-AGO2 associated with Myc-PUM1-R1147W 72% less than it did with Myc-PUM1-WT (**Figure**

265 **S13A**), in alignment with our observations in the PADDAS cell lines (**Figure 6A, B**). CNOT1
266 interactions were diminished by ~35% (**Figure S13B**). We observed no decrease in PUM1 association
267 with FMRP (**Figure S13C**), again in accord with our findings in patient-derived cells.
268 We next asked whether the R1147W mutation might be impaired in binding to WT PUM1. Myc-
269 PUM1-R1147W pulled down 51% of total GST-PUM1-WT, but the interaction between Myc-PUM1-
270 T1035S and GST-PUM1-WT remained unchanged (**Figure S13D**). The same results were observed after
271 RNase treatment (**Figure S13E**). Moreover, the combination of lower protein levels and marked protein
272 instability explains why the R1147W human phenotype is closer to that of the *Pum1* null mice than to the
273 heterozygous mice (Gennarino *et al.*, 2018).
274 To confirm that R1147W destabilizes these PUM1 interactors, we measured these RBPs in the
275 patient-derived cell lines. The proteins that lose their association with the R1147W variant also are
276 reduced in their expression (**Figure 6C, D**). Notably, MOV10's association with R1147W was greatly
277 reduced (**Figure 6A**) even though its protein levels were unchanged (**Figure 6C, D**). AGO2 and CNOT1
278 levels were unchanged in the T1035S cell line but were ~50% lower in the R1147W cell line (**Figure 6C,**
279 **D**). The mRNA levels of *PUM1*, *AGO2*, *CNOT1*, and *MOV10* did not change (**Figure S13F**), confirming
280 that the reductions in their respective protein levels were due to the loss of interaction with PUM1-
281 R1147W. Collectively, these data suggest that the R1147W variant exerts a dominant-negative effect on
282 PUM1-RBP interactors by destabilizing them.
283
284 **Shared targets are upregulated in PADDAS but not PRCA**
285 We next tested the effects of the T1035S and R1147W mutations on both shared targets and validated
286 PUM1-specific targets (Chen *et al*, 2012; Gennarino *et al.*, 2015; Zhang *et al.*, 2017) that are not in the
287 HITS-CLIP data for the other RBPs but are expressed in both fibroblasts and lymphoblasts. PUM1-
288 specific mRNA were dysregulated to very similar extents in PRCA and PADDAS patient cells, with only
289 a few targets being upregulated by as much as 20% in the adult-onset disease (**Figure S14A**).
290 Of the 175 targets shared between PUM1, PUM2, AGO2, FMRP, and RBFOX3 (**Table S5**), 54 were
291 expressed in both R1147W fibroblasts and T1035S lymphoblastoid cells. Fifty-one of those were
292 upregulated in the former but not the latter (**Figure 7A**), by an average of two-fold (ranging from a low of
293 121% for *IDS* to 347% for *TLK1*). There was little or no change in most of these targets in T1035S cells,
294 though levels of *CALM1*, *ATP2A2*, *CREB1*, and *GNAQ* fell by ~40%, and *CALM2*, *TAOK1*, and *UBE2A*
295 by ~20% (**Figure 7A**).
296 To determine whether restoring PUM1 levels would normalize expression of these shared targets, we
297 transfected Myc-PUM1-WT in R1147W cells, using transfection with an empty vector as a negative

298 control (**Figure 7B**, **Figure S14B**). WT PUM1 rescued AGO2 and CNOT1 protein levels compared to
299 age- and sex-matched healthy controls and this reduced the levels of the top 15 upregulated shared targets
300 (**Figure 7B, C**). These data confirm that the effects of the R1147W mutation, which does not impair
301 PUM1 binding to mRNA (Gennarino *et al.*, 2018), result from loss of interactions with RBPs that repress
302 the same mRNA targets. These results also support the hypothesis that the symptoms observed in adult-
303 onset SCA47 are attributable to the dysregulation of PUM1-specific target genes, while infantile-onset
304 SCA47 involves both protein partner destabilization and dysregulation of the partner proteins' targets.
305

306 **Discussion**

307 Since our initial study describing PUM1-related phenotypes (Gennarino *et al.*, 2018), we and others
308 have identified additional SCA47 patients (Bonnemason-Carrere *et al*, 2019; Gennarino *et al.*, 2018;
309 Imaizumi *et al*, 2019; Lai *et al*, 2019). In our cohort, heterozygous deletion and the R1147W mutation
310 account for the majority of infantile-onset patients, and T1035S for the majority of adult-onset cases. The
311 question that drove the present study is: why should the additional 25% drop in PUM1 levels from PRCA
312 to PADDAS produce such different phenotypes, especially when R1147W is not impaired in binding to
313 mRNA? Our data support the hypothesis that the difference is not due to a linear increase in the de-
314 repression of mRNA targets but is rather a function of an additional mechanism coming into play: the
315 destabilization of numerous interactors and the de-repression of their downstream targets. This conclusion
316 relies on five lines of evidence. First, loss of Pum1 in heterozygous and knockout mice changes the levels
317 of associated proteins, with unexpected differences emerging between brain regions and between male
318 and female mice. The odds of consistently identifying specific proteins in different brain regions and
319 sexes as false positives, across as many mice as these experiments required, are extremely low. Second,
320 we observed diminished function of the RBP interactors in the absence of Pum1, insofar as their targets
321 are dysregulated in Pum1-KO mice; moreover, the dysregulation of miRNA showed opposite patterns in
322 male and female cerebella that correlated with the sex-specific patterns of Ago2 expression. Third, the
323 levels of these proteins were reduced 40-70% in PADDAS patient cell lines, despite unaltered mRNA
324 levels, but not in PRCA patient cells; we also found that 55 shared targets expressed in both lymphoblasts
325 and fibroblasts were derepressed in infantile-onset SCA47, but not adult-onset SCA47, cells. Fourth, our
326 *in vitro* studies showed that AGO2, CNOT1, and WT PUM1 lose their interaction with PUM1-R1147W.
327 Fifth, re-expression of PUM1 in PADDAS cell lines restored the abundance of its interactors and
328 suppression of downstream targets. These results underscore the importance of examining RBP
329 interactions *in vivo*, in specific contexts (different sex or brain regions), with and without RNase
330 treatment.

There are other dosage-sensitive proteins that produce different phenotypes depending on their expression level (Tan & Zoghbi, 2019), and our results raise the possibility that interacting complexes may be disrupted once expression falls below a certain threshold, which for PUM1 appears to be around 50%. It is worth noting that a recent study found that, below a threshold of ~70% of normal levels of FMRP, there were steep decreases in IQ for each further decrement in FMRP levels, even as small as 5-10% (Kim *et al*, 2019). The amount of loss that can be sustained for a given protein would likely depend on its usual abundance, and it is possible that for some proteins, the difference in phenotype between greater and lesser abundance reflects a linear progression from mild to severe. For example, in proteopathies such as Alzheimer's or Parkinson's disease, genetic duplications of *APP* or *SNCA* cause an earlier onset of what is recognizably the same disease (Chartier-Harlin *et al*, 2004; Rovelet-Lecrux *et al*, 2006). Similarly, a mutation in *MECP2* that reduces its protein levels by only 16% is still sufficient to cause a mild form of Rett syndrome (Takeguchi *et al*, 2020).

In contrast, there are diseases in which the phenotypes do not simply range from mild to severe versions of the same symptoms, but seem to take on a different character. In the polyglutaminopathies, the disease-causing protein bears an abnormally expanded CAG tract that tends to expand upon intergenerational transmission. Although the range of normal and pathogenic repeat tract lengths differs from one polyglutamine disease to another, larger expansions are more unstable, cause earlier onset, and affect far more tissues than smaller expansions (Orr & Zoghbi, 2007). For example, adult-onset SCA7 presents as ataxia, but infantile SCA7 affects the entire nervous system, the heart, and the kidneys, and leads to death by two years of age (Bah *et al*, 2020). Another example is Huntington's disease (HD), where the juvenile form frequently lacks the classic chorea yet produces seizures, which are not a feature of the adult-onset disease; brain morphometry is also quite different in adult- and juvenile-onset cases (Tereshchenko *et al*, 2019). In this family of diseases, therefore, the mechanism is the same (repeat expansion), but different tissues have different thresholds for the CAG repeats. Moreover, the brain regions most vulnerable to HD show dramatic levels of somatic instability that correlate better with clinical outcomes than the germline polyglutamine expansion (Genetic Modifiers of Huntington's Disease, 2015; Kacher *et al*, 2021).

In the case of PUM1-related disease, it seems that an additional mechanism comes into play for the more severe phenotypes, beyond upregulation of mRNA targets. Interestingly, FMRP, which harbors a dynamic CGG repeat, is also associated with two very different phenotypes, through two different mechanisms: very large expansions silence the gene and produce Fragile X syndrome, whereas premutations cause the adult-onset Fragile-X-associated tremor/ataxia syndrome through RNA toxicity (FXTAS) (Salcedo-Arellano *et al*, 2020). Interestingly, the clinical presentation of FXTAS differs by sex.

364 Our data suggest that the three mechanisms of repression that have been proposed for PUM1—
365 collaborating with the miRNA machinery (Friend *et al.*, 2012; Kedde *et al.*, 2010; Miles *et al.*, 2012),
366 recruiting the CCR4-NOT deadenylase complex to trigger degradation (Temme *et al.*, 2014; Van Etten *et*
367 *al.*, 2012; Weidmann *et al.*, 2014), and antagonizing poly(A)-binding proteins to repress translation
368 (Goldstrohm *et al.*, 2018)—might be coordinated in neurons, insofar as PUM1, PUM2, FMRP, AGO2,
369 MOV10, CNOT1 and RBFOX3 (and related proteins in specific brain regions) either interact or are so
370 close to each other within the ribonucleosome that the loss of Pum1 or RNA can change the composition
371 of the complexes that are identified by co-IP, in ways that are specific to brain region and sex. In this
372 context it is worth noting that a very recent study found alternative splicing is altered in hippocampal
373 slices from Fmrp-deficient mice; this observation was attributed to changes in H3K36me3 levels (Shah *et*
374 *al*, 2020), but our data suggest that FMRP has a closer relationship with the RBFOX protein family and
375 alternative splicing machinery than previously imagined. Indeed, recent work has provided tantalizing
376 glimpses of close interactions among various kinds of RNA metabolism. For example, members of the
377 RBFOX family of proteins may, depending on their interactors (and perhaps cell type, sex, age, and
378 species), be involved in microRNA processing in the nucleus and translation in the cytoplasm (Conboy,
379 2017). The FMRP/MOV10 complex appears to be involved in regulating translation through miRNA,
380 with evidence that this role may change according to cell type (Kenny *et al.*, 2020). Another study used
381 quantitative mass spectroscopy to examine how Fmrp expression levels change with age in the wild-type
382 rat dentate gyrus and found differences in the levels of myriad proteins; among the 153 proteins with the
383 most significant changes in levels were Pum1, Pum2 and Papbc1 (Smidak *et al*, 2017). The region-, sex-,
384 and age-specificity of certain interactions indicates that unraveling RBP interactomes *in vivo* will require
385 considerable finesse. But creating such interactomes should lead to a more complex yet realistic picture of
386 RBP roles in neuronal function and in neurological disease.
387

388 **Acknowledgments**

389 We thank the patients and their families for participating in our study. We thank Mingyu Cao for help
390 with statistical analyses, U.N. Wasko for starting the cloning procedure with Myc and GST tag sequences
391 *in vitro*, Wayne Miles for sharing the RIP protocol and send us the HCT116-*PUM1*$^{-/-}$ cell lines, and V. L.
392 Brandt for editing the manuscript and suggesting we examine the targets of PUM1 interactors. We also
393 thank G. Struhl, V. Ambros, T. Duchaine, G. Karsenty, H. Zoghbi, M. Jovanovic, Y. Giardina, and
394 members of the Gennarino laboratory for helpful discussions and support. This work was supported by
395 the National Institute of Neurological Disorders and Stroke (NINDS; R01NS109858 to V.A.G.); the
396 National Ataxia Foundation/Young Investigator Research Grant (V.A.G.); the National Institute of

397 General Medical Sciences (NIGMS; R35GM128855 to N.G.B.); the National Human Genome Research
398 Institute (NHGRI; R01HG012216 to M.J.); the National Institute on Aging (NIA; R01AG071869 to
399 M.J.); the National Institute of General Medicine (NIGM; R35GM128802 to M.J.); the Brain & Behavior
400 Research Foundation Young Investigator Award (V.A.G.); the Paul A. Marks Scholar Program, Columbia
401 University Vagelos College of Physicians and Surgeons (V.A.G.); the TIGER Award, Taub Institute,
402 Columbia University Irving Medical Center (V.A.G.); the Columbia Stem Cell Initiative (CSCI),
403 Columbia University Irving Medical Center (V.A.G. and N.dP.). The authors declare no competing
404 interests.
405

406 **Author contributions**

407 S.B. designed and performed molecular experiments, analyzed and interpreted the data, and drafted the
408 manuscript. N.D.P. performed the qPCR experiments, *in vitro* immunoprecipitation assays, analyzed the
409 data, and edited the manuscript. A.C. performed all the brain region dissections in mice, performed the
410 qPCR experiments and maintained the *Pum1* mutant mouse colony. M.C. performed the cloning
411 experiments. P.P and R.K.S. performed mass spectrometry and helped analyze the data. C.J.T. and N.G.B.
412 developed the recombinant proteins. M.J and E.D.M performed and analyzed the proteomics studies.
413 V.A.G. conceived the study, analyzed and interpreted the data, performed molecular experiments, and
414 wrote the manuscript.
415

416 **Declaration of interests**

417 The authors declare not competing interests
418

419 **Figure legends**

420 **Figure 1. A brain-specific Pum1 interactome.** Network of putative Pum1 interactors in 10-week-old
421 mouse brain (circles connected to Pum1 by gray lines). Interactions between interactors (purple lines)
422 were inferred by g:GOSt from Corum and the Human Protein Atlas (see Materials and Methods). The
423 proteins in each of the 10 clusters are listed to the right. We combined and homogenized whole brains
424 from two 10-week-old wild-type mice per sample (1 female and 1 male), aliquoting half of each sample
425 for IP against either Pum1 or IgG, then performed six biological replicates (six samples, 12 mice total) for
426 each LC-MS/MS experiment against IP-Pum1 and IP-IgG. All putative Pum1 interactors are listed in
427 Table S1.
428

429 **Figure 2. A brain-region specific Pum1 interactome.** (**A**) Pum1 interactome from 10-week-old mouse

430 cerebellum (n=8 mice, 4 male and 4 female), hippocampus (n=10, 5/5), cortex (n=8, 4/4) and the rest of
431 the brain (i.e., excluding those three regions) for a total of 1,500 proteins (**Table S1**). Node colors
432 represent different brain regions or the overlap between two or more brain regions as noted. All
433 experiments were performed at least in triplicate. IP against IgG was used as a negative control. (**B**)
434 Bubble plots show the top categories from gene ontology analyses of Pum1 interactors from whole brain,
435 hippocampus, cortex, and cerebellum. Only the categories with fold enrichment >1.5 and FDR<0.05 are
436 shown; not all are labeled because of space limitations. The full list of gene ontology categories is
437 available in **Table S2**.
438
439 **Figure 3. Validation of Pum1 associations with post-transcriptional RNA-binding proteins in mouse**
440 **brain and HEK293T cells.** (**A**) Representative western blot of proteins pulled down by IP against Pum1
441 compared to IgG from wild-type mice brain without (*left*) and with (*right*) RNase treatment. In this panel,
442 after IP-Pum1, we immunoblotted for Pum1 (positive control), Pum2, Fmrp, Ago2, Rbfox3, Cnot1, and
443 Mov10. (see Materials and Methods.). (**B**) Representative western blots of the same proteins validated in
444 panels **A** after IP against PUM1 with or without RNase treatment from HEK293T cell lines. In panels **A**
445 and **B**, IP against IgG was used as a negative control and Input (1% from the initial protein lysate) as a
446 loading control. The numbers on the right are the respective molecular weights expressed in kilodaltons
447 (kDa). All the experiments were repeated at least four times. All mice were sacrificed at 10 weeks of age.
448
449 **Figure 4. Pum1 interactors and the microRNA machinery show brain region- and sex-specific**
450 **responses to Pum1 loss.** Representative western blots of Pum1, Pum2, Fmrp, Ago2, Rbfox3, Cnot1, and
451 Mov10 in (**A**) cerebellum, (**B**) hippocampus, and (**C**) cortex in both male (left panel) and female (right
452 panel) WT, *Pum1*$^{+/-}$, and *Pum1*$^{-/-}$ mice. All the experiments were conducted with equal numbers of 10-
453 week-old male and female mice per genotype, for a total of at least 12 mice per genotype (data represent
454 mean ± SEM). Graphs below show quantification for each protein by brain region, sex, and genotype. All
455 data were normalized to Gapdh protein levels. Data represent mean ± SEM. P values were calculated by
456 two-tailed Student's t test. *$p < 0.05$, **$p < 0.01$, ***$p < 0.001$. P1 indicates Pum1. See Figure S8 for
457 mRNA quantification for each interactor, brain region, and sex. (**D**) Heatmap showing 166 microRNAs
458 from cerebella of *Pum1*$^{-/-}$ male and female mice that were dysregulated (fold change -3 to +3) relative to
459 wild-type cerebellum. The full list of miRNA names and fold changes are available in Table S3. See
460 Figure S9 for male and female miRNA scatter plots. (**E**) Heatmap showing mRNA quantification by
461 qPCR for 49 targets co-bound by a minimum of eight dysregulated miRNAs (>25% change) from panel
462 **D**. Statistical significance and magnitude of dysregulation are illustrated for both male and female in

463 Figure S10. The entire list of targets predicted to be co-bound by at least two miRNAs is presented in
464 Table S4.
465
466 **Figure 5. Pum1 and its RNA-binding protein interactors share many neuronal mRNA targets.** (**A**)
467 Enrichment plots generated by Gene Set Enrichment Analysis (GSEA) of Pum1, Pum2, Rbfox3, and
468 Ago2 HITS-CLIP targets plotted again Fmrp ranked HITS-CLIP data. Pum1, Pum2, Rbfox3, and Ago2
469 targets are enriched at the top 10th percentile of the Fmrp targets with FDR=0. (**B**) GSEA analysis scores
470 of HITS-CLIP data from each negative control (Apc, Nova, Ptpb2, and Mbnl2) plotted against Fmrp
471 ranked HITS-CLIP data. The negative controls have a maximum enrichment score of 0.36 for Apc
472 ranking at the top 44.7% with FDR=1. (**C**) GSEA analysis scores of Pum1, Pum2, Rbfox3, and Ago2
473 HITS-CLIP data plotted against Fmrp HITS-CLIP data divided into 10-percentile ranked bins shows the
474 shared targets are among the top percentiles of targets for each protein. (**D**) GSEA analysis scores of the
475 HITS-CLIP data for Fmrp, Pum2, Ago2, Rbfox3 and four negative controls (Apc, Nova, Ptpb2, and
476 Mbnl2) against Pum1 ranked HITS-CLIP data. The targets of Fmrp, Ago2, Pum2, and Rbfox3 are
477 enriched at the top 5th to 18th percentile of Pum1 targets. (**E**) GSEA analysis of the shared targets between
478 Pum1, Pum2, Ago2, and Rbfox3 against Fmrp showing that they are enriched in the top 5th percentile of
479 Fmrp ranked targets. (**F**) Pum1, Pum2, Ago2, and Rbfox3 shared targets plotted against Fmrp ranked
480 HITS-CLIP targets and divided into 10-percentile bins shows that all of their respective targets are
481 enriched at the top 10th percentile of the Fmrp ranked targets. (**G**) GSEA analysis scores of the targets
482 shared by Pum1, Pum2, Ago2, and Rbfox3 and the four negative controls (Apc, Nova, Ptpb2, and Mbnl2)
483 plotted against Fmrp. At best the negative controls are enriched at the top 40% with a maximum ES of
484 0.41. For all the GSEA analyses, the False Discovery Rate (FDR) was provided by GSEA: **FDR<0.05
485 and ***FDR<0.01. ES=Enrichment score (blue line). Note that lowest rank at max percentage indicates
486 stronger targets in the rank (see Materials and Methods). HITS-CLIP data, and the respective rank, were
487 obtained from the literature and were initially acquired as follows: Pum1 and Pum2 (Zhang *et al.*, 2017),
488 Fmrp (Maurin *et al.*, 2018), Ago2 (Chi *et al.*, 2009), Rbfox3 (Weyn-Vanhentenryck *et al.*, 2014), Nova
489 (Zhang *et al.*, 2010), Ptpb2 (Licatalosi *et al.*, 2012), Mbnl2 (Charizanis *et al.*, 2012), and Apc (Preitner *et*
490 *al.*, 2014) (see Materials and Methods for more details). The full list of shared targets is reported in Table
491 S5.
492
493 **Figure 6. The R1147W mutation, but not T1035S, destabilizes PUM1 interactors.** (**A-B**) IP against
494 PUM1 from Subject 1 (S1, R1147W) (**A**) and Subject 2 (S2, T1035S) (**B**) compared to their respective
495 age-, sex-, and cell type- matched healthy controls confirm the interactions between PUM1 (used here as

496 a positive control), and PUM2, FMRP, AGO2, CNOT1, and MOV10. Input (1%) was used as a loading
497 control and IP against IgG was used as a negative control. (**C**) Representative western blots (*left panels*)
498 and relative quantification (*bar graphs to the right*) of protein levels for PUM1, PUM2, FMRP, AGO2,
499 CNOT1, and MOV10 in PADDAS patient-derived and PRCA patient-derived cells compared to their
500 respective controls. Data were normalized to Gapdh protein levels. From **A** to **C,** all the experiments were
501 performed at least three times. Data represent mean ± SEM. P values were calculated by two-tailed
502 Student's t test. *$p < 0.05$, **$p < 0.01$, ***$p < 0.001$.
503
504 **Figure 7. Shared targets are upregulated only in PADDAS, not in PRCA.** (**A**) mRNA level
505 quantification of PUM1 neuronal targets in common with FMRP, PUM2, AGO2, and RBFOX3 (Figure
506 5E and Table S5) in S1 (R1147W, *blue bars*) and S2 and 3 (T1035S, *orange bars*) cell lines compared to
507 their respective healthy controls. Only genes expressed in both R1147W and T1035S cell lines are
508 represented here, for a total of 54 genes. (**B**) Representative western blots (*right panel*) and relative
509 quantifications (*left panel*) of PUM1 and its interactors (AGO2, CNOT1, FMRP, and MOV10) in
510 R1147W patient-derived cell lines after Myc-PUM1-WT expression. (**C**) mRNA quantification of the top
511 15 shared target genes from panel **A** in R1147W patient-derived cell lines after Myc-PUM1-WT
512 expression. All data were normalized to GAPDH mRNA or protein levels and experiments were
513 performed at least three times. Data represent mean ± SEM. P values were calculated by two-tailed
514 Student's t test. *$p < 0.05$, **$p < 0.01$, ***$p < 0.001$. The full list of shared targets expressed in fibroblast
515 and lymphoblast cell lines is reported in Table S5.
516
517 **Supplemental figures and legends**
518 **Figure S1. Pumilio1 antibody efficiency for IP LC-MS/MS.**
519 (**A**) Volcano plot analysis showing all the proteins pulled down by IP against IgG and Pum1 from mouse
520 brain. (**B**) Principal component analysis (PCA) of IP-Pum1 followed by LC-MS/MS in WT adult mouse
521 brains compared with IP against IgG; each dot represents one sample for a total of 12 samples processed
522 by LC-MS/MS. (**C**) Pre-IP, IP, and post-IP against Pum1 and IgG from wild-type (WT) mouse brain.
523 Even at very long exposure, the post-IP (10%) Pum1 lane has no residual band at 120 kDa even though
524 10 times more protein is loaded than Input (1%). This demonstrates the specificify of the Pum1 antibody,
525 which makes it suitable for IP LC-MS/MS. The numbers on the right show molecular weight in
526 kilodaltons (kDa).
527
528 **Figure S2. Volcano plot and PCA analyses of IP:Pum1 followed by LC-MS/MS in cerebellum,**

529 **hippocampus, and cortex. (A)** Principal component analysis (PCA) of IP-Pum1 followed by LC-MS/MS
530 in cortex, hippocampus, and cerebellum from WT mice. (**B**-**D**) Volcano plots show all the proteins pulled
531 down by IP against IgG and Pum1 from (**B**) cerebellum, (**C**) cortex, and (**D**) hippocampus at 10 weeks of
532 age. IP against IgG was used as a negative control. Each dot represents a total of 3 samples processed by
533 MS for each brain region. All putative Pum1 interactors are listed in **Table S1**.
534
535 **Figure S3. Many Pum1 interactors are specific to certain brain regions and not determined by**
536 **expression level.** (**A**) Proteomic analysis in whole brain, cerebellum, hippocampus, and cortex at 10
537 weeks of age shows that Pum1 interactors are not the most highly expressed proteins. Dotted line
538 represents the mean expression of Pum1 interactors from each brain region. Proteomics was performed in
539 duplicate (one male and one female) for each brain region. (**B**) Absolute expression value of the validated
540 Pum1 interactors. Pum2 is expressed a low levels in all three brain regions but was still the strongest
541 Pum1 interactor in the cortex, suggesting a specific interaction. (**C**) Immunoblot for Pum1 (positive
542 control), Anapc1, Cnot1 and Pum2. (**D**) Western blot analysis at 10 weeks of age to evaluate Pum2
543 expression levels in eight different brain regions as well as whole brain. Pum2 is highly expressed in
544 olfactory bulbs and amygdala, and expressed at similar levels in hippocampus, cerebellum, and cortex.
545 All experiments performed in triplicate. Cerebellar and cortical tissues: n=8 wild-type mice (4 male and 4
546 female), for a total of 24 mice. Hippocampus: n=10 wild-type mice (5 female and 5 male), for a total of
547 30 mice. All mice were 10 weeks of age. IP against IgG was used as a negative control. Molecular protein
548 weights are expressed in kilodaltons (kDa). HP: hippocampus; CB: cerebellum; CX: cortex; MB:
549 midbrain; OB: olfactory bulbs; AM: amygdala; SN: substantia nigra pars compacta; BS: brain stem; WB:
550 whole brain. All the experiments were repeated at least three times.
551
552 **Figure S4. Fmrp and Pum2 IP recombinant proteins and validation of APC/C and mTOR proteins.**
553 (**A-B**) Representative western blot of PUM1 pulled down by recombinant (**A**) GST-FMRP or (**B**) GST-
554 PUM2. (**C**) Representative western blot of Rptor, Cad, Anapc1 and Fzr1 proteins pulled down by IP
555 against Pum1 (used here as positive control) from WT mice. (**D**) Representative western blot of the
556 reciprocal co-IPs against Anapc1, Fzr1, Rptor, and Cad. Each co-IP was immunoblotted against Pum1
557 and the pulled down protein used here as a reference protein to confirm the respective protein-protein
558 interaction. For **C** and **D**, IP against IgG was used as a negative control, and Input (1% from the initial
559 protein lysate) as a loading control. Molecular weights are expressed in kilodaltons (kDa) to the right. All
560 the experiments were repeated at least four times. All mice were sacrificed at 10 weeks of age with an
561 equal number or male and female.

562

563 **Figure S5. IP and co-IP against Pum1 and the interactors from whole brain in *Pum1*$^{-/-}$ and WT**
564 **mice, with and without RNase.** (**A**) IP against Pum1 in *Pum1*$^{-/-}$ mouse demonstrates the complete
565 absence of Pum1 and thus the specificity of the anti-Pum1 antibody. IP against IgG was used as a
566 negative control, and Input (1% from the initial protein lysate) as a loading control. (**B**) IP against Pum1
567 (with or without RNase treatment) shows no interaction with Ago1 or Ago3 in the mouse brain. (**C**)
568 Representative western blots of Pum1 pulled down by Pum2, Fmrp, Ago2, Cnot1 from WT and *Pum1*$^{-/-}$
569 mouse brains, with and without RNase. Molecular weights at the right are in kilodaltons (kDa).
570 All the experiments were conducted with one female and one male mouse brain at 10 weeks of age, in
571 triplicate, for a total of 6 mice. IP against IgG was used as a negative control, and Input (1% from the
572 initial protein lysate) as a loading control.
573

574 **Figure S6. Protein and mRNA quantification from WT, *Pum1*$^{+/-}$ and *Pum1*$^{-/-}$ mouse brains.** (**A**)
575 Representative western blot with relative quantifications of Pum1, Pum2, Fmrp, Ago2, Rbfox3, Cnot1,
576 and Mov10 from whole brains of WT, *Pum1*$^{+/-}$ and *Pum1*$^{-/-}$ mice. All data were normalized to Gapdh
577 protein levels. The numbers on the right are the respective molecular weights expressed in kilodaltons
578 (kDa). (**B**) mRNA level quantification by qPCR of *Pum1*, *Pum2*, *Fmrp*, *Ago2*, *Rbfox3*, *Cnot1*, and *Mov10*
579 from whole brains of WT, *Pum1*$^{+/-}$ and *Pum1*$^{-/-}$ mice. Again, all data were normalized to *Gapdh* mRNA
580 levels. All the experiments were conducted with equal number of male (at least 6 per genotype) and
581 female (at least 6 per genotype) mice at 10 weeks of age, for a total of at least 12 mice per genotype (data
582 represent mean ± SEM). The p values were calculated by the Student's t test. *$p < 0.05$, **$p < 0.01$, ***p
583 < 0.001.
584

585 **Figure S7. mRNA quantification of Pum1 interactors by brain region and sex in WT, *Pum1*$^{+/-}$ and**
586 ***Pum1*$^{-/-}$ mice.** mRNA levels in cerebellum, hippocampus, and cortex in male and female for all the
587 validated Pum1 interactors. The same number of mice were used here as in **Figure 4A-C** for a total of at
588 least 12 mice per genotype and sex at 10 weeks of age. All data were normalized to *Gapdh* mRNA levels.
589 All the experiments were performed at least six times (data represent mean ± SEM). The p values were
590 calculated by the Student's t test. *$p < 0.05$, **$p < 0.01$, ***$p < 0.001$.
591

592 **Figure S8. Volcano plots representing all the miRNAs sequenced by miRNAseq in male and female.**
593 **(A)** Principal component analysis (PCA) of miRNAseq in wild-type and *Pum1*$^{-/-}$ male and female mice
594 cerebella at 10 weeks of age. (**B**) Volcano plots show the expression profile for all the miRNAs in male

595 and female *Pum1*$^{-/-}$ mice compared to WT at 10 weeks of age. The orange dots represent the miRNAs
596 upregulated in female and downregulated in males; the blue dots represent the miRNAs downregulated in
597 female and upregulated in males (see Material and Methods).
598
599 **Figure S9. mRNA quantification of the 49 targets co-bound by at least eight dysregulated miRNAs**
600 **in mouse cerebellum.** qPCR in cerebellum of male (*left*, red) and female (*right*, blue) mice at 10 weeks
601 of age for the 49 targets co-bound by at least eight dysregulated miRNAs (with minimum 25% change in
602 expression) from **Figure 4E** and **Table S4**. All the experiments were performed in triplicate for both male
603 and female (data represent mean ± SEM). The *p* values were calculated by two-tailed Student's t test. **p*
604 < 0.05, ***p* < 0.01, ****p* < 0.001.
605
606 **Figure S10. Gene ontology analysis for all targets predicted by CoMeTa and TargetScan that are**
607 **co-bound by at least four miRNAs.** (**A**-**C**) David Gene Ontology representing the enriched (**A**)
608 biological processes, (**B**) cellular components, and (**C**) KEGG pathways for all the targets co-bound by at
609 least four miRNAs. For this analysis we set FDR<0.01 and a fold-enrichment >2. (**D**) Synaptic Gene
610 Ontology (SynGO) predicts that 117 targets are presynaptic and 124 are postsynaptic with a log10Q
611 value≥5.
612
613 **Figure S11. GSEA and Gene Ontology data pertaining to Figure 5.** (**A**) Gene Set Enrichment
614 Analysis (GSEA) of Pum1 HITS-CLIP data plotted against HITS-CLIP data from the negative controls
615 (RBPs that did not show up in the Pum1 interactome: Ptpb2, Nova, Apc, and Mbnl2) reveals no
616 significant enrichment. (**B**-**C**) Gene ontology analysis of the HITS-CLIP targets shared between Pum1,
617 Pum2, Fmrp, Ago2, and Rbfox3 reveals enrichment for certain (**B**) biological functions and (**C**) cellular
618 localization. Only categories with FDR<0.05 and fold enrichment > 5 were plotted in **B** and **C**. (**D**) Venn
619 diagram of miRNAs identified by Pum1 and Pum2 shows almost 100% overlap with the miRNAs pulled
620 down by Fmrp HITS-CLIP. For full list of shared miRNAs see **Table S6**. For all GSEA analyses the
621 False Discovery Rate (FDR) was provided by GSEA, ***FDR < 0.01. ES=Enrichment score (blue line).
622
623 **Figure S12. PUM1 R1147W retains RNA-binding activity.** (**A**-**B**) Pre-IP, IP, and post-IP against
624 PUM1 and IgG from (**A**) R1147W (infantile-onset SCA7, or PADDAS) fibroblasts and
625 (**B**) T1035S (adult-onset SCA47 or PRCA) lymphoblastoid cells. In both cell lines we were able to pull
626 down 100% of PUM1. Pre-IP represents 1% from the initial protein lysate as a loading control, while
627 10% of the protein lysate was loaded as post-IP. Molecular weights provided at right in kilodaltons (kDa).

628 **(C)** RNA-immunoprecipitation assay followed by qRT-PCR to show that T1035S is impaired in RNA-
629 binding while R1147W is not. We used *E2F3* and *CDK1* as validated PUM1 targets and E2F4 as a
630 negative control. We transfected WT and PUM1-KO HCT116 cells with 250ng of either Myc-PUM1-
631 WT, Myc-PUM1-R1147W, or Myc-PUM1-T105S. RIP was performed in triplicate.
632
633 **Figure S13. PUM1 validation experiments in patient-derived cells.** (**A**-**D**) Representative western
634 blots and relative IP quantification (*bar graphs*) of IP against Myc-PUM1-WT, Myc-PUM1-T1035S
635 (PRCA), or Myc-PUM1-R1147W (PADDAS) followed by immunoblotting for: (**A**) GST-AGO2, (**B**)
636 GST-CNOT1, (**C**) GST-FMRP, and (**D**) GST-PUM1-WT. Myc- and GST-tagged proteins were co-
637 transfected in HEK293T cells in equal quantities (250ng each). The molecular weights were expressed in
638 kilodaltons (kDa). The amount of protein pulled down compared to IP-PUM1 was quantified as
639 $[IP^{X}/(Input^{X}/GAPDH^{X})]/ [IP^{PUM1}/(Input^{PUM1}/ GAPDH^{PUM1})]$, where X is the protein of interest. (**E**)
640 Representative western blots of IP with RNase treatment against Myc-PUM1-WT, Myc-PUM1-T1035S
641 (PRCA), and Myc-PUM1-R1147W (PADDAS) followed by immunoblotting to test binding between
642 PUM1 proteins without the RNA. The numbers on the right are the respective molecular weights
643 expressed in kilodaltons (kDa). All the IPs were repeated at least three times. (**F**) mRNA quantification
644 for all of the immunoblotted proteins in **Figure 6C** in PADDAS and PRCA patient-derived cell lines
645 compared to their respective age-, sex-, and cell-type-matched controls. In all the experiments data
646 represent mean ± SEM. P values were calculated by two-tailed Student's t test. $*p < 0.05$, $**p < 0.01$,
647 $***p < 0.001$.
648
649 **Figure S14. mRNA quantification of PUM1-specific targets.** (**A**) qPCR analysis of validated PUM1-
650 specific targets from PADDAS (R1147W) patient-derived fibroblasts (blue bars) compared to three age-
651 and sex-matched fibroblast control cell lines, and PRCA (T1035S) patient-derived lymphoblastoid cell
652 lines (orange bars) compared to three age- and sex-matched lymphoblastoid control cell lines. Only genes
653 expressed in both fibroblasts and lymphoblasts are represented here, for a total of 10 genes. (**B**) mRNA
654 quantification of PUM1 from PADDAS patient-derived fibroblasts transfected with empty and Myc-
655 PUM1-WT vectors, compared to three age- and sex-matched fibroblast control cell lines. All data were
656 normalized to *GAPDH* mRNA levels and experiments performed at least three times. Data represent
657 mean ± SEM. P values were calculated by two-tailed Student's t test. $*p < 0.05$, $**p < 0.01$, $***p <$
658 0.001.
659
660 **Materials and Methods**

661

662 **Immunoprecipitation (IP) experiments using mouse brain tissue.** Mouse brain tissues were gathered
663 from an equal number of 10-week-old male and female mice. For whole brain experiments, we combined
664 and homogenized two 10-week-old wild-type mouse brains per sample (1 female and 1 male), aliquoting
665 half of each sample for IP against either Pum1 or IgG, then performed six biological replicates (12 mice
666 total) for each LC-MS/MS experiment against IP-Pum1 and IP-IgG. For experiments on the
667 hippocampus, cerebellum, and cortex, we needed much larger numbers of mice: we combined cerebellar
668 and cortical tissues from eight wild-type mice (4 male and 4 female) and performed the experiment in
669 triplicate (total of 24 mice), while for hippocampus we combined tissues from ten wild-type mice (5
670 female and 5 male) for three experiments (a total of 30 mice).

671 Samples were processed with a dounce homogenizer using a lysis buffer consisting of 200mM $NaCl_2$,
672 100mM $NaPO_4$, 20mM Hepes pH 7.4, 1% Triton X (which should disrupt all but the strongest protein-
673 protein interactions) and complemented by 1X of Xpert Protease and 1X of Phosphatase Inhibitor
674 Cocktail Solutions (GenDepot, #P3100-100, #P3200-020). Following homogenization, the samples were
675 placed on ice for 15 minutes then centrifuged at 14,800 rpm at 4°C for 25 minutes to remove the debris
676 from the supernatant. The supernatant was then moved to 1.5 ml tubes (Beckman microfuge tube
677 #357448) and spun down in a Beckman ultra-centrifuge (Optima Max XP) at 4°C for 25 minutes at
678 44,000 rpm. 10% of the protein lysate was stored as input and only 1% was loaded for western blot. The
679 protein extract was later divided into two aliquots, one for IP against the protein of interest (antibodies
680 listed below) and the other for IP against IgG, and was then incubated with 30 µL of Dynabeads™ Protein
681 G (Invitrogen, #10004D) and 5 µg of antibody overnight at 4°C on a rotisserie tube rotator. The next day,
682 the beads were washed four times with the same lysis buffer used for IP and resuspended in 40µL of
683 elution buffer (consisting of lysis buffer, NuPAGE 10X Reducing Agent [Invitrogen, #NP0009],
684 NuPAGE LDS sample buffer at 1X final concentration [Invitrogen, #NP0007]) and boiled at 95°C for
685 10 minutes before the samples were loaded in the NuPAGE 4%–12% Bis-Tris Gels (Invitrogen,
686 #NP0335BOX & #NP0336BOX) for further resolution and western blot analysis.

687 For the IP with RNase treatment, the beads were resuspended in 400 µL of lysis buffer after the three
688 final washes and divided into two separate 1.5 ml tubes of 200 µL each. To establish the dose required to
689 remove all RNA, we tested different amounts of RNase I (Invitrogen, #EN0602) and found that 4 µL was
690 enough to render RNA undetectable both by denaturing gel and cDNA amplification. This sample and the
691 negative control (i.e., one without RNase treatment) were incubated at 37°C for 15 min on a rotisserie
692 tube rotator. After incubation, all the samples were washed one last time with 500 µL of lysis buffer and
693 then eluted in 20 µL of elution buffer. We used the same protocol for all the IP processed by LC-MS/MS.

694 The antibodies used for IP were: goat α-PUM1 (Bethyl Laboratories, #A300-201A), rabbit α-PUM2
695 (Bethyl Laboratories, #A300-202A), rabbit α-FMRP (Abcam Cambridge, #ab17722), rabbit α-AGO2
696 (Abcam Cambridge, #ab32381), rabbit α-NeuN (Thermo Fisher Scientific, #PA5-37407), rabbit α-
697 CNOT1 (Cell Signaling Technology, #44613), rabbit α-MOV10 (Bethyl Laboratories, #A301-571A), and
698 rabbit α-ANAPC1 (Bethyl Laboratories, #A301-653A).
699 Please note that *in vivo* IPs from brain lysates present certain challenges that are not encountered *in*
700 *vitro*. Whereas the total lysate from cells is usually 200µl-300µl, the brain lysate is made in a large
701 volume, usually 1.5 to 2.4 ml, depending on the size of the brain or brain region. This means that in a
702 normal western blot that accommodates 30-40µl total volume, including reducing buffer and loading blue,
703 we cannot load more than 1%-3% from the total brain lysate as input. Therefore, when we pull down a
704 protein of interest (Pum1) and immunoblot for the same protein compared to a standard input (loading the
705 entire IP in one gel), the resulting IP band will be much darker than the input. We then need to expose the
706 Input from the same membrane much longer to visualize it—this is common practice when working with
707 *in vivo* tissues (De Maio *et al*, 2018; Di Grazia *et al*, 2021; Jin *et al*, 2020; Lee *et al*, 2020; Lee *et al*,
708 2008; Rousseaux *et al*, 2018).

709 **Immunoprecipitation experiments from HEK293T and patient-derived cell lines.** HEK293T cells
710 and patient-derived fibroblasts or lymphoblastoid cells were lysed by pipetting up and down with a
711 1000µl tip in a lysis buffer consisting of 200mM $NaCl_2$, 100mM $NaPO_4$, 20mM Hepes pH 7.4, 1% Triton
712 X and complemented by 1X of Xpert Protease and 1X of Phosphatase Inhibitor Cocktail (GenDepot,
713 #P3100-100, #P3200-020). The rest of the protocol is the same as described above for mouse brain tissue,
714 except that we used 2.5 µg of primary antibody for IP.
715

716 **Co-Immunoprecipitation in-gel digestion for LC-MS/MS.** Immunoprecipitated samples were separated
717 on NuPAGE 4-12% gradient SDS-PAGE (Invitrogen, #NP0335BOX & #NP0336BOX) and stained with
718 SimplyBlue (Invitrogen, #LC6060). Protein gel slices were excised and *in-gel* digestion performed as
719 previously described (Shevchenko *et al*, 2006), with minor modifications. Gel slices were washed with
720 1:1 Acetonitrile and 100mM ammonium bicarbonate for 30 min then dehydrated with 100% acetonitrile
721 for 10 min until shrunk. The excess acetonitrile was then removed and the slices dried in a speed-vacuum
722 at room temperature for 10 minutes. Gel slices were reduced with 5 mM DTT for 30 min at 56ºC in an air
723 thermostat, cooled down to room temperature, and alkylated with 11 mM IAA for 30 min with no light.
724 Gel slices were then washed with 100 mM of ammonium bicarbonate and 100% acetonitrile for 10 min
725 each. Excess acetonitrile was removed and dried in a speed-vacuum for 10 min at room temperature and

726 the gel slices were re-hydrated in a solution of 25 ng/µl trypsin in 50 mM ammonium bicarbonate for 30
727 min on ice and digested overnight at 37 ºC in an air thermostat. Digested peptides were collected and
728 further extracted from gel slices in extraction buffer (1:2 ratio by volume of 5% formic acid: acetonitrile)
729 at high speed, shaking in an air thermostat. The supernatants from both extractions were combined and
730 dried in a speed-vacuum. Peptides were dissolved in 3% acetonitrile/0.1% formic acid.
731
732 **Liquid chromatography with tandem mass spectrometry (LC-MS/MS).** The Thermo Scientific
733 Orbitrap Fusion Tribrid mass spectrometer was used for peptide tandem mass spectroscopy (MS/MS).
734 Desalted peptides were injected in an EASY-Spray™ PepMap™ RSLC C18 50cm X 75cm ID column
735 (Thermo Scientific) connected to the Orbitrap Fusion™ Tribrid™. Peptide elution and separation were
736 achieved at a non-linear flow rate of 250 nl/min using a gradient of 5%-30% of buffer B (0.1% (v/v)
737 formic acid, 100% acetonitrile) for 110 minutes, maintaining the temperature of the column at 50 °C
738 during the entire experiment. Survey scans of peptide precursors are performed from 400 to 1500 *m/z* at
739 120K full width at half maximum (FWHM) resolution (at 200 *m/z*) with a 2 x 10^5 ion count target and a
740 maximum injection time of 50 ms. The instrument was set to run in top speed mode with 3-second cycles
741 for the survey and the MS/MS scans. After a survey scan, MS/MS was performed on the most abundant
742 precursors, i.e., those ions that had a charge state between 2 and 6, and an intensity of at least 5000, by
743 isolating them in the quadrupole at 1.6 Th. We used collision-induced dissociation (CID) with 35%
744 collision energy and detected the resulting fragments with the rapid scan rate in the ion trap. The
745 automatic gain control (AGC) target for MS/MS was set to 1 x 10^4 and the maximum injection time was
746 limited to 35ms. The dynamic exclusion was set to 45s with a 10ppm mass tolerance around the precursor
747 and its isotopes. Monoisotopic precursor selection was enabled.
748
749 **LC-MS/MS data analysis.** Raw mass spectrometric data were analyzed using the MaxQuant
750 environment v.1.6.1.0 (Cox & Mann, 2008) and Andromeda for database searches (Cox *et al*, 2011) at
751 default settings with a few modifications. The default was used for first search tolerance and main search
752 tolerance (20 ppm and 6 ppm, respectively). MaxQuant was set up to search with the reference mouse
753 proteome database downloaded from Uniprot (https://www.uniprot.org/proteomes/UP000000589).
754 MaxQuant searched for trypsin digestion with up to 2 missed cleavages. Peptide, site and protein false
755 discovery rates (FDR) were all set to 1% with a minimum of 1 peptide needed for identification; label-
756 free quantitation (LFQ) was performed with a minimum ratio count of 1. The following modifications
757 were used for protein quantification: oxidation of methionine (M), acetylation of the protein N-terminus,
758 and deamination for asparagine or glutamine (NQ). Results obtained from MaxQuant were further

759 analyzed using the Perseus statistical package (Tyanova *et al*, 2016) that is part of the MaxQuant
760 distribution. Protein identifications were filtered for common contaminants. Proteins were considered for
761 quantification only if they were found in at least two replicate groups. Significant alterations in protein
762 abundance were determined by ANOVA with a threshold for significance of $P < 0.05$ (permutation-based
763 FDR correction). Pum1 protein interactors were later considered if they were found in at least five out of
764 six LC-MS/MS experiments for whole brain and in at least two out of three experiments for each
765 respective brain region with a fold-change of >1.5 between LFQ-PUM1-WT and LFQ-IgG-WT (see
766 **Table S1**).
767
768 **Protein-protein interaction map.** The protein-protein interaction map for the whole brain (Figure 1) was
769 generated by Cytoscape (https://cytoscape.org/) (Otasek *et al*, 2019) and interactions or functional
770 relationships (clusters) were inferred from Corum (Giurgiu *et al*, 2019) and the Human Protein Atlas
771 (Thul *et al*, 2017) by g:GOSt, which is a package of g:Profiler (https://biit.cs.ut.ee/gprofiler/gost)
772 (Raudvere *et al.*, 2019). The brain region-specific map (**Figure 2A**) was generated by Cytoscape
773 (Shannon *et al*, 2003).
774
775 **Quantitative proteomics from mouse brain regions.**
776 *Tissue processing for LC-MS/MS measurements*
777 Frozen brain tissues were weighted and 25-50mg (dry weight) per sample were cryopulverized and lysed
778 in Urea Buffer (8M Urea, 75mM NaCl, 50mM Tris/HCl pH 8.0, 1mM EDTA) in a final 1:10 (mg/µL)
779 tissue:buffer ratio. Protein concentration was determined by BCA assay (Pierce). 40µg of total protein per
780 sample were processed further. Disulfide bonds were reduced with 5mM dithiothreitol and cysteines were
781 subsequently alkylated with 10mM iodoacetamide. Samples were diluted 1:4 with 50mM Tris/HCl (pH
782 8.0) and sequencing grade modified trypsin (Promega) was added in an enzyme-to-substrate ratio of 1:50.
783 After 16h of digestion, samples were acidified with 1% formic acid (final concentration). Tryptic peptides
784 were desalted on C18 StageTips according to (Rappsilber *et al*, 2007) and evaporated to dryness in a
785 vacuum concentrator. Dried peptides were then reconstituted in 3% ACN / 0.2% Formic acid to a final
786 concentration of 0.5 µg/µL.
787
788 *LC-MS/MS analysis on a Q-Exactive HF*
789 About 1 µg of total peptides were analyzed on a Waters M-Class UPLC using a 25cm Thermo Scientific
790 PepMap RSLC C18 2 µm 25cm column coupled to a benchtop Thermo Fisher Scientific Orbitrap Q
791 Exactive HF mass spectrometer. Peptides were separated at a flow rate of 400 nL/min with a 160 min

792 gradient, including sample loading and column equilibration times. Data was acquired in data
793 independent mode using Xcalibur software. MS1 Spectra were measured with a resolution of 120,000, an
794 AGC target of 5e6 and a mass range from 300 to 1800m/z. MS2 spectra were measured in 47 segment
795 windows per MS1, each with an isolation window width of 32 m/z (0.5 m/z overlap with the neighboring
796 window), a resolution of 30,000, an AGC target of 3e6, and a stepped collision energy of 22.5, 25, 27.5.
797 All raw data were analyzed with SpectroNaut software version 15.6.211220 (Biognosys) using a
798 directDIA method based on a UniProt mouse database (release 2014_07, Mus musculus), performed with
799 the "BGS factory settings" including the following parameters: Oxidation of methionine and protein N-
800 terminal acetylation as variable modifications; carbamidomethylation as fixed modification; Trypsin/P as
801 the digestion enzyme; For identification, we applied a maximum FDR of 1% separately on protein and
802 peptide level. "Cross run normalization" was activated. This gave intensity values for a total of 5699
803 protein groups across all samples and replicates. "PG.Quantity" (normalized across samples) values were
804 used for all subsequent analyses.
805
806 **Protein purification of recombinant proteins.** Recombinant FMRP, PUM2, and PUM1 were purified
807 from *Escherichia coli* BL21-Codon Plus (DE3)-RIL cells. Both FMRP and PUM2 were expressed with
808 an N-terminal GST tag and isolated from the cell lysate using Glutathione Sepharose 4B (GS4B) resin.
809 The proteins were further subjected to size exclusion chromatography using 20mM HEPES pH 8.0,
810 200mM NaCl, and 1mM DTT as the buffer. MBP-SNAP-PUM1-His_6 was expressed and purified similar
811 to the previously described protocol (Elguindy & Mendell, 2021). After nickel affinity chromatography,
812 MBP-SNAP-PUM1-His_6 was buffer exchanged into 20mM HEPES pH 8.0, 200mM NaCl, and 1mM
813 DTT using PD-10 desalting columns.
814
815 **GST pull-down assay.** 500mM of purified GST-PUM2 or GST-FMRP were incubated with 1μM of HIS-
816 PUM1 with 30μl of Glutathione Sepharose 4B GST-tagged protein purification resin (Cytiva, #17075601)
817 in a final volume of binding buffer (20mM HEPES pH 8.0, 200mM NaCl, 0.5% Tween-20) for 1 hour at
818 4°C on the rocker. Resins were washed 3 times in binding buffer and centrifuged at 4000g at 4°C; resins
819 were resuspended in 30μl of elution buffer—which consisted of binding buffer, NuPAGE 10X Reducing
820 Agent (Invitrogen, #NP0009), and NuPAGE LDS sample buffer at 1X final concentration (Invitrogen,
821 #NP0007)—and boiled at 95°C for 10 minutes before the samples were loaded in the NuPAGE 4%–12%
822 Bis-Tris Gels (Invitrogen, #NP0335BOX & #NP0336BOX) for further resolution and western blot
823 analysis. 500mM of purified GST-PUM2, GST-FMRP and HIS-PUM1 were used as input controls; GST-
824 PUM2 and GST-FMRP were visualized using rabbit α-GST antibody (1:1000 [Cell Signaling

825 Technologies, #2625]), whereas for HIS-PUM1 we used rabbit α-HIS Tag antibody (1:3000, [Cell
826 Signaling Technologies, #2365]).
827
828 **Protein quantification and western blot analysis.** Patient-derived lymphoblastoid, fibroblast cell lines,
829 and control cell lines were collected at 6×10^6 cell confluence and processed for protein extraction. For
830 mouse tissues, we processed either half of the whole brain (the other half was processed for RNA
831 extraction, see below) or the entire hippocampus, cortex, or cerebellum for protein extraction. Mouse
832 tissues or cell pellets were subsequently lysed with modified RIPA buffer consisting of 25 mM Tris-HCL,
833 pH 7.6, 150 mM NaCl, 1.0% Tween 20, 1.0% sodium deoxycholate, 0.1% SDS, completed with 1X Xpert
834 Protease and 1X Phosphatase Inhibitor Cocktail Solutions (GenDepot, #P3100-100 & #P3200-020). Cells
835 were lysed by pipetting them up and down with a p1000 tip and then placed on ice for 20 min followed by
836 centrifugation at 14,800 rpm at 4°C for 25 minutes. Mouse brain tissues were pipetted up and down by
837 syringe needles—starting from an 18G 1½" (Becton Dickson, #305196), moving to 21G 1½" (Becton
838 Dickson, #305167) and finally to a 26G 1½" (Becton Dickson, #305111) needle—until the lysate passed
839 through the needle smoothly. Proteins were quantified by Pierce BCA Protein Assay Kit (Thermo
840 Scientific, # PI23225) and their absorbance measured by NanoDrop OneC (Thermo Scientific). Proteins
841 were resolved by high resolution NuPAGE 4%–12% Bis-Tris Gel (Invitrogen, #NP0335BOX &
842 #NP0336BOX) according to the manufacturer's instructions. All the blots were acquired on the G:BOX
843 Chemi XX9 machine (Syngene; Frederick, MD) using GeneSys software 1.6.5.0. Gel exposures were
844 determined by the software.
845 Antibodies used for western blot experiments were: goat α-PUM1 [1:2500, (Bethyl Laboratories,
846 #A300-201A)], rabbit α-PUM1 [1:2000, (Abcam Cambridge, #ab92545)], rabbit α-PUM2 [1:2000,
847 (Bethyl Laboratories, # A300-202A)], rabbit α-FMRP [1:1000, (Abcam Cambridge, #ab17722)], rabbit
848 α-AGO2 [1:1000, (Abcam Cambridge, #ab32381)], rabbit α-NeuN (Rbfox3) [1:1000, (Thermo
849 Scientific, #PA5-37407)], rabbit α-CNOT1 [1:1000, (Cell Signaling Technology, #44613)], rabbit α-
850 MOV10 [1:2000, (Bethyl Laboratories, #A301-571A)], and mouse α-GAPDH [1:10000, (Millipore,
851 #CB1001)].
852
853 **HEK293T cell culture and maintenance**. Human embryonic kidney immortalized 293T (HEK293T)
854 cells were grown in DMEM (GenDepot, #CM002-320) supplemented with 10% of heat-inactivated fetal
855 bovine serum (FBS [GenDepot, #F0901-050) and 1% penicillin/streptomycin (GenDepot, #CA005-010).
856 All cells were incubated at 37 °C in a humidified chamber supplemented with 5% CO_2. HEK293T cells

857 were later processed according to the needs of specific experiments (described below).
858
859 **RNA extraction and quantitative real-time PCR (qPCR).** Human fibroblast, lymphoblastoid, and
860 respective control cell lines were harvested at 6 X 10^6 confluence prior to RNA extraction. For mouse
861 tissues, half of the whole brain (the other half was processed for protein extraction, see above) or the
862 entire hippocampus, cortex, or cerebellum were processed for RNA extraction. The RNA was collected
863 for both human cells, mouse brain and brain region tissues using the miRNeasy kit (QIAGEN, # 217004)
864 according to the manufacturer's instructions. RNA was quantified using NanoDrop OneC (Thermo Fisher
865 Scientific). cDNA was synthesized using Quantitect Reverse Transcription kit (QIAGEN, # 205313)
866 starting from 1 µg of RNA. Quantitative RT-polymerase chain reaction (qRT-PCR) experiments were
867 performed using the CFX96 Touch Real-Time PCR Detection System (Bio-Rad Laboratories, Hercules)
868 with PowerUP SYBR Green Master Mix (Applied Biosystems, #A25743). Real-time PCR runs were
869 analyzed using the comparative C_T method normalized against the housekeeping human gene *GAPDH* or
870 mouse *Gapdh*, depending on the experiment (Vandesompele *et al*, 2002).
871
872 **RNA Immunoprecipitation (RIP).** HCT116 wild-type and PUM1-KO were obtained from (Lee *et al*,
873 2016). HCT116-PUM1-KO cells were grown in McCoy's 5A Media (Merck, # M4892) supplemented
874 with 10% of heat-inactivated fetal bovine serum (FBS [GenDepot, #F0901-050]) and 1%
875 penicillin/streptomycin (GenDepot, #CA005-010) for 16 hours in a 10-cm plate (80% confluency) and
876 transfected with 6µg of Myc-PUM1-WT, Myc-PUM1-R1147W, and Myc-PUM1-T1035S. After 48 hours
877 cells were collected and lysed in Polysome Lysis Buffer (PLB) (10mM HEPES-KOH pH 7, 100mM KCl,
878 5mM $MgCl_2$, 25 mM EDTA, 0.5% NP40, 2mM Dithiothreitol, 0.2 mg/ml Heparin) supplemented with
879 50U/ml of RNAse OUT™ recombinant ribonuclease inhibitor (Thermo Fischer Scientific, # 10777019),
880 50U/ml of SuperaseIN™ RNAse inhibitor (Thermo Fischer Scientific, #AM2694) and 1X of Xpert
881 Protease Inhibitor Cocktail Solutions (GenDepot, #P3100-100) for 20 minutes in ice; cells were
882 centrifuged at maximum speed at 4°C to remove cellular debris. 5µg of goat α-PUM1 (Bethyl
883 Laboratories, #A300-201A) or α-Goat-IgG with 50µl of Dynabeads™ Protein G (Invitrogen, #10004D)
884 were incubated overnight at 4°C on a rotisserie tube rotator; 100µl of lysate were removed to serve as
885 input. 3mg of lysate with 10µl of Dynabeads™ Protein G (Invitrogen, #10004D) were precleared for 30
886 minutes at 4°C on a rotisserie tube rotator; the pre-cleared lysate was incubated with antibody-conjugated
887 beads overnight at 4°C on a rotisserie tube rotator. Beads were washed 3 times with NT2 buffer (50mM
888 of Tris-HCl, 300mM NaCl, 1mM EDTA, 1% NP40, 0.1% SDS, 0.5% Na-deoxycholate supplemented
889 with 1X of Xpert Protease Inhibitor Cocktail Solutions). Beads and input were resuspended in 100µl of

890 NT2 buffer supplemented with 80U of RNAse OUT and 30µg of proteinase K and incubated for 30
891 minutes at 50°C to eliminate the proteins. RNA was extracted from the immunoprecipitated samples and
892 their input; 200µl of RLT buffer was added using RNeasy Mini Kit (Qiagen, #74104) according to the
893 manufacturer's instruction. cDNA was synthetized using SuperScript^{TM} II Reverse Transcripatse (Thermo
894 Fisher Scientific, #18064014) according to the manufacturer's instructions. Quantitative RT-polymerase
895 chain reaction (qRT-PCR) experiments were performed using the CFX96 Touch Real-Time PCR
896 Detection System (Bio-Rad Laboratories, Hercules) with PowerUP SYBR Green Master Mix (Applied
897 Biosystems, #A25743). The oligos used for qPCR are listed in **Table S7**.
898
899 **MicroRNA library construction and sequencing.** Library preparation and microRNA sequencing were
900 performed by LC Sciences (Houston, TX) according to the following criteria. Total RNA was extracted
901 from cerebellum of WT and *Pum1*$^{-/-}$ male and female at 10 weeks of age using the miRNeasy kit
902 (QIAGEN, # 217004) according to the manufacturer's instructions. The total RNA quality and quantity
903 were assessed with Bioanalyzer 2100 (Agilent Technologies, Santa Clara) with RIN number > 7.0.
904 Approximately 1 µg of total RNA were used to prepare the small RNA library according to the protocol
905 of TruSeq Small RNA Sample Prep Kits (Illumina, San Diego). Then the single-end sequencing 50bp was
906 performed on an Illumina Hiseq 2500 at LC Sciences (Hangzhou, China) following the vendor's
907 recommended protocol.
908
909 Labelling scheme:

Sample	Gender	Genotype
LCS7846_GV_KO1_F	Female	KO
LCS7846_GV_KO1_M	Male	KO
LCS7846_GV_KO2_M	Male	KO
LCS7846_GV_KO3_F	Female	KO
LCS7846_GV_KO3_M	Male	KO
LCS7846_GV_KO4_F	Female	KO
LCS7846_GV_WT1_M	Male	WT
LCS7846_GV_WT2_F	Female	WT
LCS7846_GV_WT2_M	Male	WT
LCS7846_GV_WT3_F	Female	WT
LCS7846_GV_WT3_M	Male	WT

910
911 **MicroRNA sequencing bioinformatic analysis.** Raw reads were subjected to an in-house program,
912 ACGT101-miR (LC Sciences, Houston), to remove adapter dimers, junk, common RNA families (rRNA,
913 tRNA, snRNA, snoRNA), and repeats. Subsequently, unique sequences of 18–26 nucleotides in length

914 were mapped to specific species precursors in miRBase 22.0 (http://www.mirbase.org/) by BLAST search
915 to identify known miRNAs and novel 3p- and 5p-derived miRNAs. Length variation at both 3' and 5'
916 ends and one mismatch inside of the sequence were allowed in the alignment. The unique sequences
917 mapping to specific species of mature miRNAs in hairpin arms were identified as known miRNAs. The
918 unique sequences mapping to the other arm of known specific species precursor hairpins opposite the
919 annotated mature miRNA-containing arm were considered to be novel 5p- or 3p-derived miRNA
920 candidates. The remaining sequences were mapped to other selected species precursors (with the
921 exclusion of specific species) in miRBase 22.0 by BLAST search, and the mapped pre-miRNAs were
922 further BLASTed against the specific species genomes to determine their genomic locations. The last two
923 were also defined as known miRNAs. The unmapped sequences were BLASTed against the specific
924 genomes, and the hairpin RNA structures containing sequences were predicted from the flank 80 nt
925 sequences using RNAfold software (http://rna.tbi.univie.ac.at/cgi-bin/RNAWebSuite/RNAfold.cgi). The
926 criteria for secondary structure prediction were: (1) number of nucleotides in one bulge in stem (≤12), (2)
927 number of base pairs in the stem region of the predicted hairpin (≥16), (3) cutoff of free energy (kCal/mol
928 ≤-15), (4) length of hairpin (up and down stems + terminal loop ≥50), (5) length of hairpin loop (≤20), (6)
929 number of nucleotides in one bulge in mature region (≤8), (7) number of biased errors in one bulge in
930 mature region (≤4), (8) number of biased bulges in mature region (≤2), (9) number of errors in mature
931 region (≤7), (10) number of base pairs in the mature region of the predicted hairpin (≥12), (11) percent of
932 mature region in stem (≥80).
933
934 **Gene Set Enrichment Analysis (GSEA).** GSEA was performed as previously described (Subramanian *et*
935 *al.*, 2005). The cumulative distribution function was conducted by performing 1000 random gene-set
936 membership assignments. A nominal p-value < 0.01 and an FDR < 0.25 were used to assess the
937 significance of the enrichment score (ES). HITS-CLIP data, and the respective rank, were obtained from
938 the literature and were initially acquired as follows: Pum1 and Pum2 from neonatal murine brains (Zhang
939 *et al.*, 2017), Fmrp from cerebellum, cortex, and hippocampus together (Maurin *et al.*, 2018), Ago2 from
940 neocortex at embryonic day 13 (Chi *et al.*, 2009), Rbfox3 from mouse brain (age not specified) (Weyn-
941 Vanhentenryck *et al.*, 2014), Nova from mouse brain (age not specified) (Zhang *et al.*, 2010), Ptpb2 from
942 neocortex at embryonic day 18.5 (Licatalosi *et al.*, 2012), Mbnl2 from hippocampus at 8-12 weeks of age
943 (Charizanis *et al.*, 2012), and Apc from mouse brain at embryonic day 14 (Preitner *et al.*, 2014).
944
945 **Gene ontology analyses.** Gene ontology analyses were performed with David Gene Ontology (GO). For
946 **Figure 2B, Figure S11B** and **C** only categories with FDR<0.05 were considered; while for **Figure S10**

947 only categories with FDR<0.01 were considered. David GO for the Pum1 interactome in **Figure 2B**
948 considered the entire interactome as background. For the GO regarding the HITS-CLIP targets shared
949 among Pum1, Pum2, Fmrp, Ago2, and Rbfox3 (**Figure S11B** and **C**), we considered the entire set of all
950 targetomes together as background. Regarding the Synaptic (Syn) GO analysis (**Figure S10D**), brain-
951 expressed genes were used as background (Koopmans *et al.*, 2019).
952
953 **Myc and GST cloning procedure with in vitro immunoprecipitation (IP) assays.** Human *PUM1* full-
954 length cDNA was amplified by PCR and subcloned in a pRK5 plasmid containing the Myc tag sequence
955 (Addgene, pRK5-Myc-Parkin #17612) at the N-terminal by using SalI (New England Biolabs, # R3138S)
956 and NotI (New England Biolabs, #R0189S) restriction enzymes to replace *Parkin* with *PUM1*. For GST,
957 the human full-length *PUM1* cDNA was, again, subcloned first in the pRK5 plasmid containing the GST
958 tag sequence (Addgene, pRK5-HA GST RagC wt, #19304) at the N-terminal by using SalI and NotI
959 restriction enzymes to replace *RagC* with *PUM1*. Human *FMRP*, *AGO2* and *CNOT1*, full-length cDNA
960 were cloned and contain the GST tag sequence at the N-terminal, as described for GST-*PUM1*.
961 To introduce the T1035S or R1147W mutations we used the QuikChange II XL Multi Site-Directed
962 Mutagenesis kit (Agilent Technologies, #200521). The primers for the single mutagenesis experiments
963 were designed by QuikChange software (Stratagene, San Diego, https://www.genomics.agilent.com/
964 primerDesignProgram.jsp).
965 For IP, HEK293T cells were seeded in 6-well plates for 24 h and then transfected with 250 ng of
966 either WT or mutant PUM1 plasmid with one of the interactors using the jetPRIME Transfection Reagent
967 (Polyplus transfection, #55-132) as per the manufacturer's protocol. pRK5-Myc empty plasmid (no
968 cDNA) was used as a negative control. After 48 h, the cells were collected and processed for
969 immunoprecipitation. Protein lysates were incubated overnight at 4°C with mouse α-Myc antibody
970 (1:400, [Cell Signaling Technologies, #2276]) on a rotisserie tube rotator. The next day, the beads were
971 washed four times with an IP lysis buffer and resuspended in 40 µL elution buffer (lysis buffer, NuPAGE
972 10X Reducing Agent [Invitrogen, #NP0009], NuPAGE LDS sample buffer 4X [Invitrogen, #NP0007])
973 and boiled at 95°C for 10 minutes before loading the samples in NuPAGE 4%–12% Bis-Tris Gels
974 (Invitrogen, #NP0335BOX & #NP0336BOX) for further resolution and western blot analysis. Antibodies:
975 mouse α-Myc antibody [1:2000, (Cell Signaling Technologies, #2276)], rabbit α-GST antibody [1:1000,
976 (Cell Signaling Technologies, #2625)], mouse α-GAPDH [1:10000, (Millipore, #CB1001)].
977
978 **Patient-derived cell lines**. Primary fibroblasts from the *PUM1* PADDAS patient (9-year-old female) and
979 the age- and sex-matched controls (three different 9-year-old female) were generated as previously

980 described (Gennarino *et al.*, 2018). Briefly, cells were isolated from skin biopsies taken from the patient
981 or age-matched controls using standard methodology (Barch and Association of Cytogenetic Technology,
982 1991) and placed in a transport medium (Ham's F10, Thermo Scientific, #11550043). The skin specimen
983 was later removed from the transport medium using a sterile technique (in a Class II biohazard cabinet)
984 and transferred to a sterile Petri dish where it was cut into small pieces (< 0.5 mm) using sterile scalpel
985 blades. These pieces were transferred to the lower surface of a 25 cm^2 culture flask (6-8 pieces per flask)
986 which had been pre-moistened with 1-2 mL of AmnioMAX Complete Medium (Thermo Scientific,
987 #11269016) supplemented with 1% penicillin/streptomycin (GenDepot, #CA005-010). Cell cultures were
988 maintained at 37 °C in a humidified incubator supplemented with 5% CO_2. When cell growth was
989 observed around the edges of the tissue, usually 3 to 5 days later, 2 to 3 mL of AmnioMAX Complete
990 Medium were added. Once growth was established and the tissue was anchored to the flask, another 8 mL
991 of AmnioMAX Complete Medium was added. Thereafter, the medium was renewed every 3 to 4 days
992 until ready for sub-culturing.
993 Lymphoblastoid cells from *PUM1* PRCA patients (female 59 and 58 years old, respectively) and the
994 age- and sex-matched controls (three different 58-year-old female) were generated as previously
995 described (Gennarino *et al.*, 2018). Briefly, lymphoblastoid suspension cell cultures were grown in RPMI
996 1640 medium (Invitrogen, #11875093) supplemented with 10% heat-inactivated fetal bovine serum
997 (Atlanta Biological, Flowery Branch, #S11195H) and 1% penicillin/streptomycin (GenDepot, #CA005-
998 010). Cell cultures were maintained at 37°C in a humidified incubator supplemented with 5% CO_2.
999 Medium was renewed every 2 to 3 days.
1000
1001 **Fibroblast patient-derived cell lines transfection.** Fibroblasts from age- and sex-matched healthy
1002 controls and from a female PADDAS patient were seeded at 80% of confluency in 6-well plates
1003 (~150.000 cells/well). The day after, 500ng of pRK5-CMV-Myc-Pum1 or pRK5-CMV-Myc-Empty
1004 plasmids were transfected in antibiotic-free DMEM (GenDepot, #CM002-320) using Lipofectamine LTX
1005 with Plus Reagent (Thermo Fisher, #15338030) according to the manufacturer's protocol. After 5 hours
1006 we replaced the media with new complete DMEM supplemented with 10% of heat-inactivated fetal
1007 bovine serum (FBS [GenDepot, #F0901-050]) and 1% penicillin/streptomycin (GenDepot, #CA005-010).
1008 Cells were incubated at 37 °C in a humidified chamber supplemented with 5% CO2 and collected after 72
1009 hours for RNA and protein extraction.
1010
1011 **Primers.** For the qPCR analysis to unambiguously distinguish spliced cDNA from genomic DNA
1012 contamination, specific exon primers were designed to amplify across introns of the gene tested. The

1013 primers for all genes tested were designed with Primer3 (Koressaar & Remm, 2007; Untergasser *et al*,
1014 2012). Cloning primers were manually designed to amplify the longest spliced gene isoform tested; if
1015 there was more than one isoform according to the UCSC Genome Browser (https://genome.ucsc.edu/), we
1016 chose the longest. See Table S7 for primer sequences.
1017
1018 **Ethical statement and mouse strains.** All animal procedures were approved by the Institutional Animal
1019 Care and Use Committee at Columbia University, New York under the protocol AC-AAAU8490. Mice
1020 were maintained on a 12-hr light, 12-hr dark cycle with regular chow and water ad libitum. Pum1 knock-
1021 out mice were generated as previously described (Chen *et al.*, 2012). C57BL/6J wild-type mice were
1022 purchased from Jackson Laboratory and maintained as described above. For brain dissection, mice were
1023 anesthetized with isoflurane, and the brain rapidly removed from the skull and lysed in the appropriate
1024 buffer according to the experiment (see Materials and Methods Details).
1025
1026 **Experimental design.** For protein and RNA quantification from patient-derived cell lines, we used values
1027 from at least six independent experiments with three biological replicates for each experiment. At every
1028 stage of the study, the experimenter was blinded to the identity of control and patient-derived cell lines.
1029 For example, for the data regarding both human patient-derived cell lines and mice, Experimenter #1
1030 made a list of samples and controls to be tested, and Experimenter #2 randomized this list and re-labeled
1031 the tubes; Experimenter #2 was the only person with the key to identify the samples. These samples were
1032 then distributed to Experimenter #3 to culture the cells, then to Experimenter #1 to perform western blots
1033 and qRT-PCR, and lastly Experimenters #1 and #4 analyzed the data. Only then was the key applied to
1034 identify the samples.
1035 For mouse experiments, the experimenters were randomized and blinded as described above. The
1036 number of animals used and sex, and the specific statistical tests used, are indicated for each experiment
1037 in the figure legends. Sample size was based on previous experience using the same mice (Gennarino *et*
1038 *al.*, 2015).
1039
1040 **Software and statistical analysis.** Statistical significance was analyzed using GraphPad Prism 8
1041 (https://www.graphpad.com/ scientific-software/prism/) and Excel Software (Microsoft). All data are
1042 presented as mean ± SEM. Statistical details for each experiment can be found in the figures and the
1043 legends. The range of expression levels in qPCR was determined from at least six independent
1044 experiments with three biological replicates by calculating the standard deviation of the **Δ**Ct (Pfaffl,
1045 2001). The range of expression levels in western blots was determined from at least six independent

1046 experiments with at least six biological replicates. P values were calculated by Student's T-test or analysis
1047 of variance with Tukey's post hoc analysis. For the IP in **Figure 6A** and protein quantification in patient
1048 cell lines in **Figure 6C**, we had only one PADDAS patient, so the repeated experiments were technical
1049 replicates rather than biological replicates. We therefore calculated the statistical significance based on
1050 these technical replicates in comparison to the three biological replicates (i.e., healthy controls).
1051
1052 **Study approval.** PADDAS and PRCA patient cell lines are the same as those reported previously
1053 (Gennarino *et al.*, 2018). The consent form for each subject specifically allows for sharing of medical
1054 information and physical exam findings; the sharing of cell lines from the PADDAS and PRCA subjects
1055 and the controls was approved under the Columbia University Medical Center IRB-AAAS7401
1056 (Y01M00) and the Baylor College of Medicine IRB H-34578.
1057
1058 **Data availability.**
1059 IP mass spec and quantitative proteomics raw data are available at: "pending".
1060 microRNA sequencing raw data are available at "pending"
1061
1062 **References**
1063 Agarwal V, Bell GW, Nam JW, Bartel DP (2015) Predicting effective microRNA target sites in
1064 mammalian mRNAs. *Elife* 4
1065 Bah MG, Rodriguez D, Cazeneuve C, Mochel F, Devos D, Suppiej A, Roubertie A, Meunier I, Gitiaux C,
1066 Curie A *et al* (2020) Deciphering the natural history of SCA7 in children. *Eur J Neurol* 27: 2267-
1067 2276
1068 Blackinton JG, Keene JD (2014) Post-transcriptional RNA regulons affecting cell cycle and proliferation.
1069 *Semin Cell Dev Biol* 34: 44-54
1070 Blewett NH, Goldstrohm AC (2012) A eukaryotic translation initiation factor 4E-binding protein
1071 promotes mRNA decapping and is required for PUF repression. *Mol Cell Biol* 32: 4181-4194
1072 Bohn JA, Van Etten JL, Schagat TL, Bowman BM, McEachin RC, Freddolino PL, Goldstrohm AC
1073 (2018) Identification of diverse target RNAs that are functionally regulated by human Pumilio
1074 proteins. *Nucleic Acids Res* 46: 362-386
1075 Bonnemason-Carrere P, Morice-Picard F, Pennamen P, Arveiler B, Fergelot P, Goizet C, Hellegouarch
1076 M, Lacombe D, Plaisant C, Raclet V *et al* (2019) PADDAS syndrome associated with hair dysplasia
1077 caused by a de novo missense variant of PUM1. *Am J Med Genet A* 179: 1030-1033
1078 Charizanis K, Lee KY, Batra R, Goodwin M, Zhang C, Yuan Y, Shiue L, Cline M, Scotti MM, Xia G *et*
1079 *al* (2012) Muscleblind-like 2-mediated alternative splicing in the developing brain and dysregulation
1080 in myotonic dystrophy. *Neuron* 75: 437-450
1081 Chartier-Harlin MC, Kachergus J, Roumier C, Mouroux V, Douay X, Lincoln S, Levecque C, Larvor L,
1082 Andrieux J, Hulihan M *et al* (2004) Alpha-synuclein locus duplication as a cause of familial
1083 Parkinson's disease. *Lancet* 364: 1167-1169

1084 Chen D, Zheng W, Lin A, Uyhazi K, Zhao H, Lin H (2012) Pumilio 1 suppresses multiple activators of
1085 p53 to safeguard spermatogenesis. *Curr Biol* 22: 420-425
1086 Chi SW, Zang JB, Mele A, Darnell RB (2009) Argonaute HITS-CLIP decodes microRNA-mRNA
1087 interaction maps. *Nature* 460: 479-486
1088 Conboy JG (2017) Developmental regulation of RNA processing by Rbfox proteins. *Wiley Interdiscip*
1089 *Rev RNA* 8
1090 Cox J, Mann M (2008) MaxQuant enables high peptide identification rates, individualized p.p.b.-range
1091 mass accuracies and proteome-wide protein quantification. *Nat Biotechnol* 26: 1367-1372
1092 Cox J, Neuhauser N, Michalski A, Scheltema RA, Olsen JV, Mann M (2011) Andromeda: a peptide
1093 search engine integrated into the MaxQuant environment. *J Proteome Res* 10: 1794-1805
1094 Darnell JC, Richter JD (2012) Cytoplasmic RNA-binding proteins and the control of complex brain
1095 function. *Cold Spring Harb Perspect Biol* 4: a012344
1096 Dassi E (2017) Handshakes and Fights: The Regulatory Interplay of RNA-Binding Proteins. *Front Mol*
1097 *Biosci* 4: 67
1098 De Maio A, Yalamanchili HK, Adamski CJ, Gennarino VA, Liu Z, Qin J, Jung SY, Richman R, Orr H,
1099 Zoghbi HY (2018) RBM17 Interacts with U2SURP and CHERP to Regulate Expression and Splicing
1100 of RNA-Processing Proteins. *Cell Rep* 25: 726-736 e727
1101 Di Grazia A, Marafini I, Pedini G, Di Fusco D, Laudisi F, Dinallo V, Rosina E, Stolfi C, Franze E, Sileri
1102 P *et al* (2021) The Fragile X Mental Retardation Protein Regulates RIPK1 and Colorectal Cancer
1103 Resistance to Necroptosis. *Cell Mol Gastroenterol Hepatol* 11: 639-658
1104 Elguindy MM, Mendell JT (2021) NORAD-induced Pumilio phase separation is required for genome
1105 stability. *Nature* 595: 303-308
1106 Enwerem, III, Elrod ND, Chang CT, Lin A, Ji P, Bohn JA, Levdansky Y, Wagner EJ, Valkov E,
1107 Goldstrohm AC (2021) Human Pumilio proteins directly bind the CCR4-NOT deadenylase complex
1108 to regulate the transcriptome. *RNA* 27: 445-464
1109 Friend K, Campbell ZT, Cooke A, Kroll-Conner P, Wickens MP, Kimble J (2012) A conserved PUF-
1110 Ago-eEF1A complex attenuates translation elongation. *Nat Struct Mol Biol* 19: 176-183
1111 Fu J, Peng L, Tao T, Chen Y, Li Z, Li J (2019) Regulatory roles of the miR-200 family in
1112 neurodegenerative diseases. *Biomed Pharmacother* 119: 109409
1113 Gehman LT, Meera P, Stoilov P, Shiue L, O'Brien JE, Meisler MH, Ares M, Jr., Otis TS, Black DL
1114 (2012) The splicing regulator Rbfox2 is required for both cerebellar development and mature motor
1115 function. *Genes Dev* 26: 445-460
1116 Genetic Modifiers of Huntington's Disease C (2015) Identification of Genetic Factors that Modify
1117 Clinical Onset of Huntington's Disease. *Cell* 162: 516-526
1118 Gennarino VA, D'Angelo G, Dharmalingam G, Fernandez S, Russolillo G, Sanges R, Mutarelli M,
1119 Belcastro V, Ballabio A, Verde P *et al* (2012) Identification of microRNA-regulated gene networks
1120 by expression analysis of target genes. *Genome Res* 22: 1163-1172
1121 Gennarino VA, Palmer EE, McDonell LM, Wang L, Adamski CJ, Koire A, See L, Chen CA, Schaaf CP,
1122 Rosenfeld JA *et al* (2018) A mild PUM1 mutation is associated with adult-onset ataxia, whereas
1123 haploinsufficiency causes developmental delay and seizures. *Cell* 172: 924-936 e911
1124 Gennarino VA, Singh RK, White JJ, De Maio A, Han K, Kim JY, Jafar-Nejad P, di Ronza A, Kang H,
1125 Sayegh LS *et al* (2015) Pumilio1 haploinsufficiency leads to SCA1-like neurodegeneration by
1126 increasing wild-type Ataxin1 levels. *Cell* 160: 1087-1098

1127 Giurgiu M, Reinhard J, Brauner B, Dunger-Kaltenbach I, Fobo G, Frishman G, Montrone C, Ruepp A
1128 (2019) CORUM: the comprehensive resource of mammalian protein complexes-2019. *Nucleic Acids*
1129 *Res* 47: D559-D563
1130 Goldstrohm AC, Hall TMT, McKenney KM (2018) Post-transcriptional Regulatory Functions of
1131 Mammalian Pumilio Proteins. *Trends Genet* 34: 972-990
1132 Hentze MW, Castello A, Schwarzl T, Preiss T (2018) A brave new world of RNA-binding proteins. *Nat*
1133 *Rev Mol Cell Biol* 19: 327-341
1134 Imaizumi T, Mogami Y, Okamoto N, Yamamoto-Shimojima K, Yamamoto T (2019) De novo 1p35.2
1135 microdeletion including PUM1 identified in a patient with sporadic West syndrome. *Congenit Anom*
1136 *(Kyoto)* 59: 193-194
1137 Jin Z, Feng H, Liang J, Jing X, Zhao Q, Zhan L, Shen B, Cheng X, Su L, Qiu W (2020) FGFR3 big up tri,
1138 open7-9 promotes tumor progression via the phosphorylation and destabilization of ten-eleven
1139 translocation-2 in human hepatocellular carcinoma. *Cell Death Dis* 11: 903
1140 Kacher R, Lejeune FX, Noel S, Cazeneuve C, Brice A, Humbert S, Durr A (2021) Propensity for somatic
1141 expansion increases over the course of life in Huntington disease. *Elife* 10
1142 Kedde M, van Kouwenhove M, Zwart W, Oude Vrielink JA, Elkon R, Agami R (2010) A Pumilio-
1143 induced RNA structure switch in p27-3' UTR controls miR-221 and miR-222 accessibility. *Nat Cell*
1144 *Biol* 12: 1014-1020
1145 Keene JD (2007a) Biological clocks and the coordination theory of RNA operons and regulons. *Cold*
1146 *Spring Harb Symp Quant Biol* 72: 157-165
1147 Keene JD (2007b) RNA regulons: coordination of post-transcriptional events. *Nat Rev Genet* 8: 533-543
1148 Keene JD, Lager PJ (2005) Post-transcriptional operons and regulons co-ordinating gene expression.
1149 *Chromosome Res* 13: 327-337
1150 Kenny PJ, Kim M, Skariah G, Nielsen J, Lannom MC, Ceman S (2020) The FMRP-MOV10 complex: a
1151 translational regulatory switch modulated by G-Quadruplexes. *Nucleic Acids Res* 48: 862-878
1152 Kenny PJ, Zhou H, Kim M, Skariah G, Khetani RS, Drnevich J, Arcila ML, Kosik KS, Ceman S (2014)
1153 MOV10 and FMRP regulate AGO2 association with microRNA recognition elements. *Cell Rep* 9:
1154 1729-1741
1155 Khalil B, Morderer D, Price PL, Liu F, Rossoll W (2018) mRNP assembly, axonal transport, and local
1156 translation in neurodegenerative diseases. *Brain Res* 1693: 75-91
1157 Kim K, Hessl D, Randol JL, Espinal GM, Schneider A, Protic D, Aydin EY, Hagerman RJ, Hagerman PJ
1158 (2019) Association between IQ and FMR1 protein (FMRP) across the spectrum of CGG repeat
1159 expansions. *PLoS One* 14: e0226811
1160 Koopmans F, van Nierop P, Andres-Alonso M, Byrnes A, Cijsouw T, Coba MP, Cornelisse LN, Farrell
1161 RJ, Goldschmidt HL, Howrigan DP *et al* (2019) SynGO: An Evidence-Based, Expert-Curated
1162 Knowledge Base for the Synapse. *Neuron* 103: 217-234 e214
1163 Koressaar T, Remm M (2007) Enhancements and modifications of primer design program Primer3.
1164 *Bioinformatics* 23: 1289-1291
1165 Lai KL, Liao YC, Tsai PC, Hsiao CT, Soong BW, Lee YC (2019) Investigating PUM1 mutations in a
1166 Taiwanese cohort with cerebellar ataxia. *Parkinsonism Relat Disord* 66: 220-223
1167 Lee EJ, Seo E, Kim JW, Nam SA, Lee JY, Jun J, Oh S, Park M, Jho EH, Yoo KH *et al* (2020) TAZ/Wnt-
1168 beta-catenin/c-MYC axis regulates cystogenesis in polycystic kidney disease. *Proc Natl Acad Sci U S*
1169 *A* 117: 29001-29012

1170 Lee S, Kopp F, Chang TC, Sataluri A, Chen B, Sivakumar S, Yu H, Xie Y, Mendell JT (2016) Noncoding
1171 RNA NORAD Regulates Genomic Stability by Sequestering PUMILIO Proteins. *Cell* 164: 69-80
1172 Lee Y, Samaco RC, Gatchel JR, Thaller C, Orr HT, Zoghbi HY (2008) miR-19, miR-101 and miR-130
1173 co-regulate ATXN1 levels to potentially modulate SCA1 pathogenesis. *Nat Neurosci* 11: 1137-1139
1174 Licatalosi DD, Yano M, Fak JJ, Mele A, Grabinski SE, Zhang C, Darnell RB (2012) Ptbp2 represses
1175 adult-specific splicing to regulate the generation of neuronal precursors in the embryonic brain. *Genes*
1176 *Dev* 26: 1626-1642
1177 Marrero E, Rossi SG, Darr A, Tsoulfas P, Rotundo RL (2011) Translational regulation of
1178 acetylcholinesterase by the RNA-binding protein Pumilio-2 at the neuromuscular synapse. *J Biol*
1179 *Chem* 286: 36492-36499
1180 Mauger O, Lemoine F, Scheiffele P (2016) Targeted Intron Retention and Excision for Rapid Gene
1181 Regulation in Response to Neuronal Activity. *Neuron* 92: 1266-1278
1182 Maurin T, Lebrigand K, Castagnola S, Paquet A, Jarjat M, Popa A, Grossi M, Rage F, Bardoni B (2018)
1183 HITS-CLIP in various brain areas reveals new targets and new modalities of RNA binding by fragile
1184 X mental retardation protein. *Nucleic Acids Res* 46: 6344-6355
1185 Miles WO, Tschop K, Herr A, Ji JY, Dyson NJ (2012) Pumilio facilitates miRNA regulation of the E2F3
1186 oncogene. *Genes Dev* 26: 356-368
1187 Muraro NI, Weston AJ, Gerber AP, Luschnig S, Moffat KG, Baines RA (2008) Pumilio binds para
1188 mRNA and requires Nanos and Brat to regulate sodium current in Drosophila motoneurons. *J*
1189 *Neurosci* 28: 2099-2109
1190 Orr HT, Zoghbi HY (2007) Trinucleotide repeat disorders. *Annu Rev Neurosci* 30: 575-621
1191 Otasek D, Morris JH, Boucas J, Pico AR, Demchak B (2019) Cytoscape Automation: empowering
1192 workflow-based network analysis. *Genome Biol* 20: 185
1193 Pfaffl MW (2001) A new mathematical model for relative quantification in real-time RT-PCR. *Nucleic*
1194 *Acids Res* 29: e45
1195 Preitner N, Quan J, Nowakowski DW, Hancock ML, Shi J, Tcherkezian J, Young-Pearse TL, Flanagan
1196 JG (2014) APC is an RNA-binding protein, and its interactome provides a link to neural development
1197 and microtubule assembly. *Cell* 158: 368-382
1198 Rappsilber J, Mann M, Ishihama Y (2007) Protocol for micro-purification, enrichment, pre-fractionation
1199 and storage of peptides for proteomics using StageTips. *Nat Protoc* 2: 1896-1906
1200 Raudvere U, Kolberg L, Kuzmin I, Arak T, Adler P, Peterson H, Vilo J (2019) g:Profiler: a web server for
1201 functional enrichment analysis and conversions of gene lists (2019 update). *Nucleic Acids Res* 47:
1202 W191-W198
1203 Ravanidis S, Kattan FG, Doxakis E (2018) Unraveling the Pathways to Neuronal Homeostasis and
1204 Disease: Mechanistic Insights into the Role of RNA-Binding Proteins and Associated Factors. *Int J*
1205 *Mol Sci* 19
1206 Rousseaux MWC, Tschumperlin T, Lu HC, Lackey EP, Bondar VV, Wan YW, Tan Q, Adamski CJ,
1207 Friedrich J, Twaroski K *et al* (2018) ATXN1-CIC Complex Is the Primary Driver of Cerebellar
1208 Pathology in Spinocerebellar Ataxia Type 1 through a Gain-of-Function Mechanism. *Neuron* 97:
1209 1235-1243 e1235
1210 Rovelet-Lecrux A, Hannequin D, Raux G, Le Meur N, Laquerriere A, Vital A, Dumanchin C, Feuillette
1211 S, Brice A, Vercelletto M *et al* (2006) APP locus duplication causes autosomal dominant early-onset
1212 Alzheimer disease with cerebral amyloid angiopathy. *Nat Genet* 38: 24-26

1213 Salcedo-Arellano MJ, Dufour B, McLennan Y, Martinez-Cerdeno V, Hagerman R (2020) Fragile X
1214 syndrome and associated disorders: Clinical aspects and pathology. *Neurobiol Dis* 136: 104740
1215 Shah S, Molinaro G, Liu B, Wang R, Huber KM, Richter JD (2020) FMRP Control of Ribosome
1216 Translocation Promotes Chromatin Modifications and Alternative Splicing of Neuronal Genes Linked
1217 to Autism. *Cell Rep* 30: 4459-4472 e4456
1218 Shannon P, Markiel A, Ozier O, Baliga NS, Wang JT, Ramage D, Amin N, Schwikowski B, Ideker T
1219 (2003) Cytoscape: a software environment for integrated models of biomolecular interaction
1220 networks. *Genome Res* 13: 2498-2504
1221 Shevchenko A, Tomas H, Havlis J, Olsen JV, Mann M (2006) In-gel digestion for mass spectrometric
1222 characterization of proteins and proteomes. *Nat Protoc* 1: 2856-2860
1223 Singh K, Gaur P, Prasad S (2007) Fragile x mental retardation (Fmr-1) gene expression is down regulated
1224 in brain of mice during aging. *Mol Biol Rep* 34: 173-181
1225 Singh K, Prasad S (2008) Differential expression of Fmr-1 mRNA and FMRP in female mice brain
1226 during aging. *Mol Biol Rep* 35: 677-684
1227 Smidak R, Sialana FJ, Kristofova M, Stojanovic T, Rajcic D, Malikovic J, Feyissa DD, Korz V, Hoeger
1228 H, Wackerlig J *et al* (2017) Reduced Levels of the Synaptic Functional Regulator FMRP in Dentate
1229 Gyrus of the Aging Sprague-Dawley Rat. *Front Aging Neurosci* 9: 384
1230 Subramanian A, Tamayo P, Mootha VK, Mukherjee S, Ebert BL, Gillette MA, Paulovich A, Pomeroy
1231 SL, Golub TR, Lander ES *et al* (2005) Gene set enrichment analysis: a knowledge-based approach for
1232 interpreting genome-wide expression profiles. *Proc Natl Acad Sci U S A* 102: 15545-15550
1233 Takeguchi R, Takahashi S, Kuroda M, Tanaka R, Suzuki N, Tomonoh Y, Ihara Y, Sugiyama N, Itoh M
1234 (2020) MeCP2_e2 partially compensates for lack of MeCP2_e1: A male case of Rett syndrome. *Mol*
1235 *Genet Genomic Med* 8: e1088
1236 Tan Q, Zoghbi HY (2019) Mouse models as a tool for discovering new neurological diseases. *Neurobiol*
1237 *Learn Mem* 165: 106902
1238 Temme C, Simonelig M, Wahle E (2014) Deadenylation of mRNA by the CCR4-NOT complex in
1239 Drosophila: molecular and developmental aspects. *Front Genet* 5: 143
1240 Tereshchenko A, Magnotta V, Epping E, Mathews K, Espe-Pfeifer P, Martin E, Dawson J, Duan W,
1241 Nopoulos P (2019) Brain structure in juvenile-onset Huntington disease. *Neurology* 92: e1939-e1947
1242 Thul PJ, Akesson L, Wiking M, Mahdessian D, Geladaki A, Ait Blal H, Alm T, Asplund A, Bjork L,
1243 Breckels LM *et al* (2017) A subcellular map of the human proteome. *Science* 356
1244 Trumbach D, Prakash N (2015) The conserved miR-8/miR-200 microRNA family and their role in
1245 invertebrate and vertebrate neurogenesis. *Cell Tissue Res* 359: 161-177
1246 Tyanova S, Temu T, Sinitcyn P, Carlson A, Hein MY, Geiger T, Mann M, Cox J (2016) The Perseus
1247 computational platform for comprehensive analysis of (prote)omics data. *Nat Methods* 13: 731-740
1248 Untergasser A, Cutcutache I, Koressaar T, Ye J, Faircloth BC, Remm M, Rozen SG (2012) Primer3--new
1249 capabilities and interfaces. *Nucleic Acids Res* 40: e115
1250 Uyhazi KE, Yang Y, Liu N, Qi H, Huang XA, Mak W, Weatherbee SD, de Prisco N, Gennarino VA,
1251 Song X *et al* (2020) Pumilio proteins utilize distinct regulatory mechanisms to achieve
1252 complementary functions required for pluripotency and embryogenesis. *Proc Natl Acad Sci U S A*
1253 117: 7851-7862

1254 Van Etten J, Schagat TL, Hrit J, Weidmann CA, Brumbaugh J, Coon JJ, Goldstrohm AC (2012) Human
1255 Pumilio proteins recruit multiple deadenylases to efficiently repress messenger RNAs. *J Biol Chem*
1256 287: 36370-36383
1257 Vandesompele J, De Preter K, Pattyn F, Poppe B, Van Roy N, De Paepe A, Speleman F (2002) Accurate
1258 normalization of real-time quantitative RT-PCR data by geometric averaging of multiple internal
1259 control genes. *Genome Biol* 3
1260 Wamsley B, Jaglin XH, Favuzzi E, Quattrocolo G, Nigro MJ, Yusuf N, Khodadadi-Jamayran A, Rudy B,
1261 Fishell G (2018) Rbfox1 Mediates Cell-type-Specific Splicing in Cortical Interneurons. *Neuron* 100:
1262 846-859 e847
1263 Weidmann CA, Raynard NA, Blewett NH, Van Etten J, Goldstrohm AC (2014) The RNA binding
1264 domain of Pumilio antagonizes poly-adenosine binding protein and accelerates deadenylation. *RNA*
1265 20: 1298-1319
1266 Weyn-Vanhentenryck SM, Mele A, Yan Q, Sun S, Farny N, Zhang Z, Xue C, Herre M, Silver PA, Zhang
1267 MQ *et al* (2014) HITS-CLIP and integrative modeling define the Rbfox splicing-regulatory network
1268 linked to brain development and autism. *Cell Rep* 6: 1139-1152
1269 Zamore PD, Williamson JR, Lehmann R (1997) The Pumilio protein binds RNA through a conserved
1270 domain that defines a new class of RNA-binding proteins. *RNA* 3: 1421-1433
1271 Zhang C, Frias MA, Mele A, Ruggiu M, Eom T, Marney CB, Wang H, Licatalosi DD, Fak JJ, Darnell RB
1272 (2010) Integrative modeling defines the Nova splicing-regulatory network and its combinatorial
1273 controls. *Science* 329: 439-443
1274 Zhang M, Chen D, Xia J, Han W, Cui X, Neuenkirchen N, Hermes G, Sestan N, Lin H (2017) Post-
1275 transcriptional regulation of mouse neurogenesis by Pumilio proteins. *Genes Dev* 31: 1354-1369

1276

Figure 1

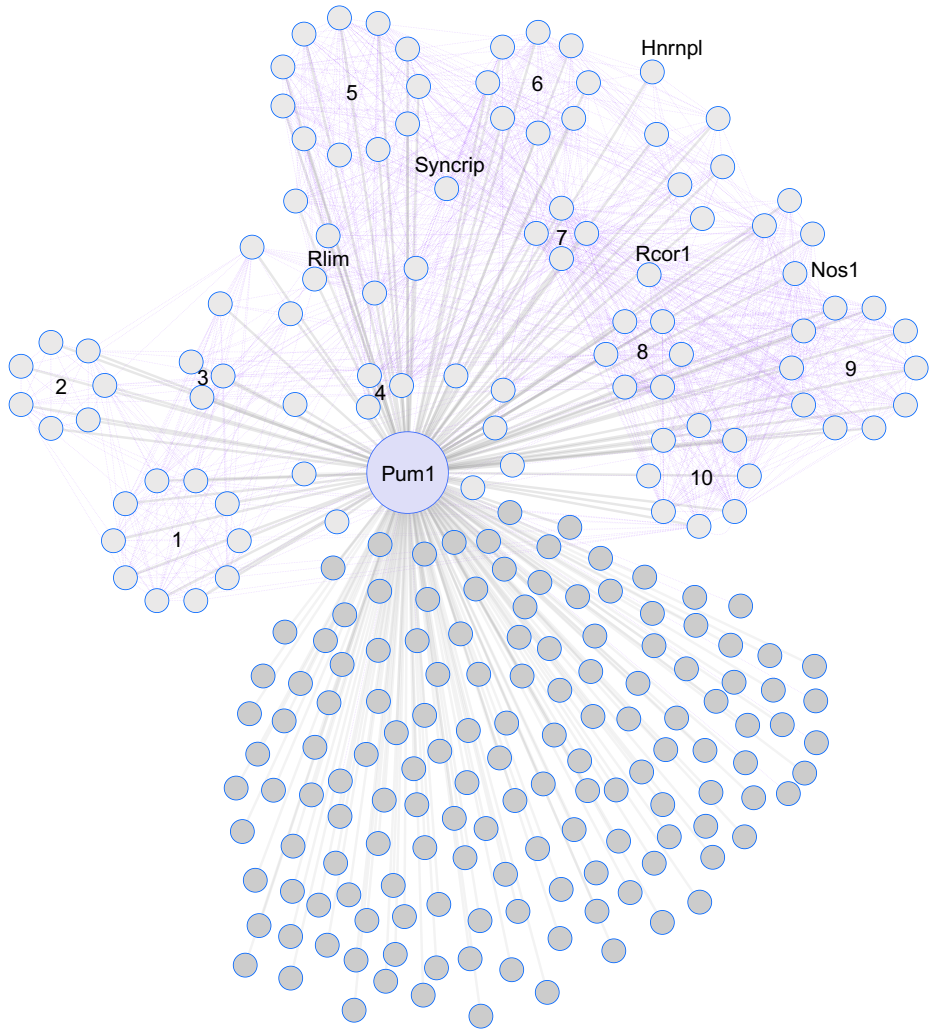

Cluster 1
Cdc16
Cdc23
Cdc27
Anapc4
Anapc1
Anapc7
Anapc5
Anapc2
Fzr1
Sh3kbp1

Cluster 2
Ppp1r12a
Ppp1r12b
Ppp1r12c
Ppp6r2
Ppp1r21
Ppp1r16b

Cluster 3
Kdm1a
Zmym2
Hdac2

Cluster 4
Mllt1
Mllt3
Aff4

Cluster 5
Hnrnpul1
Dhx15
Wdr20
Acin1
Rbm39
Snrnp200
Ddx3x
Ddx3y
Ddx17
Sf3b3
Wdr48

Cluster 6
Eif3l
Eif2s3x/y
Eif3b
Eif2s2
Ctif
Eif5
Eif3f
Eif4g3

Cluster 7
Ago2
Cnot1
Fmrp
Rbfox3

Cluster 8
Matr3
Pfkp
Pfkm
Pfkl
Pfkfb2
Pspc1

Cluster 9
Pex5l
Atg7
Snx2
Snx4
Madd
Fga
Fgb
Fgg
Rab11fip5
Pck2

Cluster 10
Rictor
Rptor
Tsc1
Tsc2
Camkk2
Cad
Lrpprc
Lppr4

Figure 2

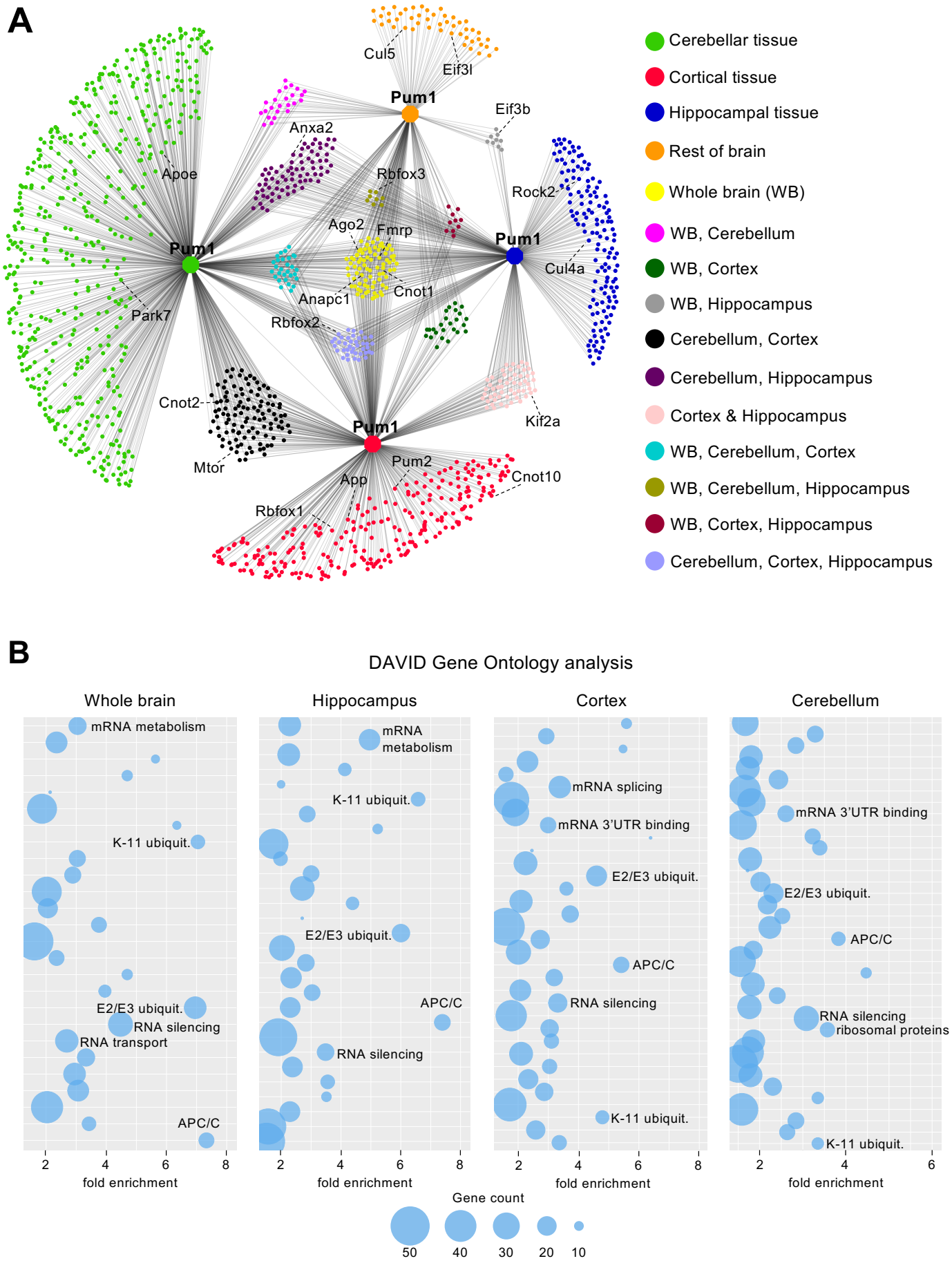
A
Cul5
Eif3l
Pum1
Eif3b
Anxa2
Apoe
Rbfox3
Rock2
Ago2
Fmrp
Pum1
Pum1
Cul4a
Anapc1
Cnot1
Park7
Rbfox2
Cnot2
Kif2a
Pum1
Mtor
Pum2
App
Cnot10
Rbfox1
Cerebellar tissue
Cortical tissue
Hippocampal tissue
Rest of brain
Whole brain (WB)
WB, Cerebellum
WB, Cortex
WB, Hippocampus
Cerebellum, Cortex
Cerebellum, Hippocampus
Cortex & Hippocampus
WB, Cerebellum, Cortex
WB, Cerebellum, Hippocampus
WB, Cortex, Hippocampus
Cerebellum, Cortex, Hippocampus
B
DAVID Gene Ontology analysis
Whole brain
Hippocampus
Cortex
Cerebellum
mRNA metabolism
K-11 ubiquit.
E2/E3 ubiquit.
RNA silencing
RNA transport
APC/C
mRNA metabolism
K-11 ubiquit.
E2/E3 ubiquit.
APC/C
RNA silencing
mRNA splicing
mRNA 3'UTR binding
E2/E3 ubiquit.
APC/C
RNA silencing
K-11 ubiquit.
mRNA 3'UTR binding
E2/E3 ubiquit.
APC/C
RNA silencing
ribosomal proteins
K-11 ubiquit.
2
4
6
8
fold enrichment
Gene count
50
40
30
20
10

Figure 3

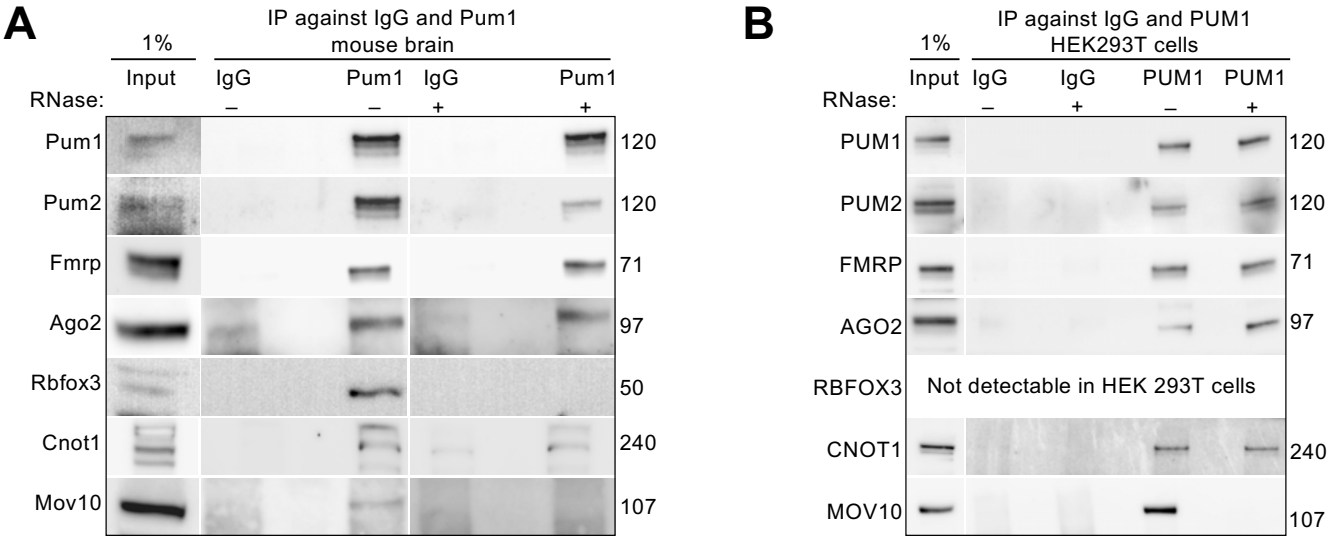
A
1%
IP against IgG and Pum1
mouse brain
Input
IgG
Pum1
IgG
Pum1
RNase:
–
–
+
+
Pum1
Pum2
Fmrp
Ago2
Rbfox3
Cnot1
Mov10
120
120
71
97
50
240
107
B
1%
IP against IgG and PUM1
HEK293T cells
Input
IgG
IgG
PUM1
PUM1
RNase:
–
+
–
+
PUM1
PUM2
FMRP
AGO2
RBFOX3
CNOT1
MOV10
Not detectable in HEK 293T cells
120
120
71
97
240
107

Figure 4

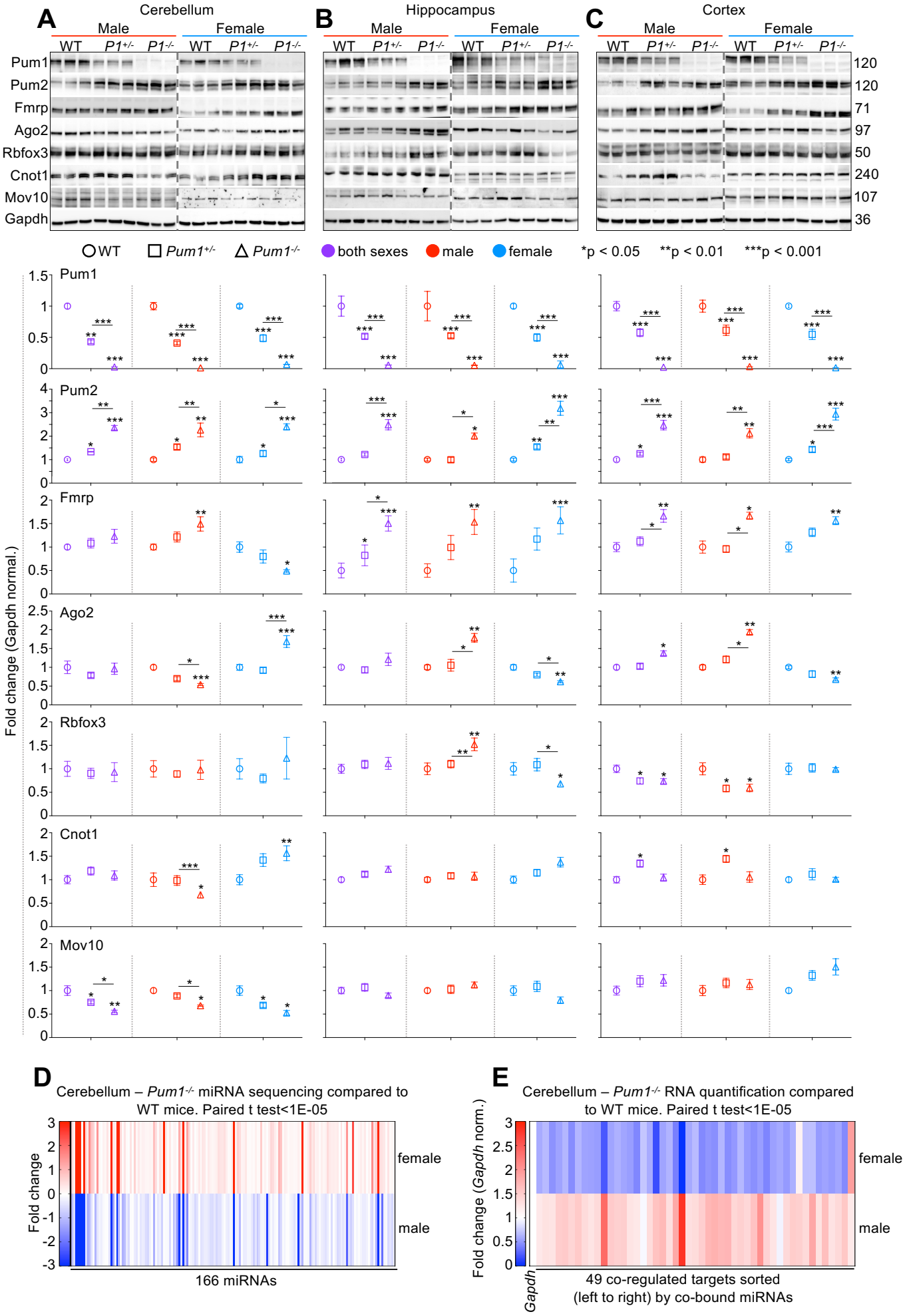
A
Cerebellum
Male
Female
WT
P1+/-
P1-/-
Pum1
Pum2
Fmrp
Ago2
Rbfox3
Cnot1
Mov10
Gapdh
B
Hippocampus
C
Cortex
120
120
71
97
50
240
107
36
WT
Pum1+/-
Pum1-/-
both sexes
male
female
*p < 0.05
**p < 0.01
***p < 0.001
Fold change (Gapdh normal.)
D
Cerebellum – Pum1-/- miRNA sequencing compared to WT mice. Paired t test<1E-05
Fold change
female
male
166 miRNAs
E
Cerebellum – Pum1-/- RNA quantification compared to WT mice. Paired t test<1E-05
Fold change (Gapdh norm.)
Gapdh
49 co-regulated targets sorted (left to right) by co-bound miRNAs

Figure 5

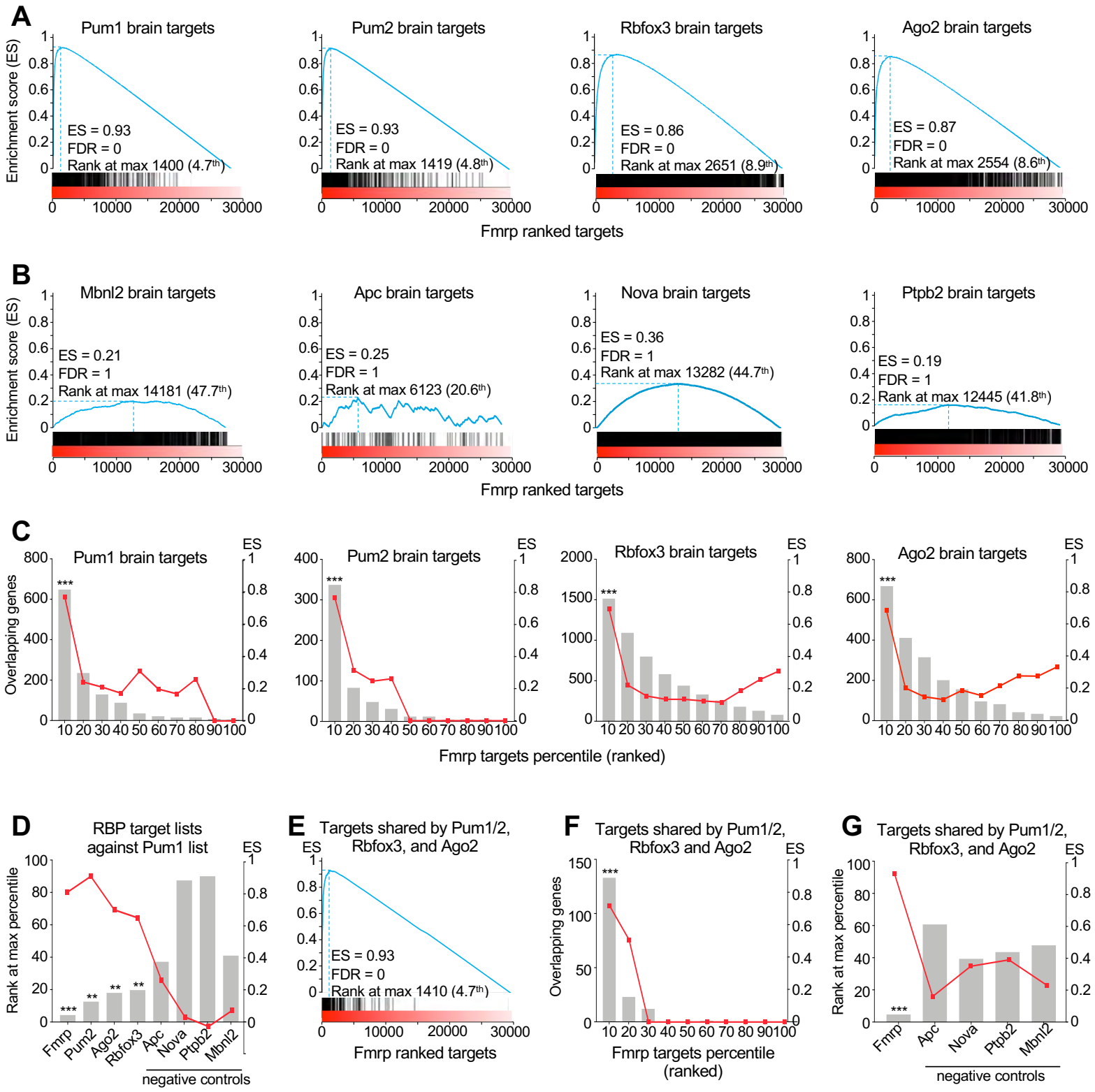
A
Pum1 brain targets
ES = 0.93
FDR = 0
Rank at max 1400 (4.7th)
Pum2 brain targets
ES = 0.93
FDR = 0
Rank at max 1419 (4.8th)
Rbfox3 brain targets
ES = 0.86
FDR = 0
Rank at max 2651 (8.9th)
Ago2 brain targets
ES = 0.87
FDR = 0
Rank at max 2554 (8.6th)
Enrichment score (ES)
Fmrp ranked targets
B
Mbnl2 brain targets
ES = 0.21
FDR = 1
Rank at max 14181 (47.7th)
Apc brain targets
ES = 0.25
FDR = 1
Rank at max 6123 (20.6th)
Nova brain targets
ES = 0.36
FDR = 1
Rank at max 13282 (44.7th)
Ptpb2 brain targets
ES = 0.19
FDR = 1
Rank at max 12445 (41.8th)
Enrichment score (ES)
Fmrp ranked targets
C
Pum1 brain targets
Pum2 brain targets
Rbfox3 brain targets
Ago2 brain targets
Overlapping genes
ES
Fmrp targets percentile (ranked)
D
RBP target lists against Pum1 list
Rank at max percentile
ES
Fmrp
Pum2
Ago2
Rbfox3
Apc
Nova
Ptpb2
Mbnl2
negative controls
E
Targets shared by Pum1/2, Rbfox3, and Ago2
ES = 0.93
FDR = 0
Rank at max 1410 (4.7th)
Fmrp ranked targets
F
Targets shared by Pum1/2, Rbfox3 and Ago2
Overlapping genes
Fmrp targets percentile (ranked)
G
Targets shared by Pum1/2, Rbfox3, and Ago2
Rank at max percentile
Fmrp
Apc
Nova
Ptpb2
Mbnl2
negative controls

Figure 6

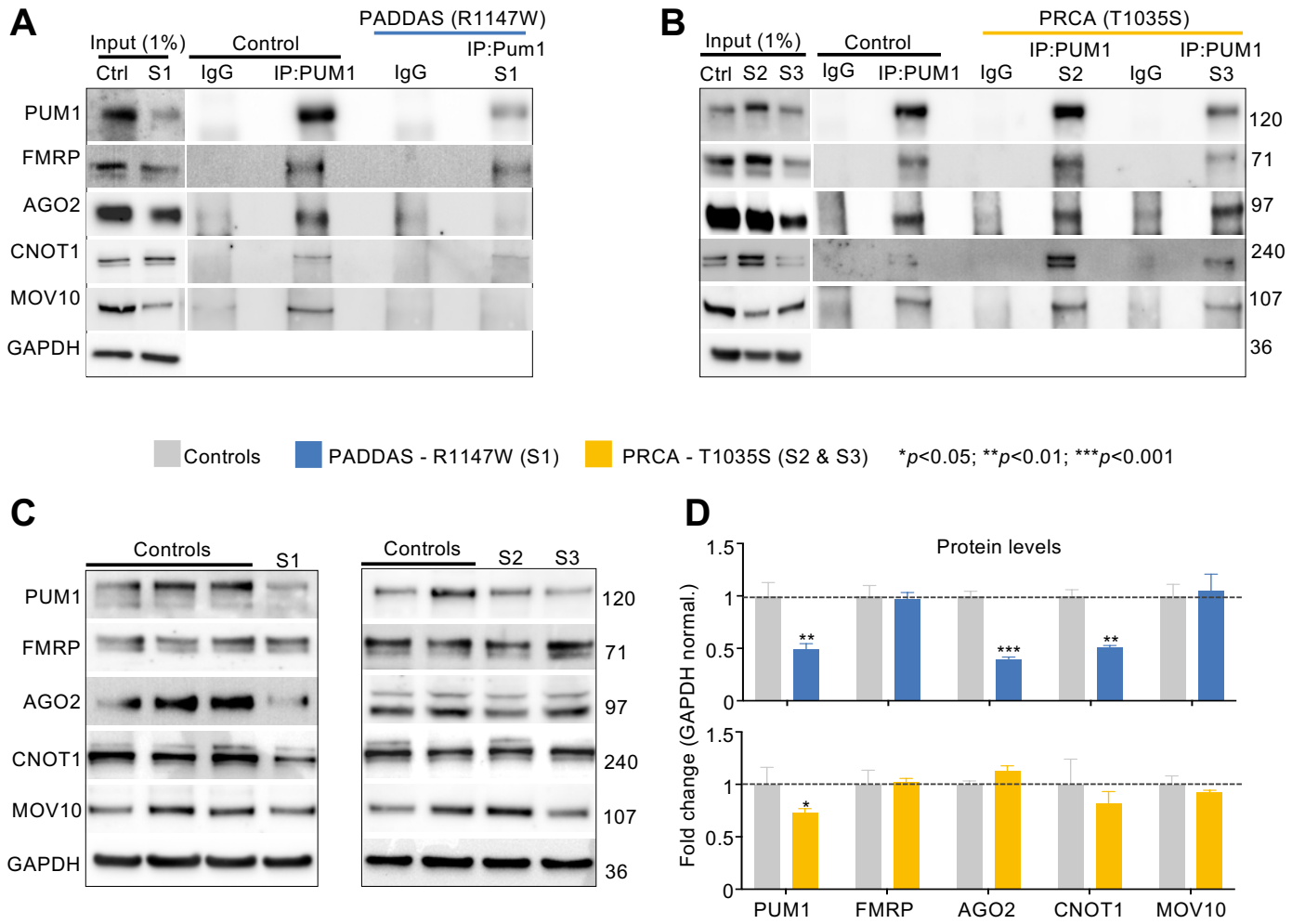
A
Input (1%)
Control
PADDAS (R1147W)
Ctrl
S1
IgG
IP:PUM1
IgG
IP:Pum1
S1
PUM1
FMRP
AGO2
CNOT1
MOV10
GAPDH
B
Input (1%)
Control
PRCA (T1035S)
Ctrl
S2
S3
IgG
IP:PUM1
IgG
IP:PUM1
S2
IgG
IP:PUM1
S3
120
71
97
240
107
36
Controls
PADDAS - R1147W (S1)
PRCA - T1035S (S2 & S3)
*p<0.05; **p<0.01; ***p<0.001
C
Controls
S1
Controls
S2
S3
PUM1
FMRP
AGO2
CNOT1
MOV10
GAPDH
120
71
97
240
107
36
D
Protein levels
Fold change (GAPDH normal.)
1.5
1
0.5
0
**
***
**
*
PUM1
FMRP
AGO2
CNOT1
MOV10

Figure 7

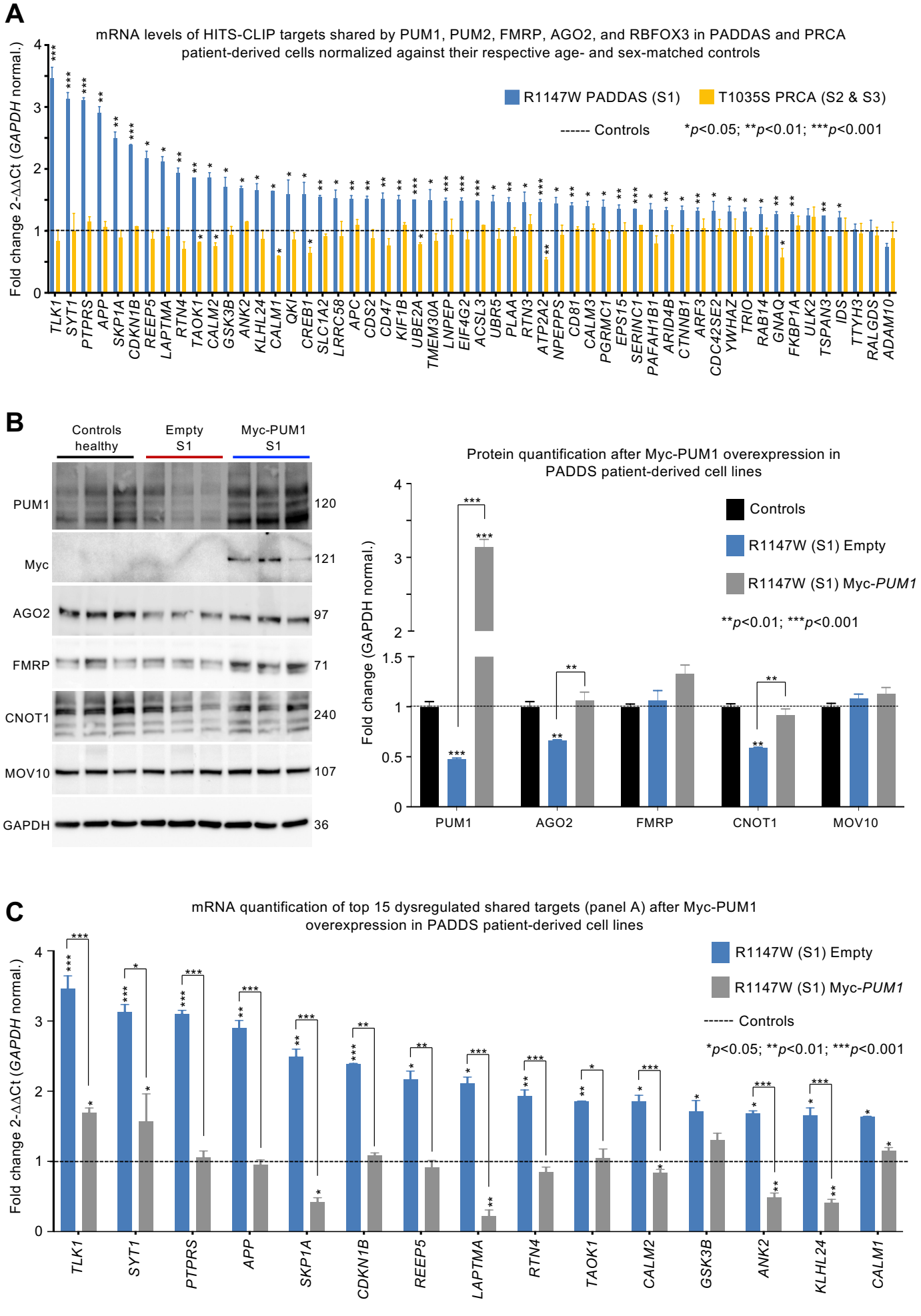
A
mRNA levels of HITS-CLIP targets shared by PUM1, PUM2, FMRP, AGO2, and RBFOX3 in PADDAS and PRCA patient-derived cells normalized against their respective age- and sex-matched controls
Fold change 2-ΔΔCt (GAPDH normal.)
R1147W PADDAS (S1)
T1035S PRCA (S2 & S3)
------ Controls
*p<0.05; **p<0.01; ***p<0.001
TLK1 SYT1 PTPRS APP SKP1A CDKN1B REEP5 LAPTMA RTN4 TAOK1 CALM2 GSK3B ANK2 KLHL24 CALM1 QKI CREB1 SLC1A2 LRRC58 APC CDS2 CD47 KIF1B UBE2A TMEM30A LNPEP EIF4G2 ACSL3 UBR5 PLAA RTN3 ATP2A2 NPEPPS CD81 CALM3 PGRMC1 EPS15 SERINC1 PAFAH1B1 ARID4B CTNNB1 ARF3 CDC42SE2 YWHAZ TRIO RAB14 GNAQ FKBP1A ULK2 TSPAN3 IDS TTYH3 RALGDS ADAM10
B
Controls healthy
Empty S1
Myc-PUM1 S1
PUM1 120
Myc 121
AGO2 97
FMRP 71
CNOT1 240
MOV10 107
GAPDH 36
Protein quantification after Myc-PUM1 overexpression in PADDS patient-derived cell lines
Fold change (GAPDH normal.)
Controls
R1147W (S1) Empty
R1147W (S1) Myc-PUM1
**p<0.01; ***p<0.001
PUM1 AGO2 FMRP CNOT1 MOV10
C
mRNA quantification of top 15 dysregulated shared targets (panel A) after Myc-PUM1 overexpression in PADDS patient-derived cell lines
Fold change 2-ΔΔCt (GAPDH normal.)
R1147W (S1) Empty
R1147W (S1) Myc-PUM1
------ Controls
*p<0.05; **p<0.01; ***p<0.001
TLK1 SYT1 PTPRS APP SKP1A CDKN1B REEP5 LAPTMA RTN4 TAOK1 CALM2 GSK3B ANK2 KLHL24 CALM1

Figure S1

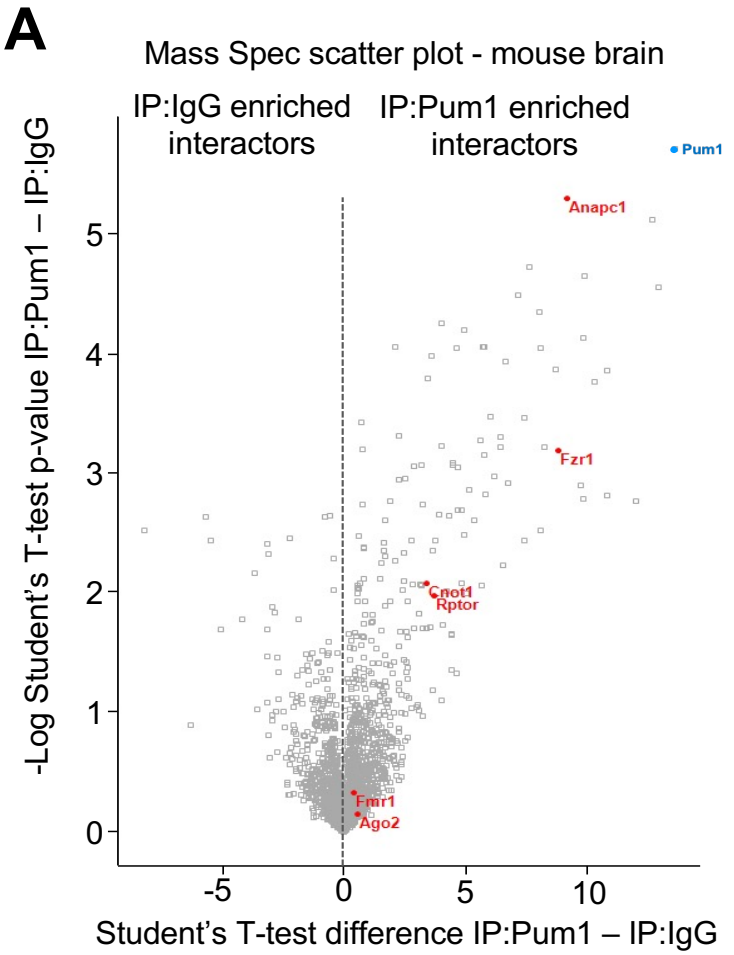
A
Mass Spec scatter plot - mouse brain
IP:IgG enriched interactors
IP:Pum1 enriched interactors
Pum1
Anapc1
Fzr1
Cnot1
Rptor
Fmr1
Ago2
-Log Student's T-test p-value IP:Pum1 – IP:IgG
Student's T-test difference IP:Pum1 – IP:IgG
-5
0
5
10
0
1
2
3
4
5

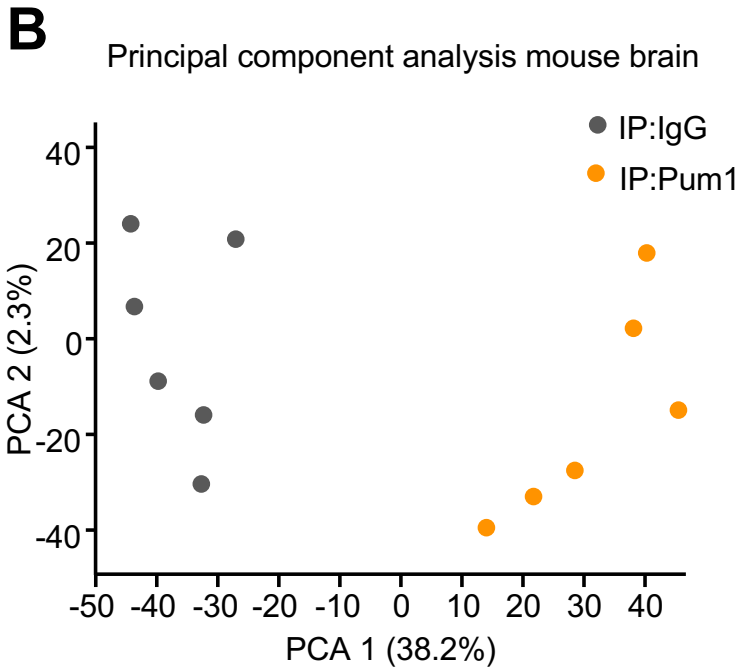
B
Principal component analysis mouse brain
IP:IgG
IP:Pum1
PCA 2 (2.3%)
PCA 1 (38.2%)
40
20
0
-20
-40
-50
-40
-30
-20
-10
0
10
20
30
40

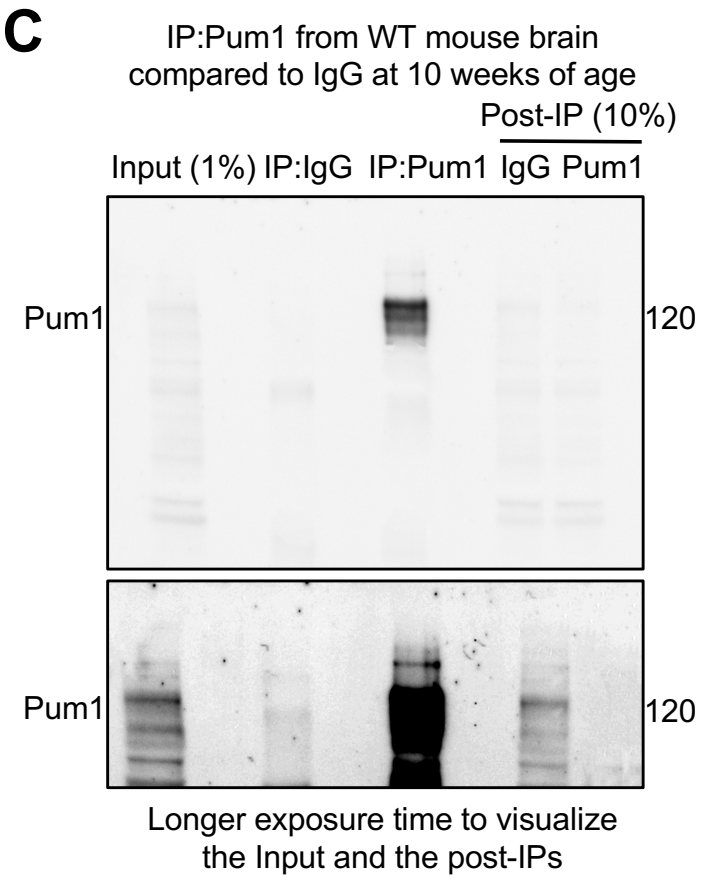
C
IP:Pum1 from WT mouse brain compared to IgG at 10 weeks of age
Post-IP (10%)
Input (1%)
IP:IgG
IP:Pum1
IgG
Pum1
Pum1
120
Pum1
120
Longer exposure time to visualize the Input and the post-IPs

Figure S2

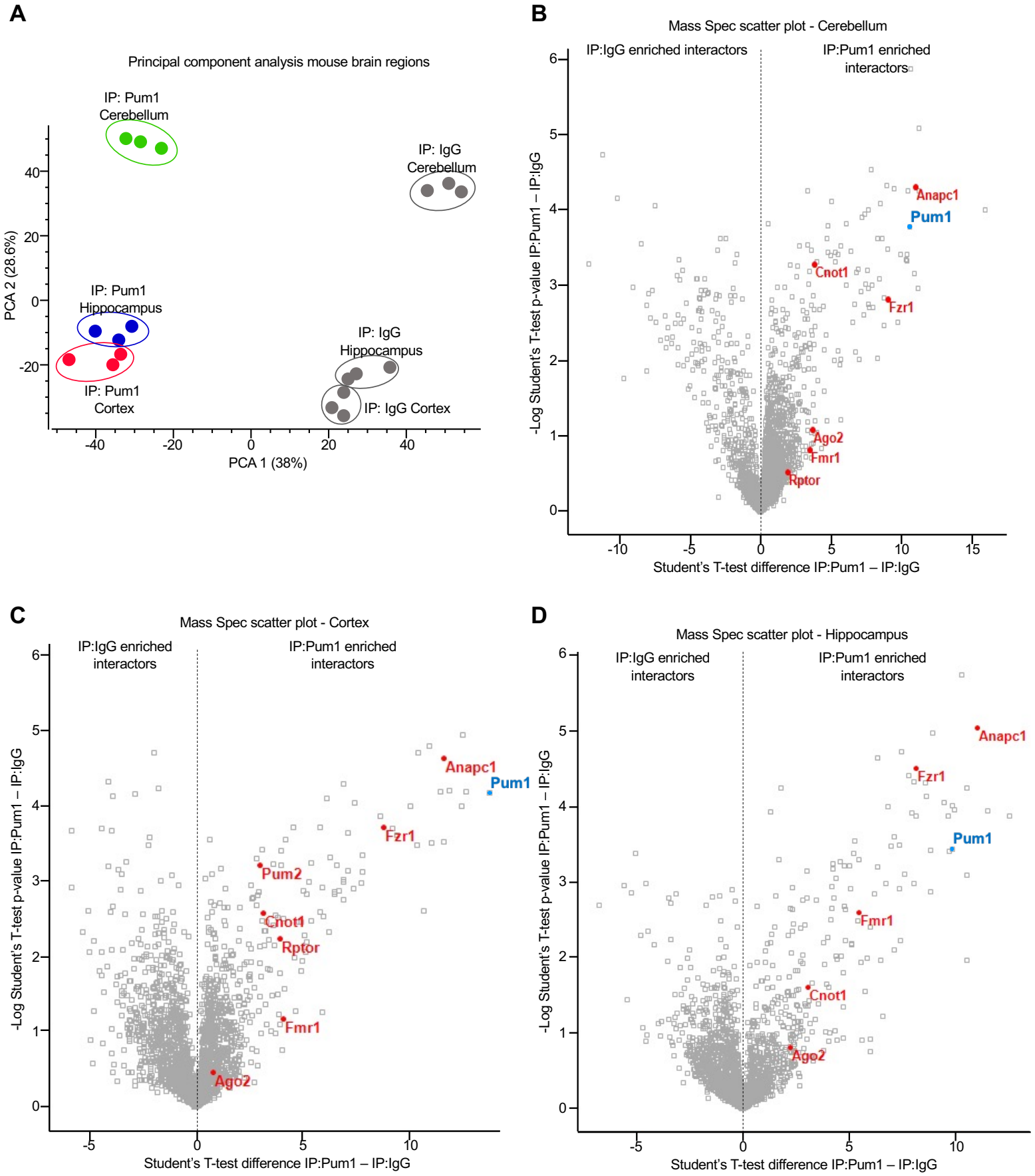
A
Principal component analysis mouse brain regions
IP: Pum1 Cerebellum
IP: IgG Cerebellum
IP: Pum1 Hippocampus
IP: IgG Hippocampus
IP: Pum1 Cortex
IP: IgG Cortex
PCA 2 (28.6%)
PCA 1 (38%)
B
Mass Spec scatter plot - Cerebellum
IP:IgG enriched interactors
IP:Pum1 enriched interactors
-Log Student's T-test p-value IP:Pum1 – IP:IgG
Student's T-test difference IP:Pum1 – IP:IgG
Anapc1
Pum1
Cnot1
Fzr1
Ago2
Fmr1
Rptor
C
Mass Spec scatter plot - Cortex
IP:IgG enriched interactors
IP:Pum1 enriched interactors
-Log Student's T-test p-value IP:Pum1 – IP:IgG
Student's T-test difference IP:Pum1 – IP:IgG
Anapc1
Pum1
Fzr1
Pum2
Cnot1
Rptor
Fmr1
Ago2
D
Mass Spec scatter plot - Hippocampus
IP:IgG enriched interactors
IP:Pum1 enriched interactors
-Log Student's T-test p-value IP:Pum1 – IP:IgG
Student's T-test difference IP:Pum1 – IP:IgG
Anapc1
Fzr1
Pum1
Fmr1
Cnot1
Ago2

Figure S3

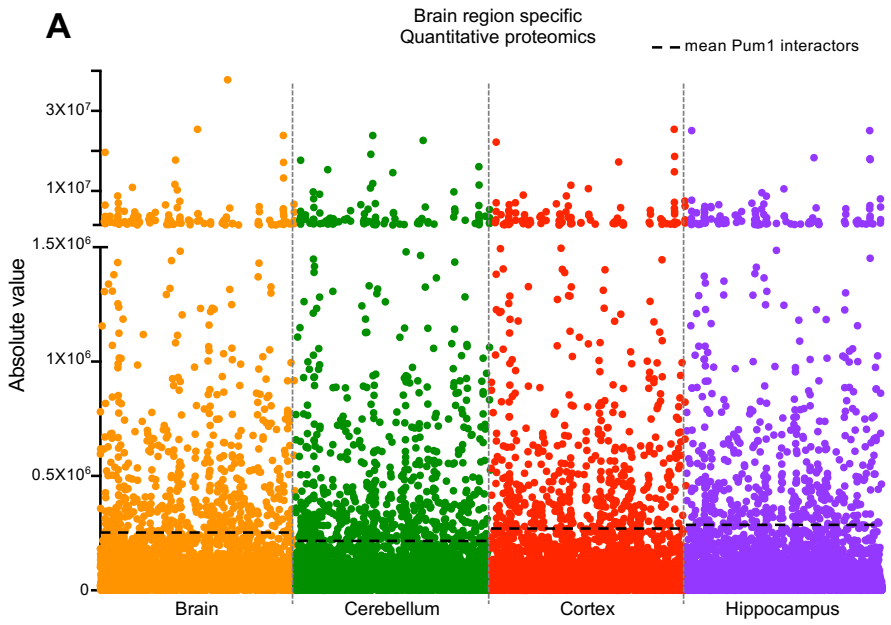
A
Brain region specific
Quantitative proteomics
mean Pum1 interactors
Absolute value
3X10^7
1X10^7
1.5X10^6
1X10^6
0.5X10^6
0
Brain
Cerebellum
Cortex
Hippocampus

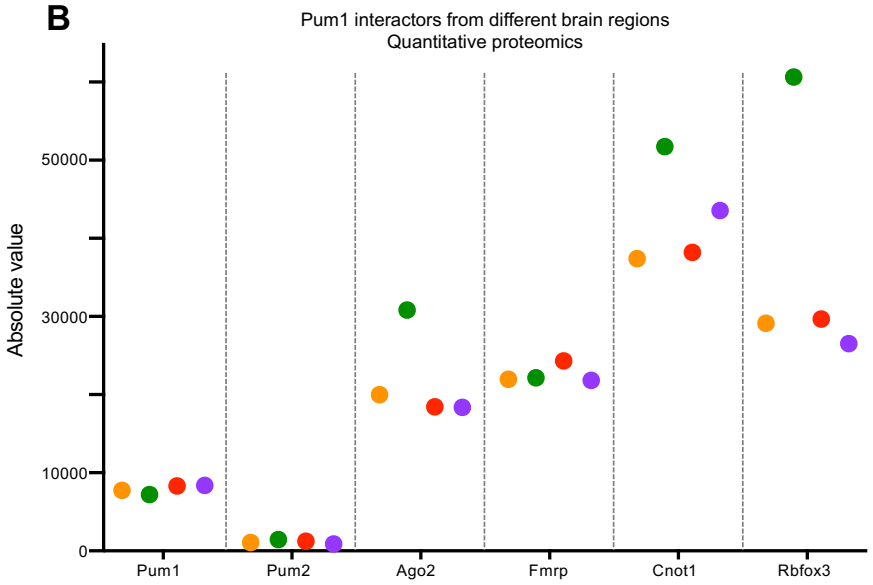
B
Pum1 interactors from different brain regions
Quantitative proteomics
Absolute value
50000
30000
10000
0
Pum1
Pum2
Ago2
Fmrp
Cnot1
Rbfox3

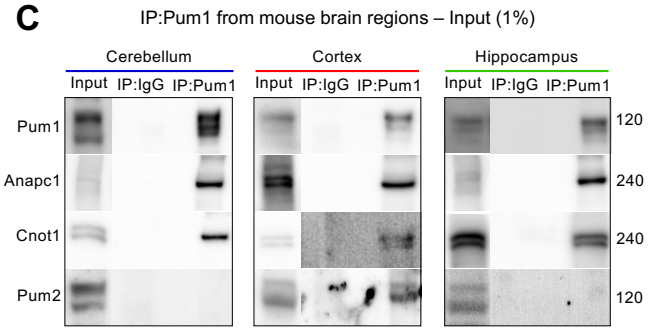
C
IP:Pum1 from mouse brain regions – Input (1%)
Cerebellum
Cortex
Hippocampus
Input
IP:IgG
IP:Pum1
Pum1
Anapc1
Cnot1
Pum2
120
240
240
120

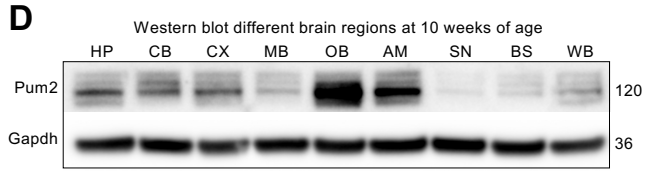
D
Western blot different brain regions at 10 weeks of age
HP
CB
CX
MB
OB
AM
SN
BS
WB
Pum2
Gapdh
120
36

Figure S4

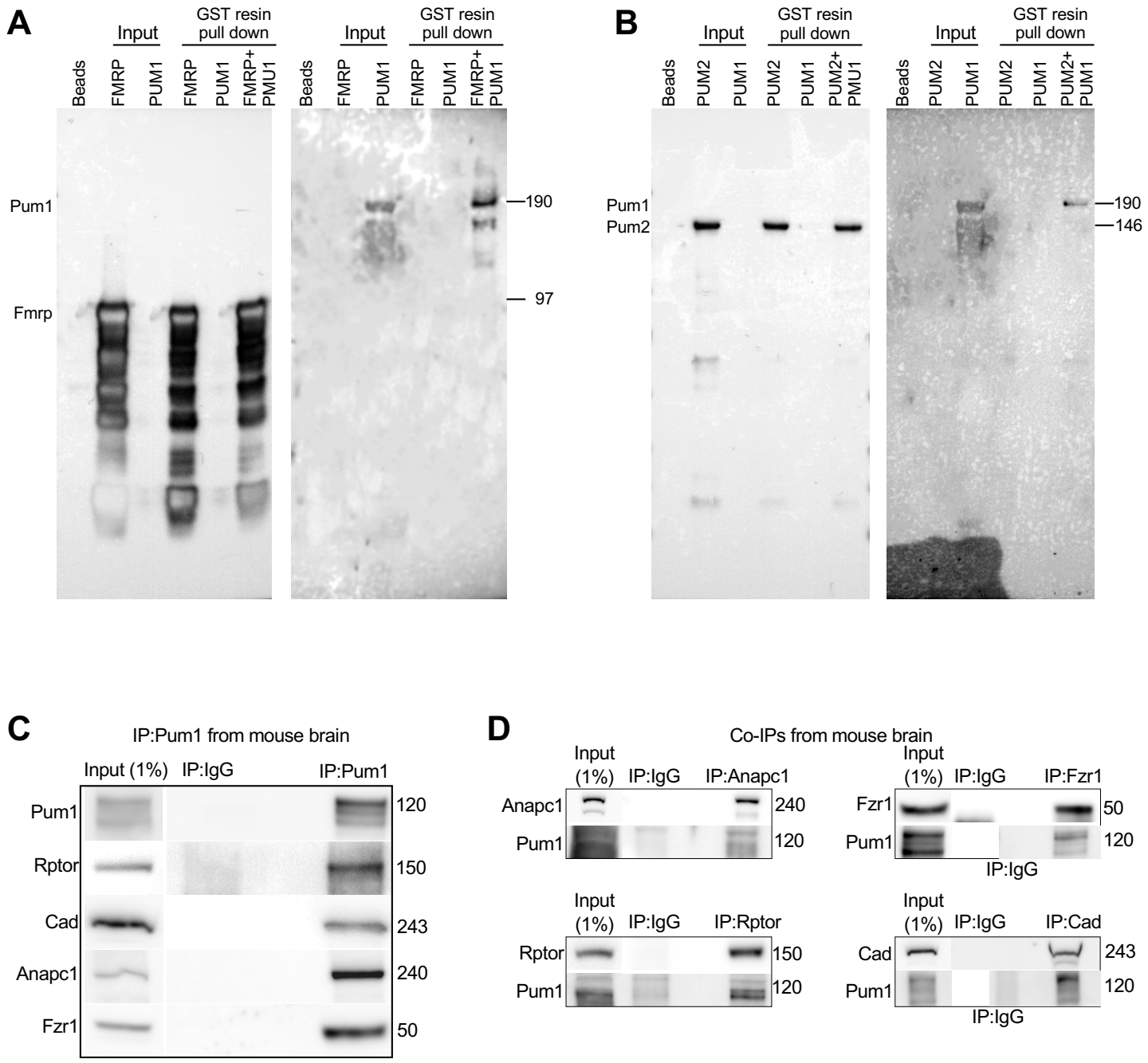
A
Input
GST resin pull down
Beads
FMRP
PUM1
FMRP
PUM1
FMRP+ PMU1
Pum1
Fmrp
190
97
B
Input
GST resin pull down
Beads
PUM2
PUM1
PUM2
PUM1
PUM2+ PMU1
Pum1
Pum2
190
146
C
IP:Pum1 from mouse brain
Input (1%)
IP:IgG
IP:Pum1
Pum1
Rptor
Cad
Anapc1
Fzr1
120
150
243
240
50
D
Co-IPs from mouse brain
Input (1%)
IP:IgG
IP:Anapc1
Anapc1
Pum1
240
120
IP:Fzr1
Fzr1
Pum1
50
120
IP:Rptor
Rptor
Pum1
150
120
IP:Cad
Cad
Pum1
243
120

Figure S5

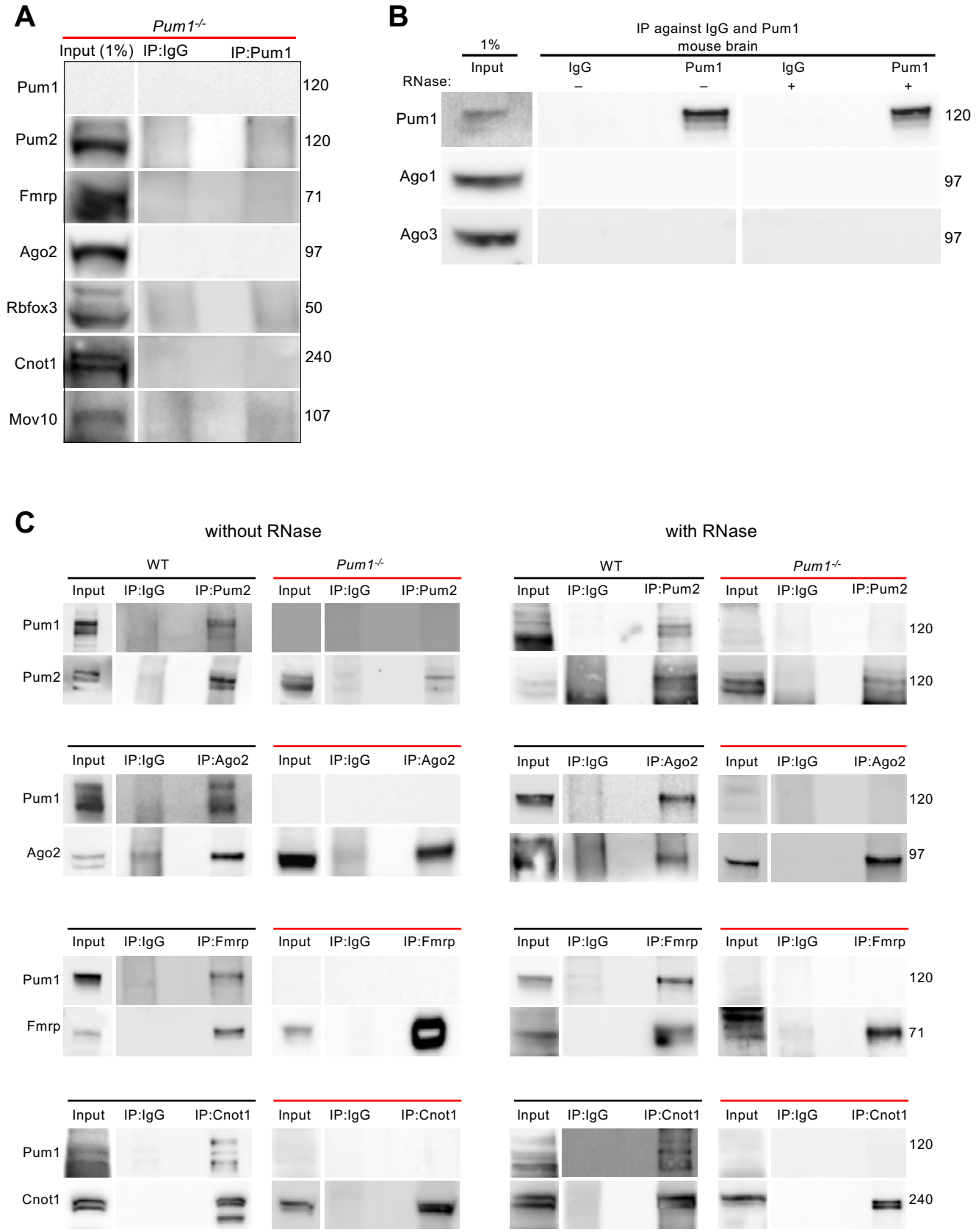
A
Pum1-/-
Input (1%)
IP:IgG
IP:Pum1
Pum1
Pum2
Fmrp
Ago2
Rbfox3
Cnot1
Mov10
120
120
71
97
50
240
107
B
IP against IgG and Pum1
mouse brain
1%
Input
IgG
Pum1
IgG
Pum1
RNase:
–
–
+
+
Pum1
Ago1
Ago3
120
97
97
C
without RNase
with RNase
WT
Pum1-/-
Input
IP:IgG
IP:Pum2
IP:Ago2
IP:Fmrp
IP:Cnot1
Pum1
Pum2
Ago2
Fmrp
Cnot1
120
120
97
71
240

Figure S6

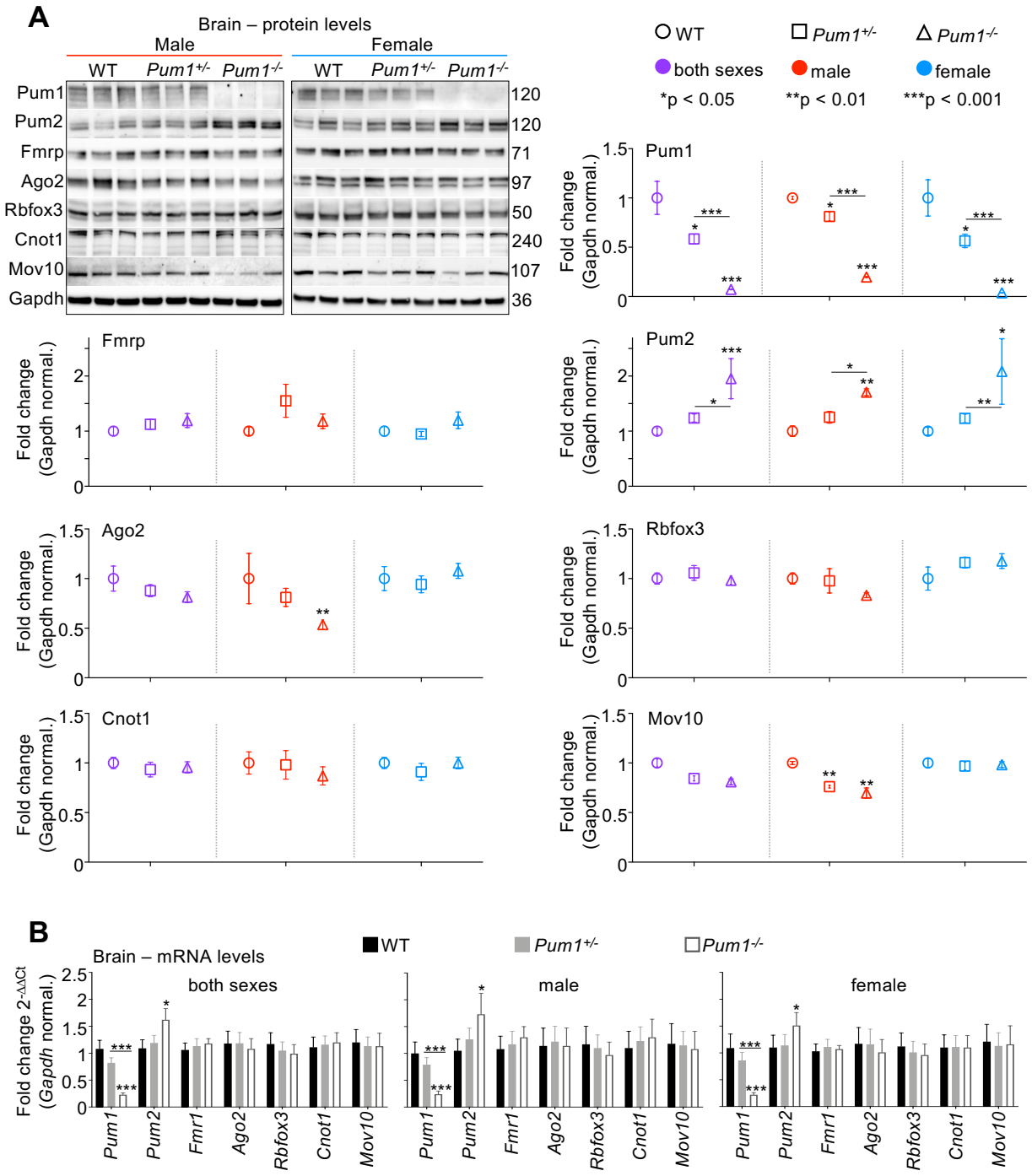
A
Brain – protein levels
Male
Female
WT
Pum1+/-
Pum1-/-
Pum1
Pum2
Fmrp
Ago2
Rbfox3
Cnot1
Mov10
Gapdh
120
120
71
97
50
240
107
36
WT
Pum1+/-
Pum1-/-
both sexes
male
female
*p < 0.05
**p < 0.01
***p < 0.001
Fold change (Gapdh normal.)
B
Brain – mRNA levels
WT
Pum1+/-
Pum1-/-
Fold change 2-ΔΔCt (Gapdh normal.)
both sexes
male
female
Pum1
Pum2
Fmr1
Ago2
Rbfox3
Cnot1
Mov10

Figure S7

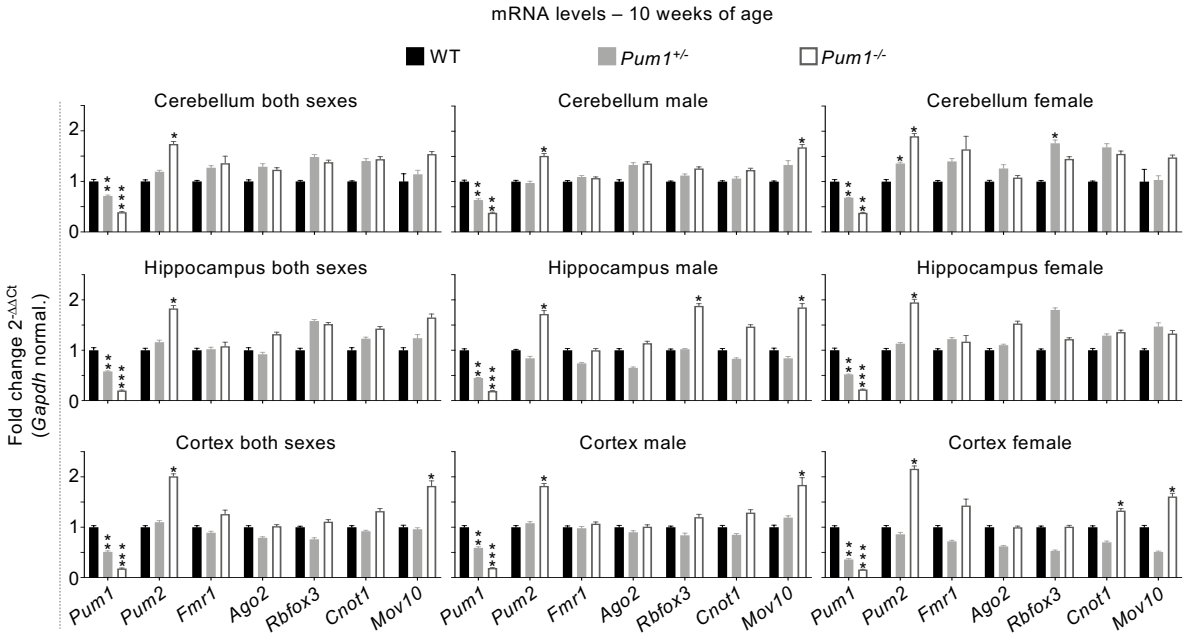
mRNA levels – 10 weeks of age
WT
Pum1+/-
Pum1-/-
Cerebellum both sexes
Cerebellum male
Cerebellum female
Hippocampus both sexes
Hippocampus male
Hippocampus female
Cortex both sexes
Cortex male
Cortex female
Fold change 2-ΔΔCt
(Gapdh normal.)
0
1
2
Pum1
Pum2
Fmr1
Ago2
Rbfox3
Cnot1
Mov10

Figure S8

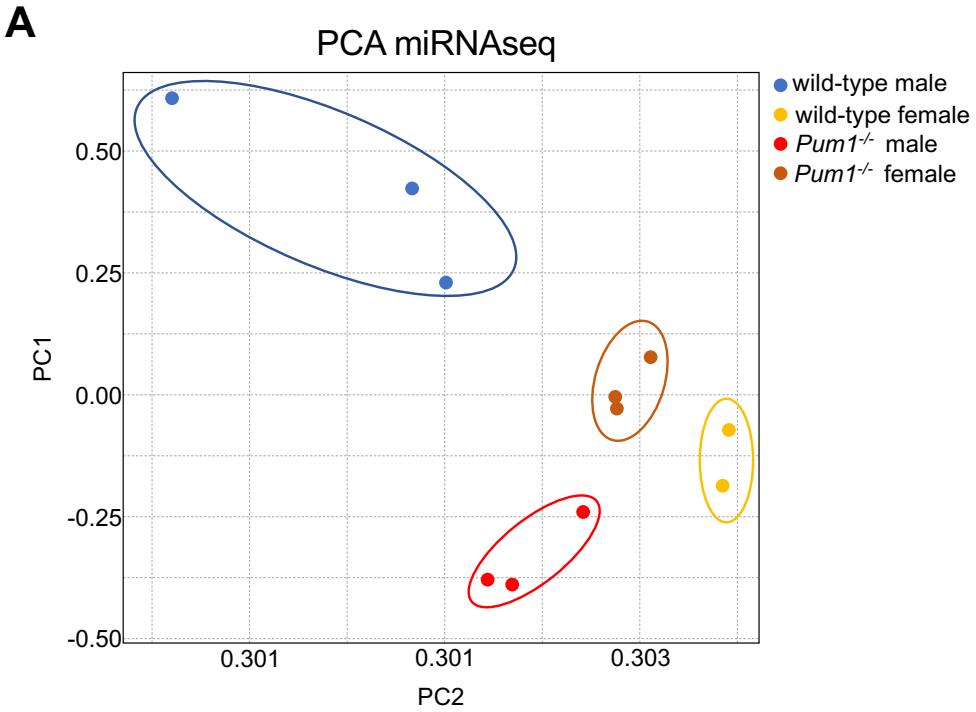
A
PCA miRNAseq
wild-type male
wild-type female
Pum1-/- male
Pum1-/- female
PC1
0.50
0.25
0.00
-0.25
-0.50
0.301
0.301
0.303
PC2

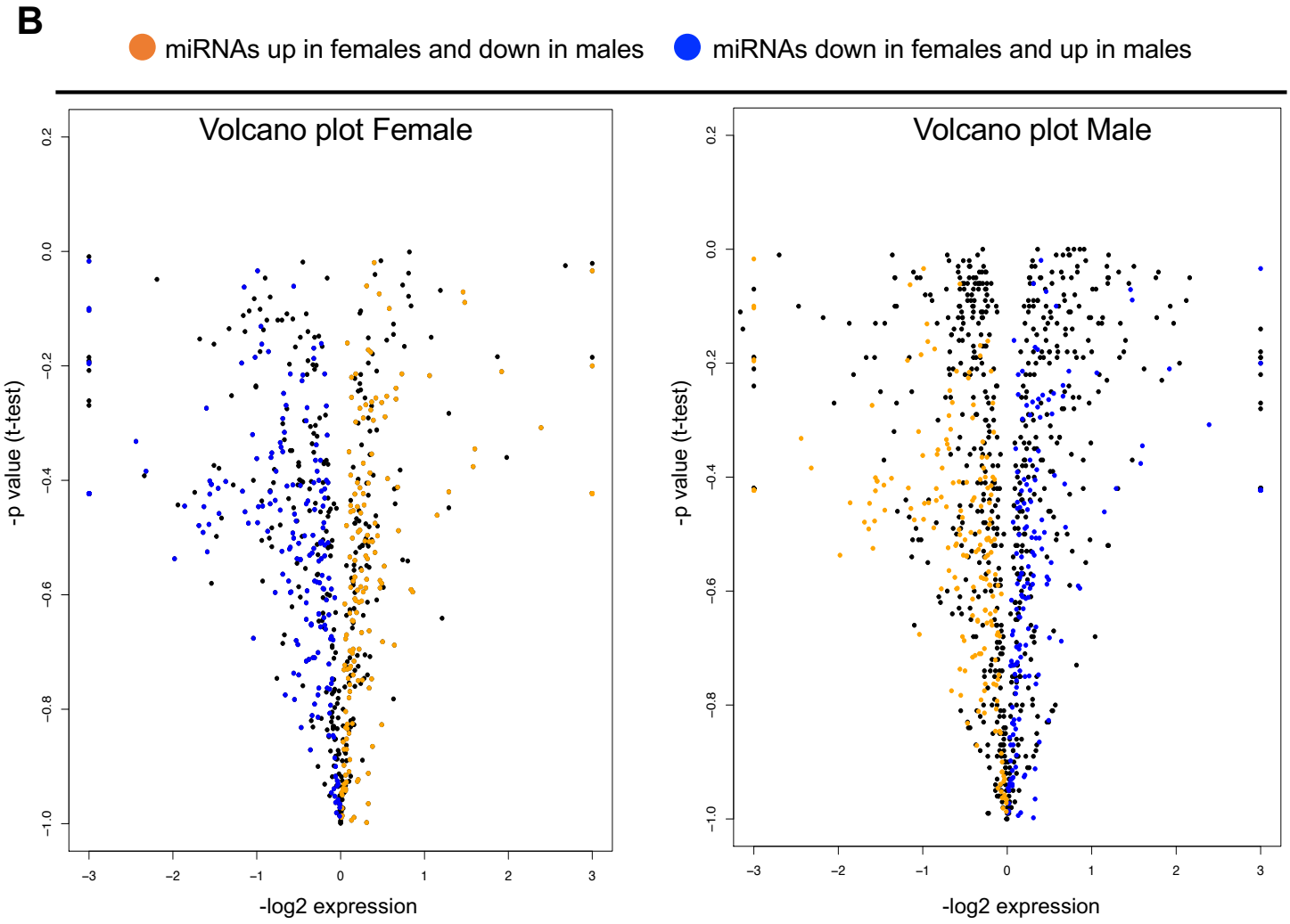
B
miRNAs up in females and down in males
miRNAs down in females and up in males
Volcano plot Female
Volcano plot Male
-p value (t-test)
-log2 expression
0.2
0.0
−0.2
−0.4
−0.6
−0.8
−1.0
−3
−2
−1
0
1
2
3

Figure S9

RNA quantification from male and female cerebellum at 10 weeks of age.
Genes plotted here sorted by number of co-bound miRNAs from **Figure 4D** with at least 25% expression change

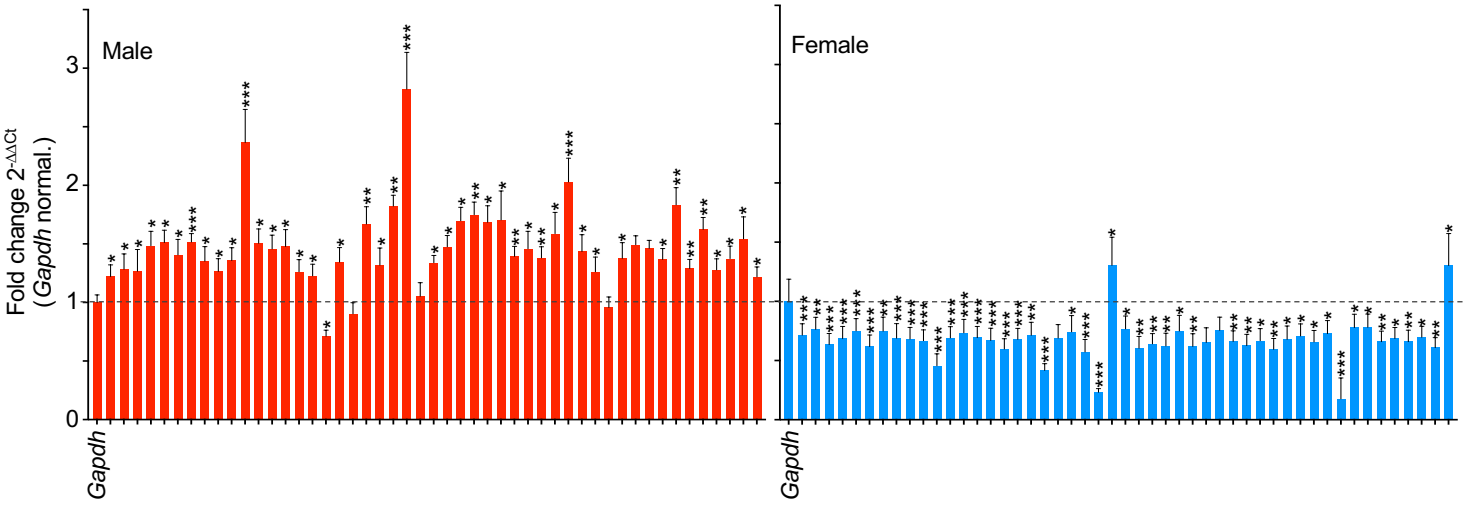

Table showing the order of gene represented in the figure above starting from *Gapdh* as represented in Figure 4E

Position in the graph	Gene	Male	Female	Error_Male	Error_Female	Co-bound miRNAs
1	*Gapdh*	1.000	1.000	0.065	0.188	11
2	*Aak1*	1.222	0.714	0.099	0.096	11
3	*Plekhm3*	1.283	0.764	0.132	0.102	11
4	*Zbtb20*	1.268	0.636	0.185	0.093	10
5	*Ago3*	1.485	0.686	0.122	0.102	10
6	*Dgkh*	1.511	0.751	0.106	0.103	10
7	*Fto*	1.407	0.618	0.132	0.097	10
8	*Grin2b*	1.517	0.749	0.071	0.117	10
9	*Lpp*	1.353	0.689	0.124	0.123	10
10	*Stx17*	1.266	0.682	0.108	0.098	10
11	*Acvr2b*	1.359	0.668	0.108	0.092	9
12	*Ap5m1*	2.366	0.456	0.282	0.101	9
13	*Chl1*	1.506	0.691	0.121	0.094	9
14	*Gpr161*	1.457	0.735	0.118	0.113	9
15	*Kcnn3*	1.477	0.694	0.145	0.094	9
16	*Klf7*	1.262	0.670	0.103	0.103	9
17	*Nfat5*	1.228	0.598	0.099	0.086	9
18	*Plxna4*	0.712	0.680	0.051	0.092	9
19	*Slc1a2*	1.344	0.713	0.125	0.111	9
20	*Slc8a1*	0.904	0.417	0.094	0.056	9
21	*Ston2*	1.669	0.690	0.148	0.114	9
22	*Tsc22d2*	1.319	0.743	0.146	0.137	9
23	*Xkr4*	1.823	0.573	0.093	0.105	9
24	*A1cf*	2.821	0.232	0.314	0.031	8
25	*Aff4*	1.053	1.304	0.116	0.238	8
26	*Clstn2*	1.340	0.768	0.062	0.109	8
27	*Cnnm2*	1.475	0.605	0.097	0.099	8
28	*Csnk1a1*	1.698	0.641	0.115	0.087	8
29	*Ctdspl2*	1.749	0.624	0.108	0.108	8
30	*Dcaf7*	1.685	0.750	0.141	0.132	8
31	*Fmnl3*	1.705	0.620	0.246	0.106	8
32	*Frmd4a*	1.394	0.654	0.085	0.123	8
33	*Grin2a*	1.459	0.755	0.148	0.112	8
34	*Hipk2*	1.381	0.662	0.094	0.088	8
35	*Kif26b*	1.588	0.627	0.181	0.094	8
36	*Klf12*	2.030	0.668	0.202	0.101	8
37	*Lmln*	1.435	0.595	0.143	0.091	8
38	*Lrrc40*	1.262	0.679	0.126	0.113	8
39	*Myo5a*	0.958	0.707	0.089	0.102	8
40	*Nav2*	1.377	0.658	0.135	0.097	8
41	*Psd3*	1.493	0.728	0.076	0.110	8
42	*Ptbp2*	1.463	0.177	0.068	0.177	8
43	*Rimkla*	1.368	0.779	0.092	0.112	8
44	*Snx30*	1.833	0.781	0.147	0.112	8
45	*Taok1*	1.290	0.660	0.078	0.088	8
46	*Zbtb10*	1.624	0.686	0.102	0.092	8
47	*Apbb2*	1.278	0.660	0.094	0.097	8
48	*Acap2*	1.374	0.697	0.107	0.093	8
49	*Acer2*	1.544	0.610	0.187	0.083	8
50	*Aebp2*	1.219	1.904	0.085	0.269	8

Figure S10

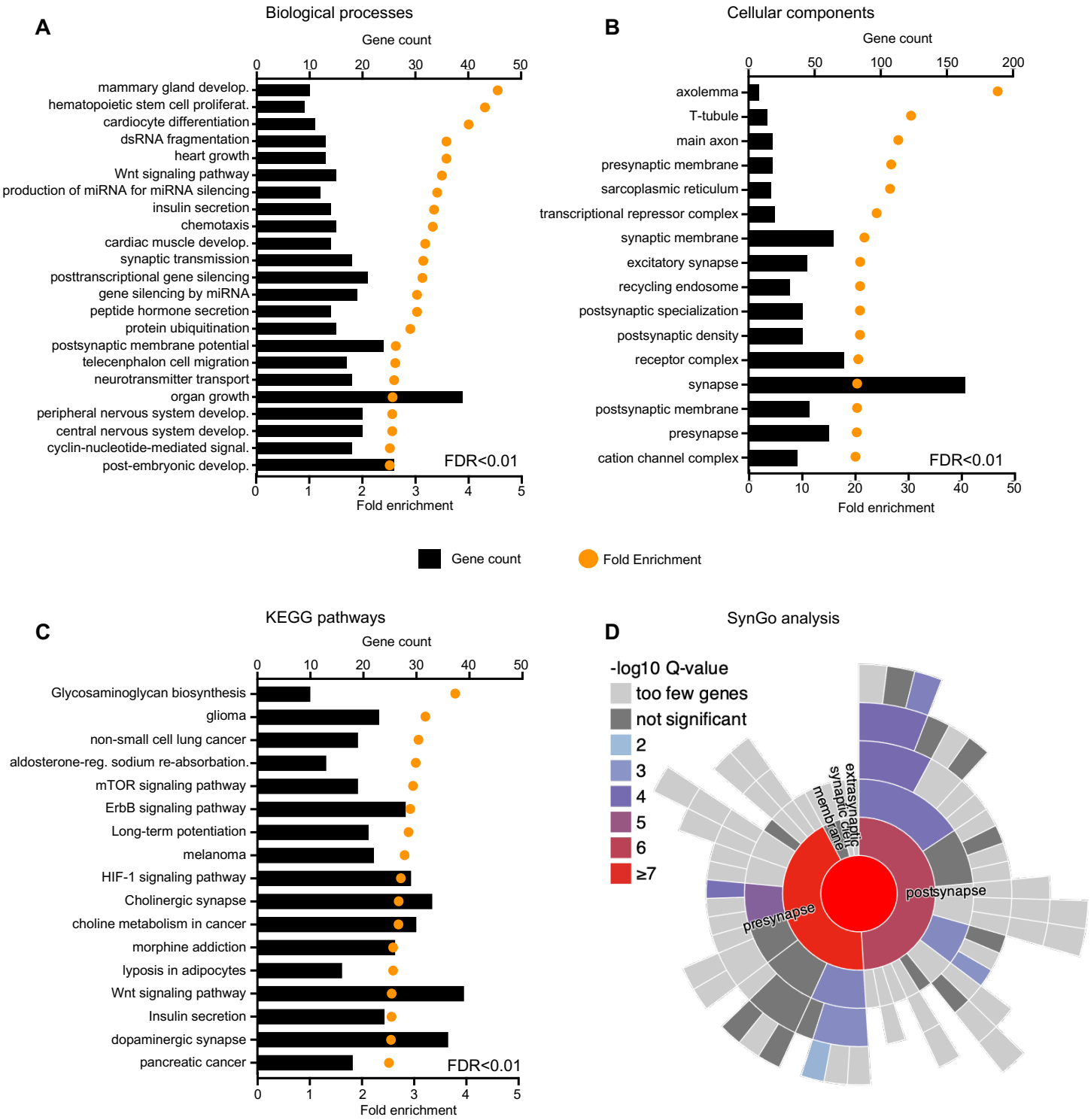
A
Biological processes
Gene count
0 10 20 30 40 50
mammary gland develop.
hematopoietic stem cell proliferat.
cardiocyte differentiation
dsRNA fragmentation
heart growth
Wnt signaling pathway
production of miRNA for miRNA silencing
insulin secretion
chemotaxis
cardiac muscle develop.
synaptic transmission
posttranscriptional gene silencing
gene silencing by miRNA
peptide hormone secretion
protein ubiquitination
postsynaptic membrane potential
telecenphalon cell migration
neurotransmitter transport
organ growth
peripheral nervous system develop.
central nervous system develop.
cyclin-nucleotide-mediated signal.
post-embryonic develop.
FDR<0.01
0 1 2 3 4 5
Fold enrichment
B
Cellular components
Gene count
0 50 100 150 200
axolemma
T-tubule
main axon
presynaptic membrane
sarcoplasmic reticulum
transcriptional repressor complex
synaptic membrane
excitatory synapse
recycling endosome
postsynaptic specialization
postsynaptic density
receptor complex
synapse
postsynaptic membrane
presynapse
cation channel complex
FDR<0.01
0 10 20 30 40 50
Fold enrichment
Gene count
Fold Enrichment
C
KEGG pathways
Gene count
0 10 20 30 40 50
Glycosaminoglycan biosynthesis
glioma
non-small cell lung cancer
aldosterone-reg. sodium re-absorbation.
mTOR signaling pathway
ErbB signaling pathway
Long-term potentiation
melanoma
HIF-1 signaling pathway
Cholinergic synapse
choline metabolism in cancer
morphine addiction
lyposis in adipocytes
Wnt signaling pathway
Insulin secretion
dopaminergic synapse
pancreatic cancer
FDR<0.01
0 1 2 3 4 5
Fold enrichment
D
SynGo analysis
-log10 Q-value
too few genes
not significant
2
3
4
5
6
≥7
extrasynaptic synaptic cleft membrane
postsynapse
presynapse

Figure S11

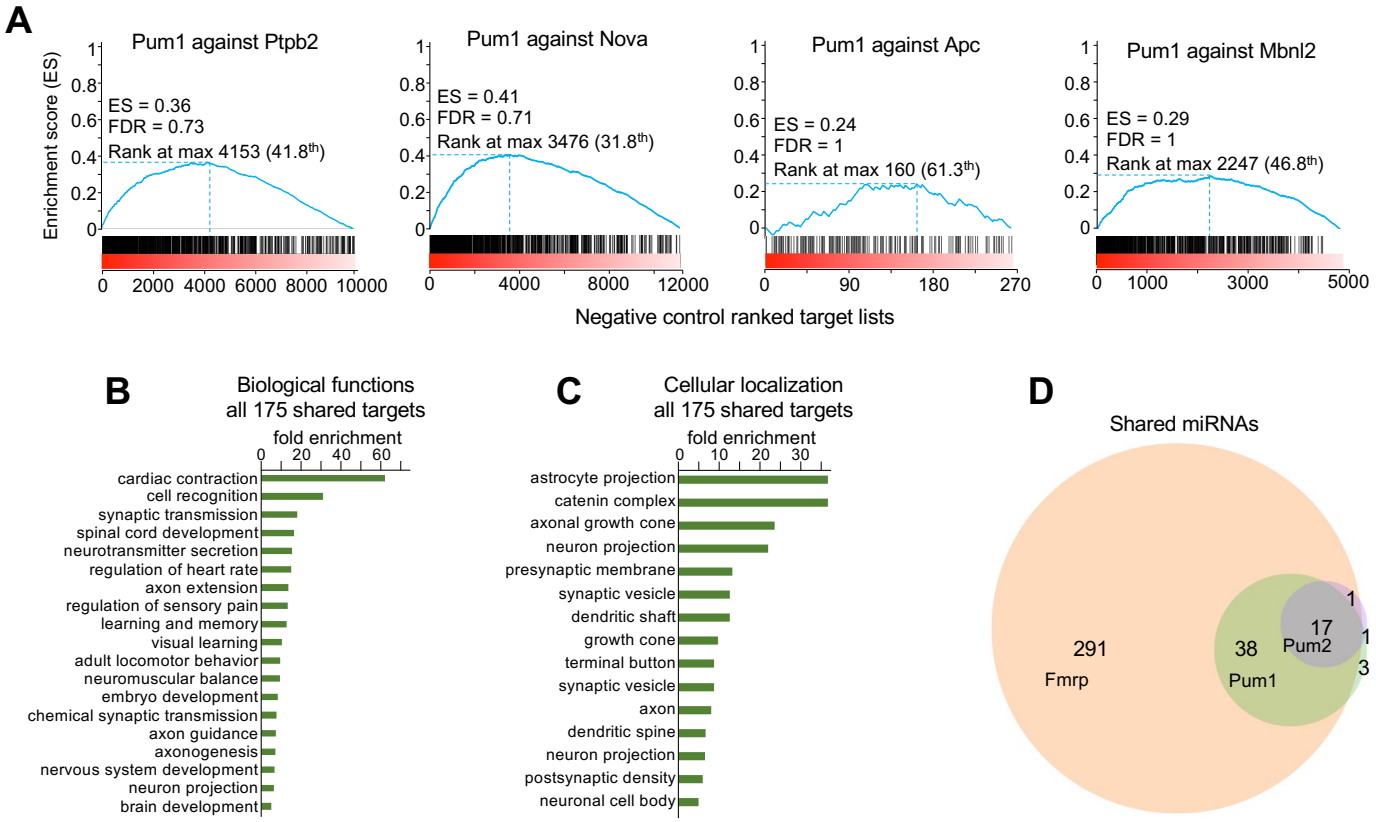
A
Pum1 against Ptpb2
ES = 0.36
FDR = 0.73
Rank at max 4153 (41.8th)
Pum1 against Nova
ES = 0.41
FDR = 0.71
Rank at max 3476 (31.8th)
Pum1 against Apc
ES = 0.24
FDR = 1
Rank at max 160 (61.3th)
Pum1 against Mbnl2
ES = 0.29
FDR = 1
Rank at max 2247 (46.8th)
Enrichment score (ES)
Negative control ranked target lists
B
Biological functions
all 175 shared targets
fold enrichment
cardiac contraction
cell recognition
synaptic transmission
spinal cord development
neurotransmitter secretion
regulation of heart rate
axon extension
regulation of sensory pain
learning and memory
visual learning
adult locomotor behavior
neuromuscular balance
embryo development
chemical synaptic transmission
axon guidance
axonogenesis
nervous system development
neuron projection
brain development
C
Cellular localization
all 175 shared targets
fold enrichment
astrocyte projection
catenin complex
axonal growth cone
neuron projection
presynaptic membrane
synaptic vesicle
dendritic shaft
growth cone
terminal button
synaptic vesicle
axon
dendritic spine
neuron projection
postsynaptic density
neuronal cell body
D
Shared miRNAs
291
Fmrp
38
Pum1
17
Pum2
1
1
3

Figure S12

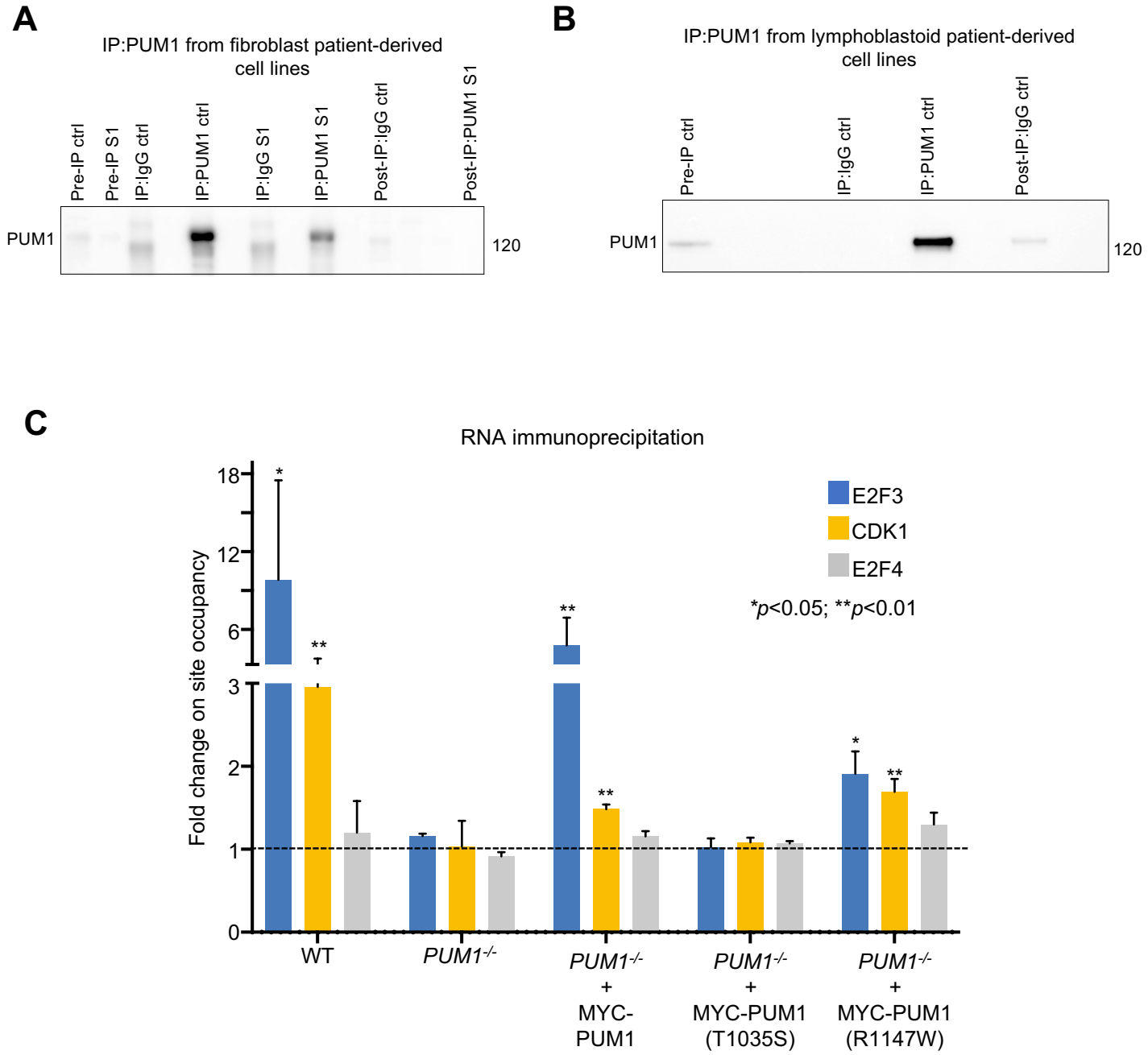
A
IP:PUM1 from fibroblast patient-derived cell lines
Pre-IP ctrl
Pre-IP S1
IP:IgG ctrl
IP:PUM1 ctrl
IP:IgG S1
IP:PUM1 S1
Post-IP:IgG ctrl
Post-IP:PUM1 S1
PUM1
120
B
IP:PUM1 from lymphoblastoid patient-derived cell lines
Pre-IP ctrl
IP:IgG ctrl
IP:PUM1 ctrl
Post-IP:IgG ctrl
PUM1
120
C
RNA immunoprecipitation
Fold change on site occupancy
E2F3
CDK1
E2F4
*p<0.05; **p<0.01
WT
PUM1-/-
PUM1-/- + MYC-PUM1
PUM1-/- + MYC-PUM1 (T1035S)
PUM1-/- + MYC-PUM1 (R1147W)

Figure S13

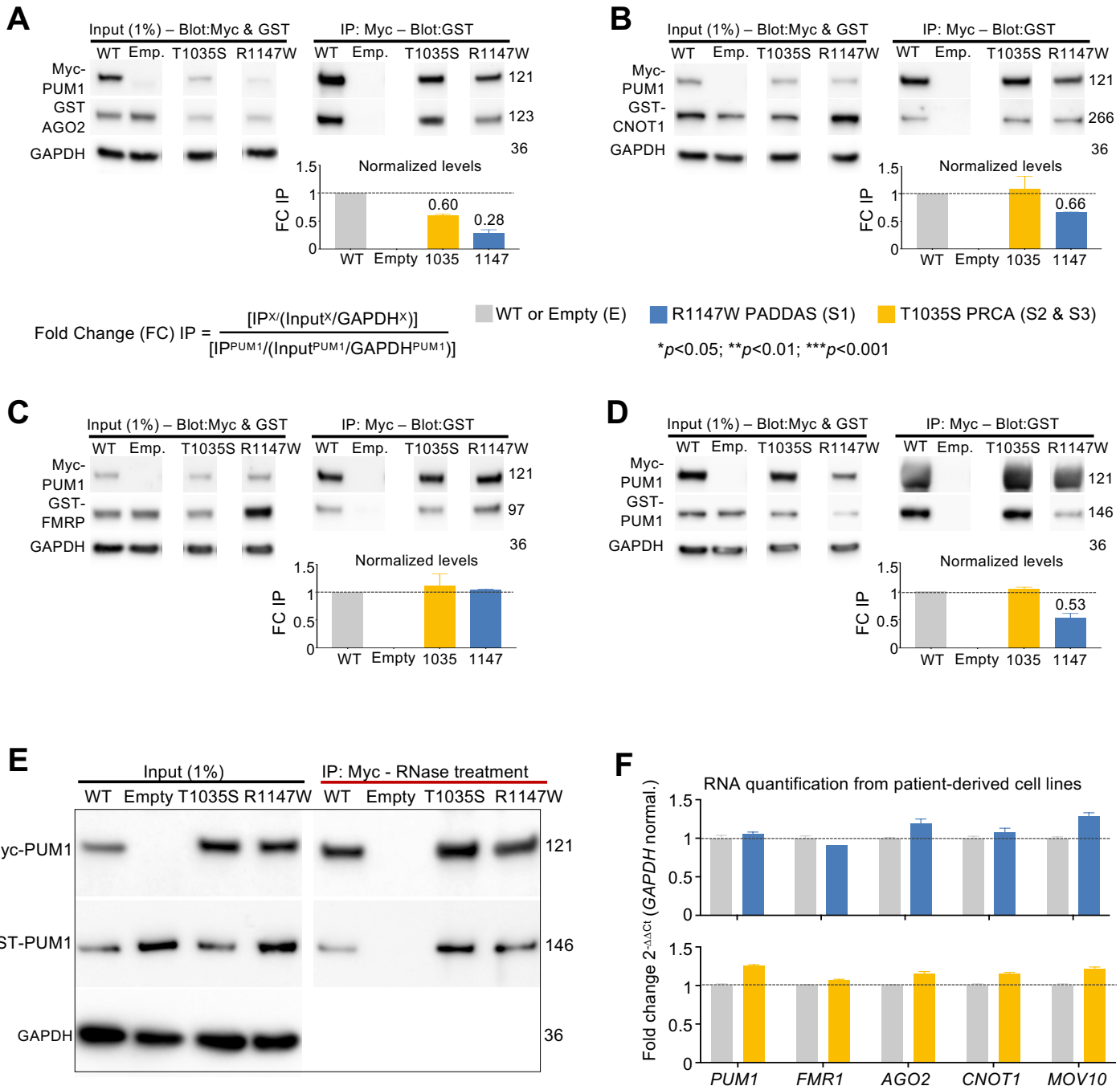
A
Input (1%) – Blot:Myc & GST
IP: Myc – Blot:GST
WT Emp. T1035S R1147W WT Emp. T1035S R1147W
Myc-PUM1
GST AGO2
GAPDH
121
123
36
Normalized levels
FC IP
0.60
0.28
WT Empty 1035 1147
B
Input (1%) – Blot:Myc & GST
IP: Myc – Blot:GST
WT Emp. T1035S R1147W WT Emp. T1035S R1147W
Myc-PUM1
GST-CNOT1
GAPDH
121
266
36
Normalized levels
FC IP
0.66
WT Empty 1035 1147
Fold Change (FC) IP = [IP^X/(Input^X/GAPDH^X)] / [IP^PUM1/(Input^PUM1/GAPDH^PUM1)]
WT or Empty (E)
R1147W PADDAS (S1)
T1035S PRCA (S2 & S3)
*p<0.05; **p<0.01; ***p<0.001
C
Input (1%) – Blot:Myc & GST
IP: Myc – Blot:GST
WT Emp. T1035S R1147W WT Emp. T1035S R1147W
Myc-PUM1
GST-FMRP
GAPDH
121
97
36
Normalized levels
FC IP
WT Empty 1035 1147
D
Input (1%) – Blot:Myc & GST
IP: Myc – Blot:GST
WT Emp. T1035S R1147W WT Emp. T1035S R1147W
Myc-PUM1
GST-PUM1
GAPDH
121
146
36
Normalized levels
FC IP
0.53
WT Empty 1035 1147
E
Input (1%)
IP: Myc - RNase treatment
WT Empty T1035S R1147W WT Empty T1035S R1147W
Myc-PUM1
GST-PUM1
GAPDH
121
146
36
F
RNA quantification from patient-derived cell lines
Fold change 2^-ΔΔCt (GAPDH normal.)
PUM1 FMR1 AGO2 CNOT1 MOV10

Figure S14
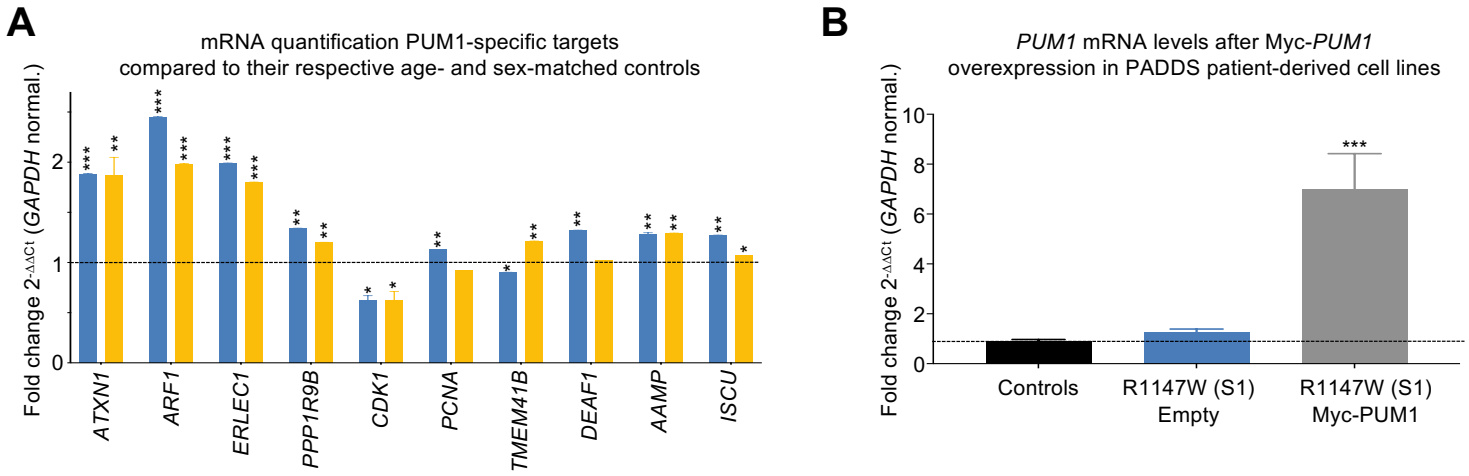
--- Age- and sex- matched control cell lines ■ Controls (Healthy) ■ R1147W PADDAS (S1) ■ T1035S PRCA (S2 & S3) *p<0.05; **p<0.01; ***p<0.001